Dissertation zur Erlangung des Doktorgrades

der Fakultät für Chemie und Pharmazie

der Ludwig-Maximilians-Universität München

Evaluation of the Proteasome as a Trigger and Target

in Idiopathic Pulmonary Fibrosis

Nora Kristine Semren (geb. Pfister)

aus

München, Deutschland

2015

Für Ella und Daniel

TABLE OF CONTENTS

SUMMARY

Idiopathic pulmonary fibrosis (IPF) is an irreversible and progressive disease of the lungs, which is characterized by aberrant tissue remodeling and massive deposition of extracellular matrix proteins. This process is mainly conducted by myofibroblasts, an activated fibroblast phenotype. During the pathogenesis of IPF, the fine alveolar structure is destroyed and gas exchange declines, finally resulting in organ failure. So far, pharmacological treatment options are very limited and lung transplantation still remains the only curative therapy.

Pathologic tissue remodeling in IPF is closely connected to altered cell and protein homeostasis. The ubiquitin-proteasome system is critical for degradation of polyubiquitinated proteins in a spatially and timely controlled manner, thereby regulating protein levels. The proteasome is a multicatalytic enzyme complex consisting of a barrel shaped 20S catalytic core particle (CP) and one or two 19S regulatory particles (RP), thus forming active 26S/30S proteasomes. Dysregulation of the proteasome has been reported for several chronic diseases of the heart, brain, and also lung. Furthermore, inhibition of the proteasome has been shown to provide antifibrotic effects in different organs, including the lung.

As nothing is known about proteasome function in the pathogenesis of IPF, the first aim of the present study was to analyze proteasomal regulation during tissue remodeling and myofibroblast differentiation.

For that, lung fibroblasts were treated with transforming growth factor-β (TGF-β) and proteasome activity as well as composition was examined. For *in vivo* testing, the bleomycin mouse model of lung fibrosis was used and human lung tissue of IPF patients was analyzed. It was found that induction of myofibroblast differentiation by TGF-β mediated assembly of 19S RPs with 20S CPs, thereby forming 26S/30S complexes, which was critically dependent on the regulatory particle non-ATPase 6 subunit (Rpn6). In addition, silencing of Rpn6 in primary human lung fibroblasts counteracted TGF-β-induced myofibroblast differentiation. During bleomycin-induced fibrotic remodeling of mouse lungs, increased formation of 26S/30S proteasomes was accompanied by augmented expression of Rpn6 in fibrotic lungs. Here, Rpn6 was highly expressed in hyperplastic alveolar epithelial cells and Clara cells. Overexpression of Rpn6 was also observed in myofibroblasts and hyperplastic bronchiolar basal cells of fibrotic lung tissue of IPF patients and accompanied by enhanced polyubiquitination of proteins.

As therapeutic application of proteasome inhibitors in pulmonary fibrosis showed controversial results including beneficial antifibrotic effects but also toxicity, the second aim of this study was

to test whether site-specific inhibition of the proteasome, using the novel second generation inhibitor oprozomib, provides antifibrotic effects in the absence of systemic side effects after local pulmonary application.

Oprozomib was compared to the FDA-approved proteasome inhibitor bortezomib and tested on the human alveolar epithelial cancer cell line A549 and on primary mouse alveolar epithelial type II cells regarding its cytotoxic effects. Oprozomib was less toxic than bortezomib and provided high selectivity for the chymotrypsin-like active site of the proteasome. In primary mouse lung fibroblasts, oprozomib showed significant antifibrotic effects like reduction of collagen I and α-smooth muscle actin expression at non-toxic doses. When applied locally into the lungs of healthy mice via instillation, oprozomib was well tolerated and effectively reduced pulmonary proteasome activity. In bleomycin-challenged mice, however, locally applied oprozomib resulted in accelerated weight loss and increased mortality. Furthermore, oprozomib failed to reduce fibrosis in these mice, but rather augmented fibrotic lung remodeling in bleomycin-challenged animals.

To conclude, this study identified a novel mechanism for fibrotic remodeling of the lungs involving 26S/30S proteasome activation via Rpn6 upon TGF-β-mediated myofibroblast differentiation. Increased levels of Rpn6 and polyubiquitinated proteins in IPF lungs further suggest an important contribution of the ubiquitin-proteasome system to the pathogenesis of this disease. Inhibition of the proteasome with the novel site-specific proteasome inhibitor oprozomib provided low toxicity and antifibrotic effects in alveolar epithelial cells and pulmonary fibroblasts. These results could not be confirmed in pulmonary fibrosis of bleomycin-treated mice, as oprozomib treatment showed high toxicity in fibrotic animals.

In light of these data, current proteasome inhibitors, which block the catalytic core, might be too toxic as therapeutic agents for the treatment of fibrotic lung diseases. However, interference with the formation of 26S/30S proteasomes, as shown by Rpn6 knockdown, might provide a novel concept for therapeutic regulation of proteasome activity in lung fibrosis.

1 INTRODUCTION

1.1 Idiopathic Pulmonary Fibrosis

"IPF is defined as a specific form of chronic, progressive fibrosing interstitial pneumonia of unknown cause, occurring primarily in older adults, limited to the lungs, and associated with the histopathologic and/or radiologic pattern of UIP."

Definition by the Official ATS/ERS/JRS/ALAT Statement on Idiopathic Pulmonary Fibrosis (Raghu et al., 2011).

1.1.1 Clinical phenotypes, prognosis, and risk factors of IPF

Idiopathic pulmonary fibrosis (IPF), a form of usual interstitial pneumonia (UIP), is a devastating, irreversible, and chronic pulmonary disease, which is characterized by a progressive destruction of the fine alveolar architecture and loss of lung function. So far, treatment options in IPF are very limited resulting in a poor prognosis for affected patients. As IPF mainly occurs in middle-aged to elderly adults (50 years and onwards), it is regarded as an age-related disease (Raghu et al., 2011). Even though IPF is not a very common disease, its incidence is rising and is currently estimated to be between 4.6 and 16.3 per 100,000 people, and seems to be more frequent in men than women (King et al., 2011). The aggressive nature of IPF is also reflected by a poor median survival of only up to 2-3 years after initial diagnosis (Raghu et al., 2011). A long asymptomatic period in the beginning of the disease often leads to late diagnosis, as most IPF patients consult a medical doctor for the first time at an already advanced stage of the disease (Figure 1.1). At the onset of symptoms, three major progression types can be distinguished. Most patients experience a slow but progressive clinical and functional decline. This can be accompanied by acute exacerbations, which, in IPF, often occur in the absence of specific reasons such as infection, heart failure, or pulmonary embolism. Acute exacerbations often indicate the beginning of the final phase of the disease. Few patients face a fast progressive course with a short time of survival. These patients are predominantly male smokers, and activation of cigarette smoke-induced inflammatory pathways has been reported. In addition, heavy smokers are also likely to show a combination of pulmonary fibrosis and emphysema, leading to a faster progression of the disease than in patients with IPF alone (King et al., 2011).

Even though IPF is defined as a disease of unknown etiology, various potential risk factors have been reported. Cigarette smoking (Baumgartner et al., 1997) and environmental exposure to

dust, especially from metal or wood, have been strongly associated with IPF. But also chronic viral infection or gastroesophageal reflux linked to a presumed microaspiration of gastric acid have been assumed to contribute to the pathogenesis of the disease (Raghu et al., 2011).
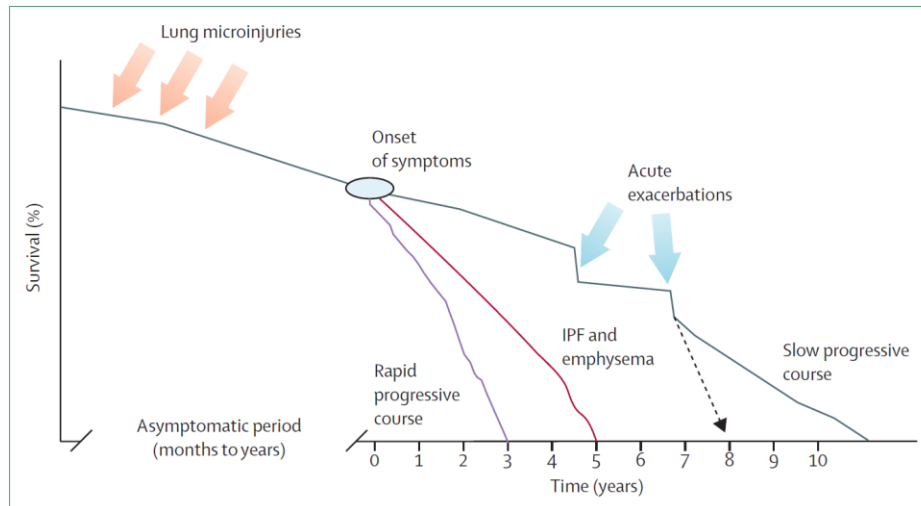
Figure 1.1. Clinical phenotypes of IPF
A long asymptotic period is followed by an acute onset of symptoms, which usually is also the time of diagnosis. Three main phenotypes are distinguished: A slow progressive phenotype, experienced by 10% of patients, exhibits a slow, clinical and functional decrease, which can be worsened by episodes of acute exacerbations. In contrast, patients with a rapid progressive course have a very short duration of illness. Heavy smokers might also develop an intermediate phenotype which is characterized by additional presence of emphysema. (Taken from King et al., 2011)

Several studies provide evidence for genetic predisposition of pulmonary fibrosis and account for about 5% of IPF cases. Most common disease-linked mutations in familial forms of IPF have been identified in the surfactant protein C gene (SFTPC) (Thomas et al., 2002), in the promotor region of the mucin 5B gene (MUC5B) (Seibold et al., 2011), and in genes encoding telomerase (TERT and TERC) (Armanios et al., 2007).

1.1.2 Pathological characteristics of IPF

A final diagnosis of IPF can be obtained by histological analysis of lung biopsies and non-invasive diagnostic procedures, such as lung function testing and high resolution computed tomography (HRCT).

A common histological feature of IPF at low magnification is the proximity of alternating normal and scarred lung areas, resulting in a patchy distribution (Figure 1.2A). Hereby, scarred areas predominate in subpleural/paraseptal regions, whereas the centrolobule may show regions with normal lung structure (Figure 1.2B). The lung architecture, normally presented by fine alveolar structures, is distorted and large airspaces, so called honeycombs, which are encompassed by bronchial epithelium and often filled by inflammatory cells or mucus, are present. In contrast to emphysema, the background of honeycombs consists of destroyed lung tissue (Figure 1.2C) (Cavazza et al., 2010). A typical feature in the histology of IPF is the presence of so called fibroblast foci, which consist of proliferating, extracellular matrix (ECM) deposing, spindle-shaped myofibroblasts embedded in a myxoid matrix (Figure 1.2D). Fibroblast foci indicate areas of acute fibrotic remodeling, whereas honeycombing and fibrotic scars prevail in areas of past fibrotic injury (Cavazza et al., 2010; Raghu et al., 2011; Wolters et al., 2014).
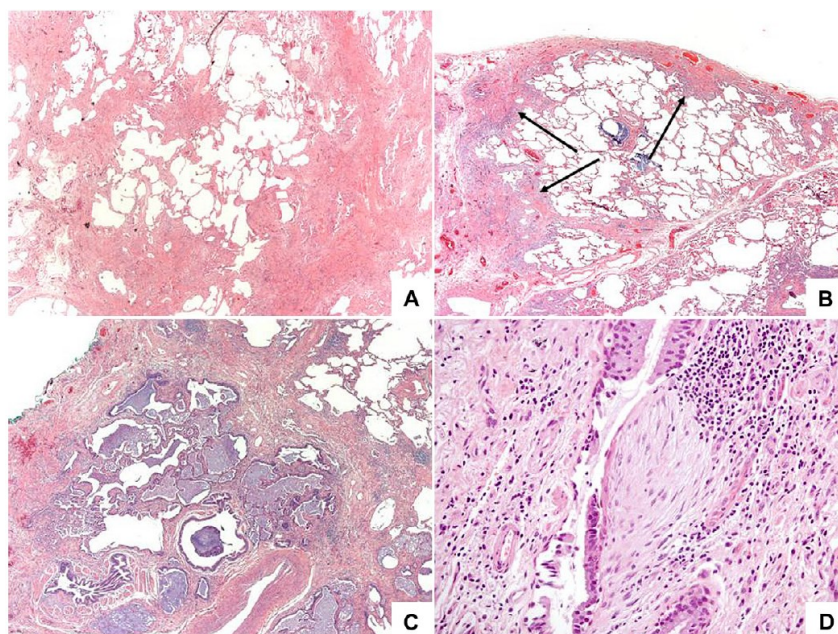
Figure 1.2. Histopathology of IPF (H&E)
(**A**) Patchwork pattern of scarred and normal lung areas (20x magnification). (**B**) Arrows indicate fibrosis in the peripheral, subpleural, and paraseptal area (20x magnification). (**C**) Honeycombing (20x magnification) and (**D**) fibroblast focus consisting of proliferating myofibroblasts (20x magnification). (Taken from Cavazza et al., 2010)

Honeycombing is also a typical criterion for a definite diagnosis of IPF by HRCT. Here, it is manifested as reticular opacities mainly in the subpleural region with well-defined walls (Figure 1.3) (King et al., 2011; Raghu et al., 2011).
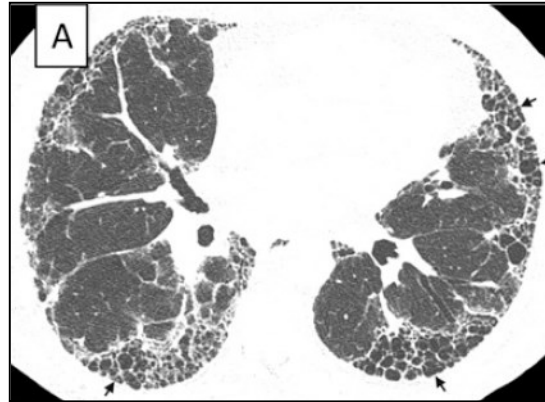
Figure 1.3. HRCT of a typical pattern of UIP
Axial HRCT image shows a typical UIP pattern with multiple layers of extensive honeycombing in basal regions, indicated by arrows. (Taken from Raghu et al., 2011)

1.1.3 Pathomechanisms in IPF

Despite the identification of a variety of risk factors, which are discussed to trigger the initiation of lung fibrosis, the origin of IPF and its underlying pathomechanism is not completely understood yet.

Most of these risk factors such as smoking, exposure to air pollutants or viral infection might lead to perpetuated microinjuries of the alveolar epithelium and might trigger a dysregulation within the wound healing process. This finally results in excessive and ongoing deposition of extracellular matrix proteins, thereby causing distortion of the fine alveolar structure and finally organ failure (Wynn, 2011). Therefore, IPF is also widely regarded as unrestrained wound healing response (Fernandez & Eickelberg, 2012b).

Normal wound healing consists of four distinct phases including clotting and coagulation, migration of inflammatory cells, fibroblast activation and finally tissue remodeling and resolution. In the lung, epithelial cells release inflammatory mediators after disruption to start an antifibrinolytic-coagolation cascade and to recruit inflammatory cells like neutrophils, lymphocytes, eosinophils and macrophages to the site of injury. These leukocytes further release profibrotic cytokines such as interleukin-1β (IL-1β), tumor necrosis factor (TNF), interleukin-13 (IL-13) and transforming growth factor-β (TGF-β) to induce fibroblast migration, proliferation, and activation (Wynn, 2011). Further, activated macrophages and neutrophils

remove dead cells and attack invading organisms. Activated fibroblasts, so-called myofibroblasts, express α-smooth muscle actin (αSMA) and secrete ECM proteins. During the tissue remodeling step, myofibroblasts mediate wound contraction to finally facilitate migration of dividing epithelial cells over the present matrix to regenerate the damaged tissue. However, in IPF the wound healing process is dysregulated, myofibroblasts remain activated and excessively dispose ECM, leading to scar formation and finally tissue destruction (Figure 1.4) (King et al., 2011; Wynn, 2011).
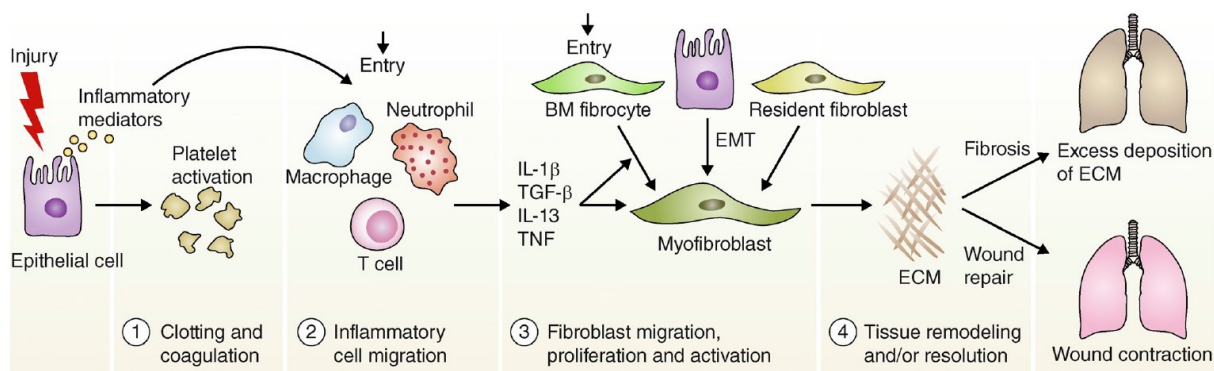
Figure 1.4. Wound healing process in normal and fibrotic lungs
Lung regeneration after injury can be divided into four phases: During the clotting and coagulation phase affected epithelial cells release inflammatory mediators and initiate an antifibrinolytic-coagolation cascade. Inflammatory cells migrate and secrete profibrotic cytokines to induce myofibroblast activation. Myofibroblasts then release ECM components and mediate the final tissue remodeling phase. In healthy lungs, the epithelium integrity is restored whereas in IPF myofibroblasts stay activated and continue the remodeling process, leading to an excessive deposition of ECM. (Taken from Wynn, 2011)

1.1.3.1 The alveolar epithelium

IPF primarily occurs in the alveolar region of the lung. The alveolar epithelium consists of type I epithelial cells (AECI or ATI), responsible for the gas exchange, and type II epithelial cells (AECII or ATII) that produce large amounts of surfactant proteins and are discussed to be progenitor cells of AECI (Barkauskas & Noble, 2014). A typical histological feature in IPF is the presence of abnormal hyperplastic and hypertrophic AECII, which overlay fibroblastic foci (Katzenstein & Myers, 1998). These cells are highly active, showing both apoptosis and proliferation, and indicate ongoing dysregulated repair processes without persistent stimulus (King et al., 2011; Korfei et al., 2011). In IPF it is hypothesized that the alveolar epithelium is unable to mediate normal tissue regeneration. This is supported by human genetic studies in familial cases of pulmonary fibrosis, reporting gene mutations that effect proteins, which are mainly expressed in alveolar epithelial cells (Wolters et al., 2014). For example gene mutations

in surfactant proteins C and A2, which are expressed exclusively in AECIIs, might activate the unfolded protein response (UPR) (Noble et al., 2012; Wolters et al., 2014). The UPR involves a variety of conserved signaling pathways and monitors the chaperone-mediated folding capacity of the endoplasmic reticulum (ER). ER-stress occurs when the ER is unable to restore proper protein folding, as shown for the mentioned mutant surfactant proteins, leading to accumulation of misfolded proteins (Meiners et al., 2015; Walter & Ron, 2011). As a consequence, the UPR is activated via three ER transmembrane transducers: Inositol requiring enzyme 1 (IRE1) induces expression of chaperones and proteins involved in ER-associated protein degradation (ERAD) to enhance degradation of misfolded proteins by the ubiquitin-proteasome system (UPS). Next to proteasomal protein degradation, autophagy is activated during UPR to dispose aggregates of misfolded proteins via lysosomes (Senft & Ronai, 2015). Activating transcription factor 6 (ATF6) also elevates expression of chaperones and protein kinase RNA-like ER kinase (PERK) activation reduces overall protein translation (Christianson & Ye, 2014; Walter & Ron, 2011; Wei et al., 2013). Further, the UPR can increase ER abundance, thereby enhancing its capacity for protein folding and processing to prevent accumulation of misfolded proteins and to restore homeostasis (Wei et al., 2013). Successful UPR results in UPR-attenuation, but in case ER-stress remains the UPR promotes apoptosis (Shore et al., 2011) as proposed for AECIIs in sporadic cases of IPF (Tanjore et al., 2012). Impaired autophagy has also been proposed to contribute to accelerated senescence in epithelial cells with ER-stress responses (Araya et al., 2012) and to be involved in TGF-β-mediated myofibroblast activation (Araya et al., 2012; Patel et al., 2012).

Furthermore, pulmonary surfactant is crucial to maintain alveolar stability during respiration and insufficient production might lead to alveolar damage (Hardie et al., 2010). Seibold et al. identified a common polymorphism in the promoter region of MUC5B leading to an overexpression of the gel-forming mucin in bronchial epithelial cells. Excessive concentrations of mucin are discussed to impair the mucosal host defence and to reduce lung clearance of microorganisms, inhaled particles or dissolved chemicals. This might cause an persistent exaggerated lung injury and trigger development of IPF (Seibold et al., 2011).

Short dysfunctional telomeres are associated with premature aging as seen in patients with dyskeratosis congenital. Armanios et al. could identify mutations in the genes hTERT and hTR encoding telomerase reverse transcriptase and telomerase RNA in familial IPF. Impaired telomerase function, resulting in short dysfunctional telomeres, are known to activate a DNA damage response which results in apoptosis or senescence. This might lead to a reduced regenerative capacity of the alveolar epithelium in the lung and a progressive loss of alveolar

cells, leading to damage of the epithelium and development of fibrotic lesions (Armanios et al., 2007; Wolters et al., 2014).

The interplay of several factors like age, environmental exposure to smoke or dust, genetic factors, gastroesophageal reflux, viral infections or unknown endogenous factors might finally contribute to the diseases pathogenesis (Raghu et al., 2011). Thereby, loss of proteostasis, as indicated by persistent ER-stress, UPR, and impaired autophagy may play a crucial role to promote an alveolar epithelium which is susceptible to an abnormal tissue repair, finally leading to IPF (Balch et al., 2014).

1.1.3.2 *Myofibroblast activation*

Fibroblast foci are histological hallmarks of IPF and ECM releasing myofibroblasts strongly contribute to the scarring process and the destruction of the fine alveolar structure. Myofibroblasts are key effector cells in IPF, which are discussed to originate from various sources including bone marrow derived, circulating fibrocytes, resident fibroblasts or epithelial-to-mesenchymal transition (EMT) (Fernandez & Eickelberg, 2012b; Phan, 2012). They are highly contractile due to expression of αSMA in stress fibres, which is also a common marker for this cell type. Myofibroblast differentiation in the lung is mainly induced by mediators, released by alveolar epithelial cells in response to lung injury as described in chapter 1.1.3.1 (King et al., 2011; Klingberg et al., 2013).

The presence of high local concentrations of biologically active TGF-β, high mechanical stress, and specialized ECM-components such as the extra domain A (ED-A) splice variant of fibronectin (Fn) are discussed to act as main drivers of myofibroblast differentiation (Hinz et al., 2007). High levels of TGF-β are a characteristic feature of IPF lungs and are proposed to be mainly released by macrophages and epithelial cells in response to epithelial injury or by activated myofibroblasts within the remodeling process. TGF-β is commonly regarded as key initiator of fibroblast differentiation into ECM-secreting myofibroblasts (Duffield et al., 2013; Fernandez & Eickelberg, 2012a; Wynn & Ramalingam, 2012).

When TGF-β is activated from its latent complex, it binds to TGF-β transmembrane type I (TβRI) and type II (TβRII) serine/threonine kinase receptors and induces their heterodimerization. Subsequently, TβRII transphosphorylates TβRI, which finally phosphorylates receptor-specific transcription factors (R-SMADs: SMAD2 and SMAD3) (Massagué, 2012) (Figure 1.5). Translocation of phosphorylated SMADs into the nucleus is then mediated by SMAD4, and transcription of profibrotic genes, including ECM components such as collagens, αSMA, and

fibronectin, is activated after association of the R-SMAD/SMAD4 complex with the genomic SMAD-binding element (SBE). Transcriptional regulation by SMADs can be antagonized by nuclear proteins SKI and SNO (also SnoN). Furthermore, SMAD7, an inhibitory SMAD (I-SMAD), counteracts TGF-β signaling through various mechanisms. R-SMADs can also regulate TGF-β-mediated transcription via SMAD-induced miRNA processing (Akhurst & Hata, 2012; Massagué, 2012).

Resident fibroblasts are regarded as the main source of myofibroblasts in lungs of IPF patients. Under normal conditions, they regulate ECM homeostasis by expression and secretion of ECM proteins to build up matrix and by release of matrix metalloproteinases and tissue inhibitors of matrixmetalloproteinases to degrade or remodel ECM. Residing in the subepithelial region, they show little actin-associated cell-cell or cell-matrix interactions (Bagnato & Harari, 2015; Hinz et al., 2007). After injury of the epithelium, the release of profibrotic markers, mainly TGF-β, induces fibroblast differentiation in highly contractile, proliferating myofibroblasts which then migrate to the area of epithelial disruption to deposit ECM, thereby mediating initial wound contraction and closure (Phan, 2012).
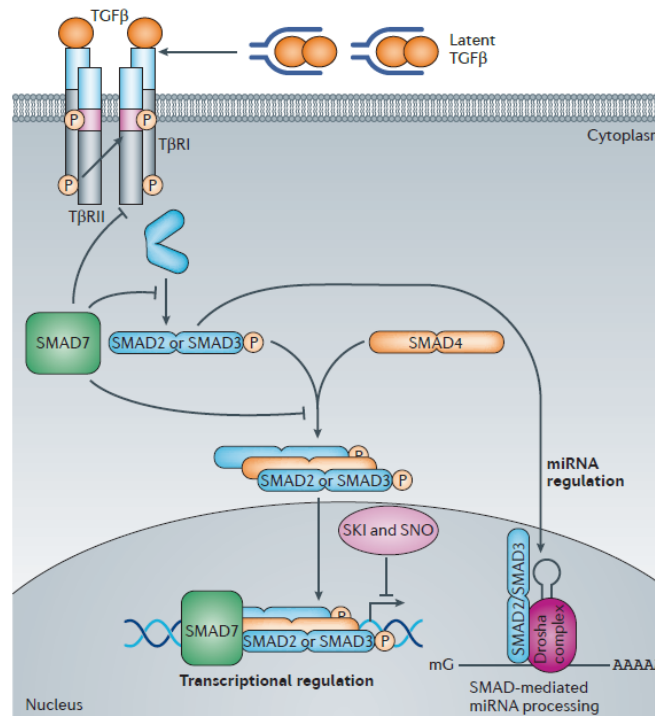
Figure 1.5. SMAD-dependent TGF-β signaling
TGF-β mediates phospholyation of TβRII and TβRI, which then phosphorylates R-SMADs, thereby activating their translocation into the nucleus. R-SMADs may also regulate gene expression via SMAD-mediated miRNA processing. I-SMAD, SKI and SNO act as inhibitory factors of the TGF-β pathway. (Taken from Akhurst & Hata, 2012)

Fibrocytes are a special subpopulation of leukocytes and have been shown to infiltrate into IPF lungs from the blood. They have been described in areas of active fibrotic remodeling in proximity of newly formed scar tissue. Fibrocytes combine features of hematopoietic and mesenchymal cells like expression of CD45 and CD34 together with expression of collagen I and fibronectin. Alveolar epithelial cells in IPF lungs express the chemokine CXCL12, thereby inducing chemotaxis of fibrocytes towards the injured epithelium. Subsequent TGF-β mediated differentiation at the site of injury might add to the excessive accumulation of myofibroblasts in IPF (King et al., 2011; Maharaj et al., 2013).
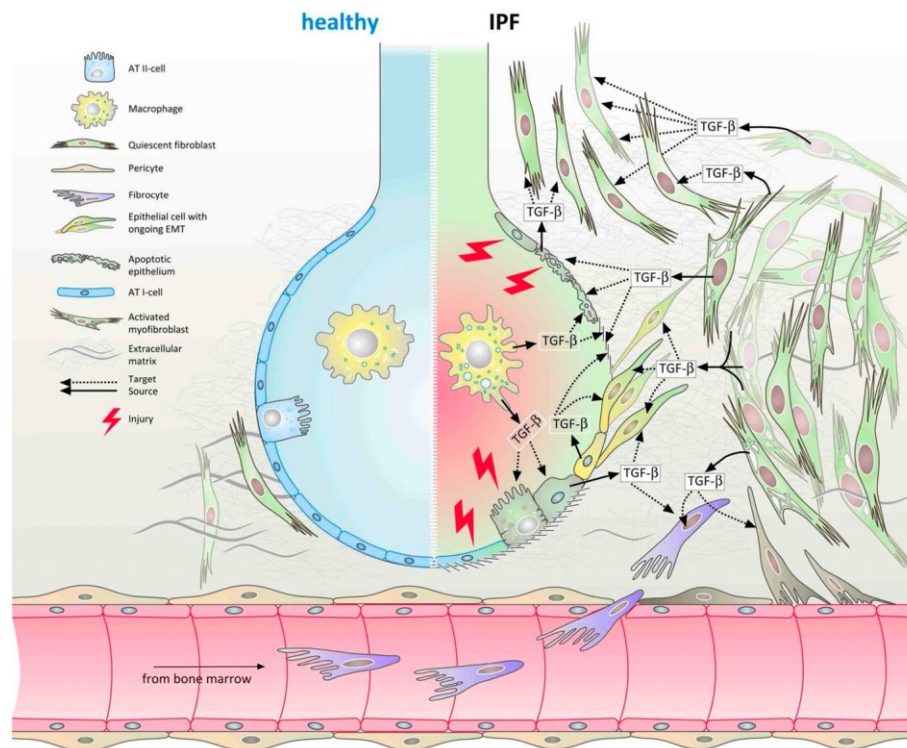
Figure 1.6. Proposed sources of myofibroblasts in IPF
TGF-β is released by AECs, macrophages or activated myofibroblasts in response to epithelial injury. Bone marrow-derived fibrocytes and resident fibroblasts are recruited and differentiate into highly contractile, ECM-releasing myofibroblasts. AECs undergo EMT and contribute to the myofibroblast pool. In IPF the aberrant wound healing process persists and myofibroblasts stay activated. (Taken from Fernandez & Eickelberg, 2012a)

Another proposed source of myofibroblasts is the alveolar epithelium itself. Within the process of EMT, AECs loose epithelial cell markers and polarity and acquire a mesenchymal phenotype indicated by single cell motility and synthesis of ECM (Fernandez & Eickelberg, 2012a). There is strong evidence for TGF-β as main driver of EMT in lungs of IPF patients. AECs in IPF lungs show high levels of SNAI1 and SNAI2 transcription factors, which have been shown to be main effectors of TGF-β mediated EMT in the lung (Jayachandran et al., 2009).

Within normal tissue repair, myofibroblasts undergo apoptosis once the healing process is finished. In IPF, this does not happen in fibroblast foci and myofibroblasts stay activated resulting in an ongoing remodeling process and excessive deposition of ECM (Figure 1.6). The underlying mechanism is not completely understood yet but might involve persistent profibrotic TGF-β signaling by AECs, macrophages and myofibroblasts (Fernandez & Eickelberg, 2012a, 2012b).

1.1.4 Treatment strategies in IPF

Due to the devastating character of IPF, its fast progression and a general late diagnosis, therapeutic interventions are very limited. Despite extensive research efforts during the past decades medical science was not able to establish an effective curative pharmacological therapy for the treatment of IPF. Although pirfenidone was approved for the treatment of IPF in Japan (2008), Europe (2011) and USA (2014), the official guidelines for diagnosis and management of IPF of the American Thoracic Society (ATS), the European Respiratory Society (ERS), the Japanese Respiratory Society (JRS) and the Latin America Thoracic Society (ALAT) do not in general recommend any specific pharmacologic therapy but rather suggest to apply non-pharmacological interventions (Raghu et al., 2011).

1.1.4.1 Pharmacological therapies and drug candidates

Just recently, a phase III trial to study therapeutic effects of pirfenidone, an orally available pyridine derivative, was completed successfully. Compared to placebo, treatment with pirfenidone significantly reduced disease progression in IPF patients and was associated with decreased mortality (King et al., 2014). Pirfenidone provides pleiotropic antifibrotic, anti-inflammatory, and antioxidative effects, but the underlying mechanism of action is not well understood. *In vivo* and *in vitro* studies with pirfenidone suggest downregulation of profibrotic cytokines, chemokines and growth factors (especially TGF-β) and inhibition of myofibroblast differentiation together with reduced synthesis of ECM components (Ahluwalia et al., 2014).

Common treatment strategies for IPF patients so far include antioxidant therapy (N-acetylcystein), immunomodulators (corticosteroids, cyclosporine A, azathioprine, cyclophosphamide, interferon-γ 1b), agents that antagonize myodifferentiation (pirfenidone, nintedanib) and anticoagulants (warfarin, heparin). However, none of these therapies provides strong evidence for a better outcome in IPF as clinical trials often show controversial results, but they seem to be beneficial in individual cases (Ahluwalia et al., 2014; Raghu et al., 2011). To date, several promising drug candidates that act on various different profibrotic processes in IPF

are in phase II and III clinical trials. Table 1.1 and Figure 1.7 summarize these candidates.

Table 1.1. Ongoing and recently completed phase II/III trials in IPF (Ahluwalia et al., 2014)~modified

Agent	Mechanism of action	Study phase
Tralokinumab	IL-13 monoclonal antibody	Phase II
Lebrikizumab	IL-13 monoclonal antibody	Phase II
Pirfenidone	Antifibrotic, antiinflammatory, antioxidant	Phase III (completed)
Nintedanib	Tyrosine kinase inhibitor targeting VEGFR, FGFR, PDGFR	Phase III (completed)
STX-100	Integrin $\alpha v \beta 6$ monoclonal antibody	Phase II
FG-3019	CTGF inhibitor	Phase II
BMS-986020	Lysophosphatidic acid receptor antagonist	Phase II
Simtuzumab	LOXL2 monoclonal antibody	Phase II
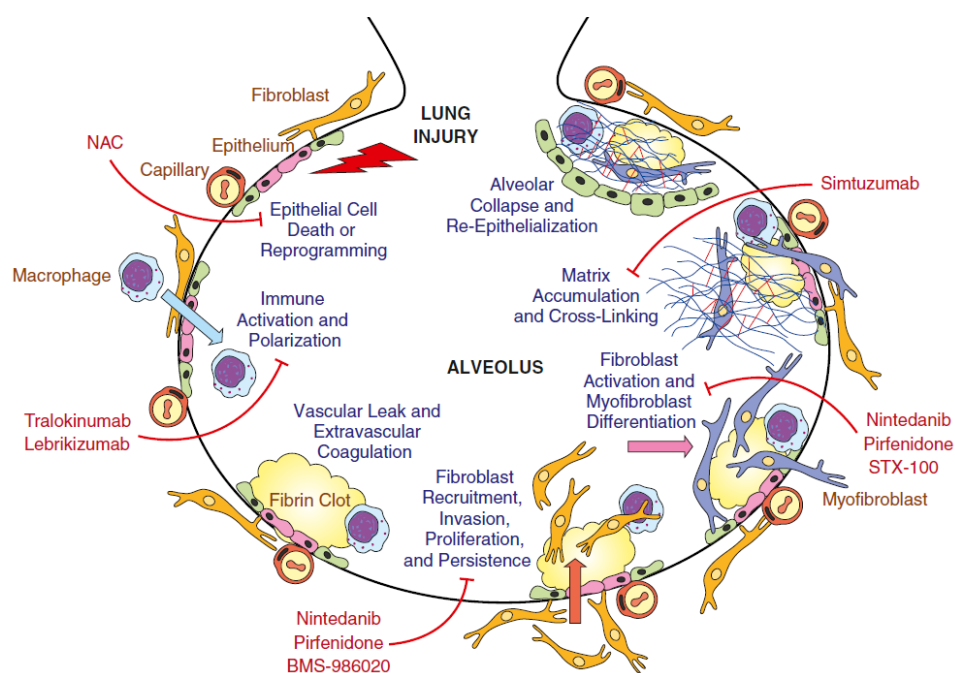
Figure 1.7. Promising investigational therapies for IPF and their pharmacologic interaction
Several promising drug candidates with different mechanisms of action are in ongoing and recently completed clinical studies for therapeutic intervention of IPF. (Taken from Ahluwalia et al., 2014)

1.1.4.2   Non-pharmacological interventions

Non-pharmacological treatment options have been shown to provide beneficial effects in IPF patients. The official guidelines of the ATS, ERS, JRS and ALAT recommend long-term oxygen therapy for IPF patients with resting hypoxemia and suggest pulmonary rehabilitation, involving aerobic training, strength and flexibility training, educational lectures, nutritional interventions and psychological support. Despite all efforts to establish curative treatment strategies, the most

effective therapy to prolong survival of IPF patients to date still remains lung transplantation (Rafii et al., 2013; Raghu et al., 2011).

1.1.5   The bleomycin mouse model for pulmonary fibrosis

Several animal models have been established to study the pathomechanism or therapeutic interventions of pulmonary fibrosis. Pulmonary fibrosis in mice can be induced by various stimuli including exposure to silica, asbestos, fluorescein isothiocyanate (FITC), overexpression of TGF-β or radiation (Moore et al., 2013). The most commonly used and best studied animal model for pulmonary fibrosis is the bleomycin mouse model. Bleomycin, a cytotoxic glycopeptide antibiotic, is a well-known drug in cancer therapy. In tumor cells, it causes DNA double strand breaks thereby inducing apoptosis. One severe side effect of bleomycin in cancer patients is the development of pulmonary fibrosis. This observation led to the establishment of the bleomycin animal model for the investigation of pulmonary fibrosis (Mouratis & Aidinis, 2011).

The most common application route in the murine model is a single intratracheal instillation of bleomycin into the lungs. Bleomycin initially causes acute lung injury by epithelial cell damage and inflammation, followed by fibrotic tissue remodeling in a very short time of about 7 to 9 days after instillation. During the initial inflammatory phase (until day 7 post-bleomycin) proinflammatory cytokines such as IL-1β, TNFα, IL-6 or interferon-γ (INFγ) are elevated (Moeller et al., 2008). The profibrotic response peaks around day 14 with increased expression of TGF-β, collagens and fibronectin, accumulation of ECM, and fibrotic remodeling, and persists up to 28 days after bleomycin challenge (Moore et al., 2013; Mouratis & Aidinis, 2011).

However, fibrotic remodeling in the bleomycin mouse model is reversible and fibrosis resolves, depending on the mouse strain, within 56 days after bleomycin instillation. Due to the slow, irreversible, and progressive course of the disease in IPF patients, the bleomycin mouse model therefore cannot completely reflect the pathogenesis of this disease. Also, some characteristic hallmarks of IPF such as fibroblast foci are missing in bleomycin-induced pulmonary fibrosis (Moeller et al., 2008; Moore et al., 2013; Mouratis & Aidinis, 2011). Despite these limitations, the bleomycin mouse model remains the best characterized and probably most convenient model for studying the pathogenesis of IPF and testing of novel antifibrotic therapies, so far (Mouratis & Aidinis, 2011).

1.2   The Ubiquitin-Proteasome System

The ubiquitin-proteasome system (UPS) is the major degradation pathway for intracellular proteins. Substrate recognition and degradation within the ubiquitin-proteasome system is highly controlled and therefore guarantees a specific regulation of protein levels in numerous cellular processes. The key protease within the ubiquitin-proteasome system is the proteasome, a multicatalytic enzyme complex of over 2.5 megadaltons (Ciechanover, 2013; Finley, 2009).

1.2.1   The proteasome

The proteasome consists of a barrel-like structured catalytic core particle (CP), also named 20S proteasome, and one or two 19S regulatory particles (RP). To avoid uncontrolled proteolysis of cellular proteins, the proteasome provides a unique secure arrangement to only allow highly specific degradation. Protein cleavage occurs inside the catalytic core of the 20S particle, which is closed in its inactive state by the obstacle of a narrow entry pore. Opening and therefore activation of the CP occurs when the 19S RP associates with the 20S CP in an ATP-dependent manner (Finley, 2009; Groll et al., 2000). Activation of the proteasome is not exclusively implemented by the 19S RP, which can bind to one or both ends of the 20S CP to form 26S or 30S proteasomes, respectively. There are two more types of proteasome activators (PA), the 11S complexes PA28α/β and PA28γ, and PA200, which are able to open the channel to the catalytic core independent of ATP. However, the 19S RP is the only activator, which is able to recognize and process K48-polyubiquitinated proteins, thereby assuring highly specific protein degradation (Kish-Trier & Hill, 2013; Meiners et al., 2014; Stadtmueller & Hill, 2011).

1.2.1.1   The 20S catalytic particle

The 20S CP is symmetrically composed of two outer rings, which are formed by seven α-subunits (α1-7) in each case, that enclose two inner rings of seven β-subunits (β1-7), respectively (Groll et al., 1997).

Assembly of the CP starts with the formation of the heptameric α-ring, which then serves as a template for the β-ring, resulting in half 20S proteasomes still missing β7. Two so-called half-mers (-β7) then dimerize to active 20S proteasomes by incorporation of β7 (Murata et al., 2009). 20S assembly is tightly regulated and assisted by a variety of chaperones: Proteasome assembling chaperone 1 (PAC1)-PAC2 and PAC3-PAC4 heterodimers assist to form the α-ring and to avoid uncontrolled aggregation of α-subunits. Ubiquitin-mediated proteolysis 1 (UMP1) is required for initial β2 association on the α-ring. Further intramolecular chaperones, which are propeptides of β1, β2, β5, β6, and β7 mediate orderly incorporation of the β-subunits into the

ring complex and finally promote dimerization of the half-mers (Gu & Enenkel, 2014; Murata et al., 2009).

Three of the seven β-subunits, β1, β2, and β5, contain proteolytic activity and cleave proteins after different amino acids into oligomeric peptides of 3-28 amino acids length. The β1 subunit prefers cleavage on the C-terminal side of acidic residues, β2 cleaves after basic residues and β5 after hydrophobic residues. According to their cleavage site-specificity, they are classified as chymotrypsin-like (CT-L), trypsin-like (T-L), and caspase-like (C-L) active sites (Figure 1.8) (Borissenko & Groll, 2007; Groll et al., 2000).
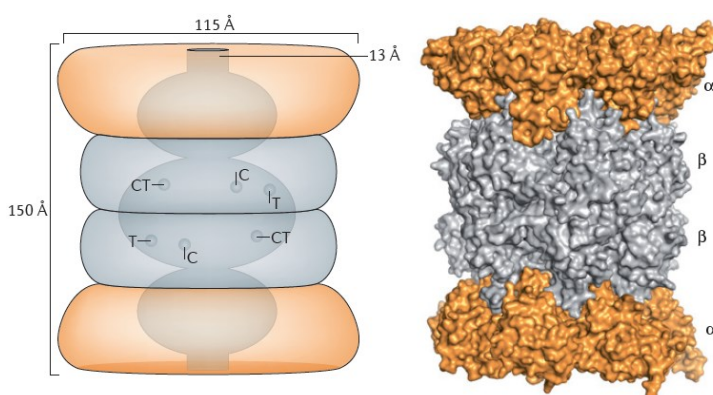
Figure 1.8. Architecture of the 20S proteasome complex
Schematic of the 20S CP (left) provides insight into the channel and the arrangement of the catalytic sites. Each site, namely caspase-like (C), trypsin-like (T) and chymotrypsin-like (CT) active site, is present twice per complex. They reside within the β-rings. The three-dimensional structure of the 20S CP (right) shows the arrangement of the α- (orange) and β-rings (grey). (Taken from Makino et al., 2013)

Each active site contains an N-terminal threonine which provides the catalytic nucleophile and the primary proton acceptor, responsible for hydrolysis of peptide bonds. In a first step the substrate peptide forms an ester bond with the N-terminal threonine which is then hydrolysed by incorporation of a nucleophilic water molecule into the product. Cleavage site specificity is provided by specificity pockets which stabilize the substrate and orientate it from its N- to its C-terminus (Borissenko & Groll, 2007).

The active sites are safely situated inside the catalytic core particle, which is closed in its inactive state to avoid uncontrolled protein degradation, as described above. Hereby, the outer α-rings block the entrance to the proteolytic chamber in its closed conformation. The 19S RP promotes gate opening and therefore activation of the CP by binding to specific sites of the α-subunits, which leads to a rearrangement of the α-rings resulting in channel-opening and

activation of the CP (Bhattacharyya et al., 2014; Finley, 2009; Groll et al., 2000). Next to the 19S RP, the other PAs PA28α/β, PA28γ, and PA200 are able to open the CP in an ATP-independent manner. Their role in proteasomal degradation is not completely understood yet, but might involve specific degradation of certain proteins or the formation of hybrid proteasomes, when assembled with 26S proteasomes, to modulate protein degradation (Meiners et al., 2014).

1.2.1.2   *The 19S regulatory particle*

The 19S regulatory particle, also known as PA700, consists of at least 18 subunits which form a lid complex, containing not less than eight regulatory particle non-ATPase (Rpn) proteins (Rpn3, Rpn5-9, Rpn11, Rpn12) with Rpn11 as deubiquitinating enzyme (DUB) and a base, consisting of six regulatory particle triple A ATPases (Rpt) (Rpt1-6) and four non-ATPase proteins (Rpn1, Rpn2, Rpn10 and Rpn13), whereas Rpn10 and Rpn13 serve as ubiquitin receptors (Gu & Enenkel, 2014; Lander et al., 2012). The RP enables binding of polyubiquitinated proteins, recycling of ubiquitin via deubiquitination, and ATP-dependent unfolding of protein chains to funnel them into the 20S catalytic core (Figure 1.9) (Lander et al., 2013; C.-W. Liu & Jacobson, 2013; Tomko & Hochstrasser, 2013).

Assembly of the 19S RP is a very complex process and not completely understood yet. Lid and base of the 19S RP might assemble independently from each other, but also assembly of the base on top of the 20S CP, thereby using it as a template, has been proposed (Gu & Enenkel, 2014). The six homologous ATPase subunits of the base (Rpt1-6) assemble together with Rpn1 and Rpn2 into a hexameric ring. This process is guided by RP base-dedicated chaperones S5b, p27, p28, and Rpn14, which interact with one or two base-subunits. Further, Rpn14 and p28 seem to be involved in the docking process of the base to the 20S CP. Once the base is assembled, association of lid and base occur by an unknown mechanism, which might involve S5a/Rpn10 (Besche et al., 2009).

Only little is known about the assembly of the lid. Data from yeast indicate the formation of two subunit-agglomerates consisting of Rpn5, Rpn6, Rpn8, Rpn9 and Rpn11 or Rpn3, Rpn7, Rpn12 and Rpn15. In this model Rpn3 and Rpn5 form a connection (Murata et al., 2009; Sharon et al., 2006). Furthermore, the molecular chaperone Hsp90 is proposed to assist in assembly and maintenance of the lid (Murata et al., 2009).

In order to form an effectively operating 26S proteasome, the 19S RP somehow has to be attached to the 20S CP. This mechanism is barely understood, but there are some factors known to stabilize this interaction: Association of the 19S RP with the 20S CP results in

plugging in the C-terminal residues of the two base-ATPase subunits of Rpt2 and Rpt5 into defined pockets of the α-ring of the 20S CP. This interaction requires ATP binding, therefore the intracellular ATP-levels might be a possible key player in 26S formation (Smith et al., 2007). Furthermore, ATP is necessary for appropriate 26S functions such as deubiquitination and unfolding of polyubiquitinated proteins and hydrolysis (Braun et al., 1999; C.-W. Liu et al., 2006). It has also been shown that intracellular ATP levels influence proteasome activity in both directions by a yet unknown mechanism (Huang et al., 2010).
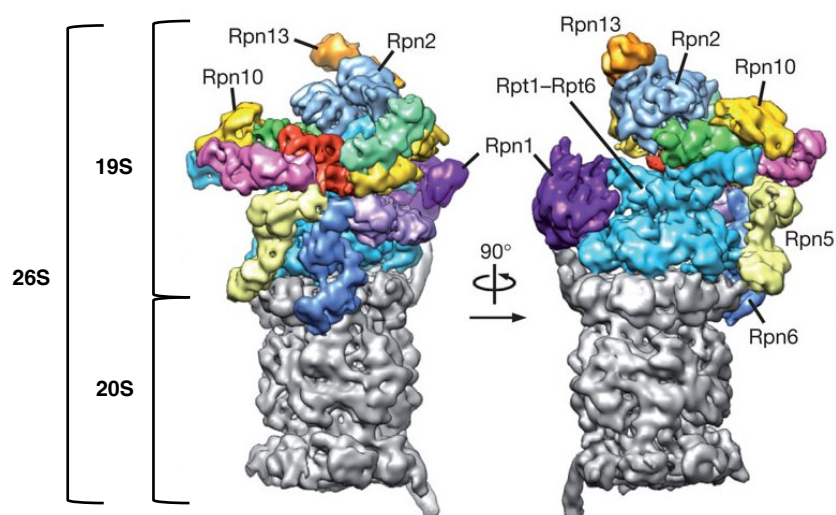
Figure 1.9. Three-dimensional reconstruction of the 26S proteasome
The subnanometre cryoelectron microscopy reconstruction of the 26S proteasome is shown in two views. Subunits of the 19S RP are depicted in different colours building a 26S complex with the 20S CP (grey). (Taken from Lander et al., 2012)~modified

Upregulation of proteasome activity by increased assembly of 26S and 30S proteasomes has recently been described for embryonic stem (ES) cells by Vilchez et al. In this study, ES cells provided high proteasome activities, which decreased upon differentiation into neural progenitor cells (NPCs) or further differentiation into neurons. Increased proteasome activities were mediated by formation of 26S and 30S proteasomes leading to a higher substrate turnover in these cells. In parallel, the 19S lid subunit Rpn6 was highly expressed in ES cells in comparison to NPCs and identified as a rate limiting factor that promotes formation of highly active 26S and 30S proteasomes (Vilchez, Boyer, et al., 2012). In addition, Pathare et al. showed by crystal- and cryostructure analysis that Rpn6 closely interacts with 19S ATPase Rpt6 and the α2 subunit of the 20S CP within the 26S complex. Here, Rpn6 acts like a clamp holding together the

otherwise weakly stabilized 26S proteasome (Figure 1.9) (Pathare et al., 2012). These structural findings are supported by data from yeast that show impaired formation of 26S proteasomes upon Rpn6 depletion (Isono et al., 2005; Santamaria et al., 2003).

Taking into account the complexity of 19S assembly and association with 20S CP to form 26S proteasomes, this proposes a strong overall regulation on different levels such as presence of chaperones or possible rate limiting subunits as shown for Rpn6. However, up to now there is only limited knowledge about the factors which might influence 19S assembly and its association with the 20S CP to balance protein degradation to an appropriate level adjusted to the need of the cell.

1.2.2   *Protein degradation by the ubiquitin-proteasome system*

The ubiquitin-proteasome system is responsible for the controlled degradation of about 90% of all intracellular proteins, thereby representing the main protein destruction machinery of the cell (Meiners et al., 2014). To avoid uncontrolled protein degradation, their disposal via the ubiquitin-proteasome system is a highly regulated process.

For degradation, proteins are specifically recognized by E3 ubiquitin ligases and covalently tagged with polyubiquitin chains that are linked via the lysine 48 (K48) residue of the ubiquitin moiety as a degradation signal for the ubiquitin-proteasome system. Next to K48, ubiquitin chains can also be linked via other lysines such as K11 or K63 to regulate cell signaling or in case of K63 to promote degradation via autophagy. Also attachement of monoubiqutins is possible. However, there are a variety of different ubiquitin chain modifications but only little is known about their function within the cell (Komander & Rape, 2012).

Ubiquitination is initiated by linkage of one ubiquitin molecule to an ubiquitin-activating enzyme (E1) and further transfer to an ubiquitin-conjugating enzyme (E2). The E3 ligase finally links the ubiquitin to the protein. E2 enzymes promote further linkage of ubiquitin molecules, thereby forming a polyubiquitin chain on the protein (Ciechanover, 2015).

Disposable proteins are recognized via their polyubiquitin tags by the non-ATPase subunits Rpn10 and Rpn13 of the 19S lid complex. The deubiquitinase Rpn11 then cleaves off the ubiquitin chain in an ATP dependent manner and the protein substrate is unfolded and carried into the catalytic core to undergo degradation into oligomeric peptides (Figure 1.10) (Lander et al., 2013).

Proteasomes are present in the cytoplasm and nucleus, regulating levels of proteins involved in numerous cellular processes such as cell cycle control (Benanti, 2012; Teixeira & Reed, 2013),

MHC class I antigen processing (Sijts & Kloetzel, 2011), protein quality control (Meiners & Eickelberg, 2012), gene transcription (Geng et al., 2012), or differentiation (Cenci, 2012). Also the TGF-β pathway is highly regulated by the ubiquitin-proteasome system. During TGF-β signaling, proteasomes adjust protein levels of several factors by controlling their degradation. Smurf E3 ligases for example ubiquitinate R-SMADs and mediate their degradation, leading to repression of TGF-β signaling whereas Arkadia, another E3 ligase, promotes ubiquitination and degradation of inhibitory proteins such as SMAD7 or SnoN leading to enhanced signaling (David et al., 2013; Imamura et al., 2013; Soond & Chantry, 2011).
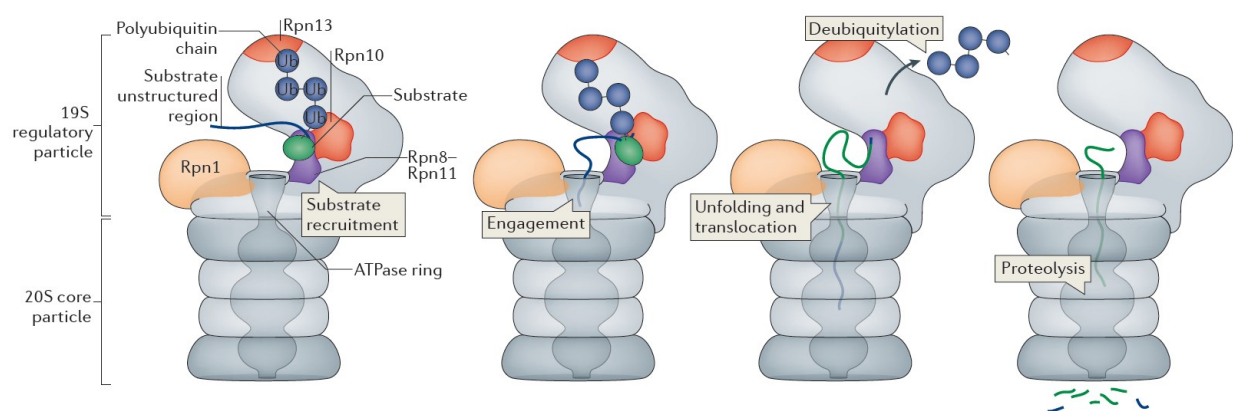
Figure 1.10. Degradation of polyubiquitinated proteins by the proteasome
Proteins, which are tagged with K48-linked ubiquitin chains are recognized by the lid of the 19S RP (Rpn10 and Rpn13), deubiquitinated (Rpn11), unfolded and carried into the catalytic core of the 20S CP. The active sites within the catalytic core promote substrate cleavage into oligomeric peptides. (Taken from Bhattacharyya et al., 2014)

1.2.3   Inhibition of the proteasome

Approval of the first proteasome inhibitor, bortezomib (BZ) (Velcade®), for the treatment of multiple myeloma by the FDA in 2003 can be regarded as a major milestone in the therapy of this disease, greatly improving response rates and survival of patients (Kane et al., 2003). Since then, a variety of compounds has been designed to covalently bind or reversibly interact with the active sites of the 20S CP, thereby inhibiting the proteasome (Beck et al., 2012; Finley, 2009). Next to these conventional inhibitors, new concepts are arising to interfere with protein degradation by the ubiquitin-proteasome system such as inhibition of ubiquitin E3 ligases, proteasome recognition inhibitors or inhibition of 19S deubiquitinases by small molecules (Dou & Zonder, 2014).

1.2.3.1   Inhibitors of the 20S core particle

Inhibitors of the 20S CP are designed to bind to the N-terminal threonine residues inside the catalytic core that form the active sites of the β1, β2 and β5 subunits. Most of them are peptide-like compounds that have a similar binding mode to the N-terminal threonine as natural substrates. Active site-specificity can be achieved by modification of their side chains. Covalently binding inhibitors show a common principle, combining a peptide scaffold with an electrophilic anchor such as aldehydes, vinyl sulfones, boronates, α,β-epoxyketones, α-ketoaldehydes and β-lactones (Beck et al., 2012; Huber & Groll, 2012).

In the past years, a variety of second generation proteasome inhibitors have been developed to provide higher selectivity for specific active sites (Dick & Fleming, 2010). Just recently, the chymotrypsin-like site-specific α,β-epoxyketone inhibitor carfilzomib (Krypolis®) has been FDA-approved for the treatment of multiple myeloma (Herndon et al., 2013). In contrast to boronate inhibitors, like bortezomib, which form a reversible tetrahedral transition state with the nucleophilic Thr1O$^\gamma$ of the N-terminal threonine with high binding specificity to the chymotrypsin-like and caspase-like active sites (Beck et al., 2012; Huber & Groll, 2012), α,β-epoxyketone inhibitors irreversibly and selectively bind to the chymotrypsin-like active site by formation of a morpholino structure with the N-terminal threonine within the catalytic core particle (Herndon et al., 2013) (Table 1.2).
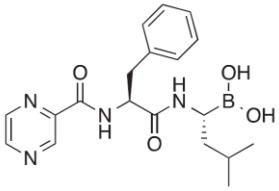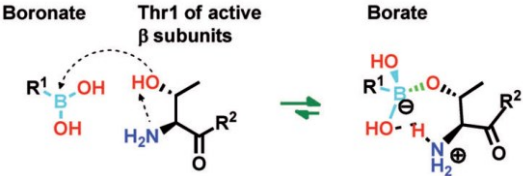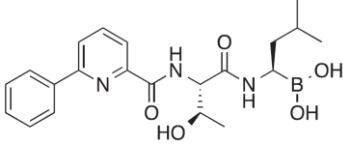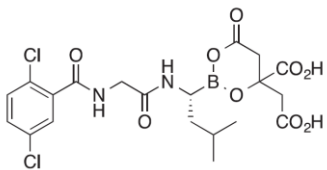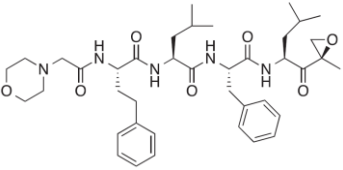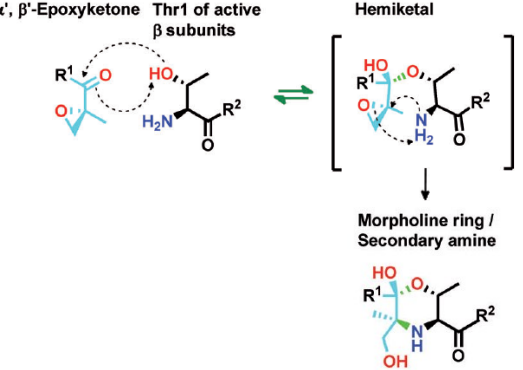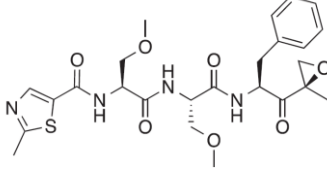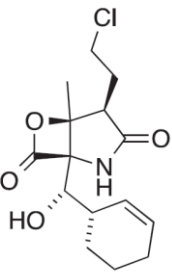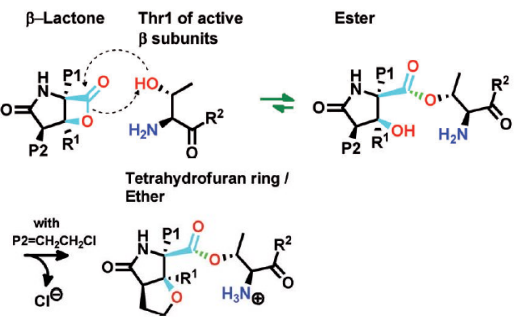
Next to the FDA-approved inhibitors bortezomib and carfilzomib, a variety of promising drug candidates are currently under clinical investigation for treatment of multiple myeloma, solid tumors, lymphoma or leukemia (Dou & Zonder, 2014) and are summarized in Table 1.2.

Oprozomib (OZ) (former ONX0912) is a novel modified derivate of carfilzomib, bearing the same epoxyketone pharmacophore. Oprozomib is the first orally available proteasome inhibitor (Chauhan et al., 2010; Roccaro et al., 2010) and currently in clinical phase II for the treatment of multiple myeloma (Teicher & Tomaszewski, 2015).

Other promising candidates are ixazomib, an orally available boronic ester prodrug, the boronic ester delanzomib and the β-lactone marizomib (Beck et al., 2012; Dou & Zonder, 2014; Kubiczkova et al., 2014). Like bortezomib, delanzomib and the prodrug ixazomib citrate, which is hydrolyzed in aqueous solution to its active form, exhibit high affinity to the chymotrypsin-like active site but also bind to the caspase-like site at higher concentrations. Marizomib, also known as salinosporine A, a secondary metabolite of the obligate marine actinomycetes bacterium *Salinispora tropica*, is the only non-peptidic 20S inhibitor in clinical trial so far (Beck et al., 2012). It binds irreversibly to all three active sites of the catalytic core. Hereby, the Thr1O$^\gamma$ of the

N-terminal threonine attacks the carbonyl carbon atom of marizomib and opens its β-lactone ring resulting in a hydroxyl group and an acyl-enzyme ester (Huber & Groll, 2012).

Table 1.2. Bortezomib and second generation inhibitors (Dou & Zonder, 2014; Huber & Groll, 2012)~modified

Proteasome Inhibitor	Chemical Structure	Inhibition Profile	Structural Class and Reaction Mechanism
Bortezomib		Reversible β5>β1	Boronate
Delanzomib		Reversible β5>β1	
Ixazomib citrate		Reversible β5>β1	
Carfilzomib		Irreversible β5	Epoxyketone
Oprozomib		Irreversible β5	
Marizomib		Irreversible β5>β2>β1	β-lactone

1.2.3.2   *Novel inhibitors of the ubiquitin-proteasome system*

Next to the 20S CP, the ubiquitin-proteasome system provides a variety of other potential druggable targets to interfere with protein degradation. Several compounds, targeting the ubiquitin-proteasome system via E1, E2 and E3 ligases or interfering with the 19S RP are currently under investigation:

E3 ligases play a crucial role in controlled protein degradation, as they specifically ubiquitinate proteins to promote their degradation by the proteasome. Inhibition of specific E3 ligases therefore leads to accumulation of their substrates (Micel et al., 2013). Several E3 ligase inhibitors are currently in clinical trial including inhibitors for HDM2, causing accumulation of its target, the tumor suppressor protein p53 (Micel et al., 2013; Weathington & Mallampalli, 2014) or inhibitors for the inhibitors of apoptosis protein (IAP), resulting in enhancement of proapoptotic proteins (Beug et al., 2012). Just recently, a novel mechanistic activity as inhibitor of the E3 ligase Cereblon has been investigated for the immunomodulatory agent thalidomide and its derivatives lenalidomide and pomalidomide (Chamberlain et al., 2014).

Other possibilities to target proteasomal protein degradation include inhibition of the ubiquitin-ubiquitin interface of K48-linked chains by ubistatins, which has been shown to disrupt substrate recognition by the 19S RP resulting in cell cycle arrest (Verma et al., 2004). Furthermore, inhibition of deubiquitinases of the 19S RP led to accumulation of polyubiquitinated proteins and induction of G_2/M cell cycle arrest (D'Arcy et al., 2011).

A novel concept of proteasome inhibition arises in the possibility to target protein-protein interactions within the complex, thereby destabilizing subunit interactions or impairing assembly as for example shown for rapamycin, which prevents attachment of the 19S to the 20S proteasome (Gaczynska & Osmulski, 2015).

1.2.3.3   *Cellular effects of proteasome inhibition*

Due to their cytotoxic effects, proteasome inhibitors of the 20S catalytic core have mainly been developed as powerful agents for the treatment of cancer and revolutionized the therapy of multiple myeloma, a hematological malignancy (Teicher & Tomaszewski, 2015). As the proteasome plays a fundamental role in cellular homeostasis, biological effects of proteasome inhibition are multifactorial. However, for bortezomib, some key signaling pathways have been identified to mainly contribute to its mechanism of action, which may also be transferable to other catalytic core inhibitors of the proteasome.

The transcription factor nuclear factor κB (NF-κB) is involved in numerous tumor-related processes such as suppression of apoptosis, angiogenesis, cell proliferation and migration. In the cytoplasm, it is bound to its inhibitor I-κB, preventing its translocation to the nucleus. Activation of NF-κB occurs, when I-κB is phosphorylated as a trigger for polyubiquitination and subsequent degradation by the 26S proteasome. Inhibition of the proteasome in various cancer cells therefore prevents activation of NF-κB leading to downregulation of genes related to angiogenesis, survival, and growth while apoptosis is upregulated (Hideshima et al., 2001).

Furthermore, proteasome inhibition has been shown to activate several apoptotic pathways via accumulation of proapoptotic factors like p53, Bcl-2-associated X protein (Bax) and NOXA and downregulation of antiapoptotic mediators such as B-cell lymphoma 2 (Bcl-2) and IAP. This might contribute to cytotoxic effects of proteasome inhibitor in cancer cells (Frankland-Searby & Bhaumik, 2012).

Cell cycle progression is tightly controlled by cyclins and cyclin dependent kinases (CDKs), which are also substrates of the proteasome (Benanti, 2012). Proteasome inhibition therefore has been shown to induce accumulation of cyclins and CDKs, leading to disruption of cell cyle progression (Frankland-Searby & Bhaumik, 2012; Kubiczkova et al., 2014).

Next to these cytotoxic events of proteasome inhibition on cancer cells, low non-toxic doses of proteasome inhibitors also have been shown to provide protective effects in several organs. This includes antiinflammatory, antiproliferative and antifibrotic actions, which have been explained by interference of proteasome inhibition with the corresponding pathways such as NF-κB, as described above, or TGF-β (Meiners et al., 2014; Meiners, Ludwig, et al., 2008). Here, it has been shown that non-toxic proteasome inhibition counteracted TGF-β mediated SMAD activation by upregulation of the transcriptional repressor SnoN (also SNO) (Sakairi et al., 2011) or by upregulation of the nuclear hormone receptor peroxisome proliferator-activated receptor γ (PPARγ), a suppressor of SMAD-mediated transcription (Mutlu et al., 2012).

1.2.3.4   Proteasome inhibitors in pulmonary fibrosis

Inhibitors of the 20S catalytic core of the proteasome have been shown to provide antifibrotic effects in several organs including heart, kidney, skin, and lung (Fineschi et al., 2006; Meiners et al., 2004; Mutlu et al., 2012; Sakairi et al., 2011).

For the lung, there are conflicting data regarding the antifibrotic effects of proteasome inhibitors in the bleomycin model of lung fibrosis: While Fineschi et al. reported that the daily application of the clinically approved proteasome inhibitor bortezomib, starting one day after bleomycin

instillation, did not show any protective effects (Fineschi et al., 2008), Mutlu et al. observed that bortezomib promoted normal repair and prevented lung fibrosis until day 21 post-bleomycin when given at modest doses only at day 7 and 14 after the initial bleomycin lung damage. They also reported that application of both drugs, bortezomib and bleomycin, at the same time, resulted in excess mortality in these mice (Mutlu et al., 2012). These data indicate that there is only a very small therapeutic window for proteasome inhibitors of the CP which has also been reported for other disease applications (Di Napoli & McLaughlin, 2005; Meiners, Ludwig, et al., 2008).

1.3   Objectives

The ubiquitin-proteasome system plays a central role to control protein levels in the cell by degradation of old, misfolded, or unneeded proteins to maintain homeostasis. It is involved in virtually all cellular functions and its dysregulation has been associated with various lung diseases including pulmonary fibrosis (Meiners et al., 2014; Weiss et al., 2010). Therefore, the overall goal of this study was to provide a better understanding of proteasomal regulation in IPF and to evaluate a novel therapeutic intervention in pulmonary fibrosis, by local application of the highly specific, second generation proteasome inhibitor oprozomib.

To achieve this goal, aims were defined as follows:

1. Analysis of proteasome activity during myofibroblasts differentiation and fibrotic remodeling *in vitro* and *in vivo*.

2. Identification and characterization of factors, which modulate proteasome activity during myofibroblasts differentiation.

3. Evaluation of specificity, toxicity and antifibrotic effects of oprozomib *in vitro*.

4. *In vivo* evaluation of therapeutic potential of oprozomib after local pulmonary application.

For these purposes, myofibroblast differentiation was induced by TGF-β, the bleomycin mouse model for pulmonary fibrosis was applied and lung tissue samples were analyzed. Protein lysates of cells, mouse, and human lung tissues were assayed for their proteasome content on mRNA and protein levels and proteasome activity was examined. Intracellular proteasome function was further characterized by siRNA-mediated gene knockdown and proteasome inhibition using specific inhibitors. Animal experiments were performed to investigate antifibrotic effects of a novel proteasome inhibitor after local intratracheal instillation into the lung or oral gavage.

Collectively, this study should provide a better insight into proteasomal regulation during lung fibrosis and address the ubiquitin-proteasome system as a novel target for antifibrotic therapies in IPF.

2 MATERIALS AND METHODS

2.1 Materials

2.1.1 Antibodies

Table 2.1. Primary antibodies

Antigen	Host	Application (Dilution)	Manufacturer
Anti-Collagen I (600401103)	Rabbit	WB (1:5000), IF (1:200)	Rockland, Gilbertsville, USA
Anti-Cyclin D1 (2978)	Rabbit	WB (1:1000)	Cell Signaling, Danvers, USA
Anti-Fibronectin (sc-9068)	Rabbit	WB (1:1000)	Santa Cruz, Dallas, USA
Anti-KRT5 (ab75869)	Rabbit	IHC (1:200)	Abcam, Cambridge, UK
Anti-PSMD11 (Rpn6) (NBP1-46191)	Rabbit	WB, NG (1:2000), IHC (1:75), IF (1:200)	Novus Biologicals, Littleton, USA
Anti-TBP1 (Rpt5) (A303-538A)	Rabbit	WB, NG (1:5000)	Biomol, Hamburg, Germany
Anti-TTF1 (ab76013)	Rabbit	IHC (1:75)	Abcam, Cambridge, UK
Anti-Ubi-K48 (05-1307)	Rabbit	WB (1:3000), IHC (1:75)	Millipore, Billerica, USA
Anti-αSMA (A5288)	Mouse	WB, NG (1:1000), IF (1:1000)	Sigma-Aldrich, St. Louis, USA
Anti-αSMA (ab5694)	Rabbit	IHC (1:200)	Abcam, Cambridge, UK
Anti-β1 (20S) (sc-67345)	Rabbit	NG (1:250)	Santa Cruz, Dallas, USA
Anti-β-actin-peroxidase (A3854)	Mouse	WB (1:50000)	Sigma-Aldrich, St. Louis, USA
Anti-20S α3 (ab119419)	Mouse	WB (1:1000)	Abcam, Cambridge, UK
Anti-20S α1-7 (ab22674)	Mouse	WB, NG (1:1000)	Abcam, Cambridge, UK

Western blot (WB); Native gel (NG); Immunohistochemistry (IHC); Immunofluorescence (IF); Primary antibodies for WB were diluted in Roti-Block and for IF in Roti-Immunoblock.

Table 2.2. Secondary antibodies

Antigen	Host	Application	Manufacturer
Horse anti-mouse IgG HRP-linked (7076S)	Horse	WB, NG (1:50000)	Cell Signaling, Danvers, USA
Goat anti-rabbit IgG HRP-linked (7074S)	Goat	WB, NG (1:50000)	Cell Signaling, Danvers, USA
Alexa Fluor 488 goat anti-mouse IgG (A11001)	Goat	IF (1:250)	Life Technologies, Carlsbad, USA
Alexa Fluor 488 goat anti-rabbit IgG (A11008)	Goat	IF (1:250)	Abcam, Cambridge, UK

Western blot (WB); Native gel (NG); Immunofluorescence (IF)

2.1.2 Buffers, solutions and chemicals

Table 2.3. Buffers and solutions for protein extraction from cells and tissue

Buffer	Reagent	Concentration	Manufacturer
Hypoosmotic lysis solution: (WB, NG)	cOmplete® protease inhibitor (11697498001)	1x	Roche Diagnostics, Mannheim, Germany
	PhosSTOP® phosphatase inhibitor (04906845001)	1x	Roche Diagnostics, Mannheim, Germany
RIPA extraction buffer: (WB)	Tris/HCl pH 7.5	50 mM	AppliChem, Darmstadt, Germany
	NaCl	150 mM	AppliChem, Darmstadt, Germany
	Nonident P40	1% (v/v)	AppliChem, Darmstadt, Germany
	Sodiumdeoxycholate	1% (w/v)	Carl Roth, Karlsruhe, Germany
	SDS	0.1% (w/v)	AppliChem, Darmstadt, Germany
	cOmplete® protease inhibitor	1x	Roche Diagnostics, Mannheim, Germany
TSDG buffer: (WB, NG)	Tris/HCl pH 7.0	50 mM	AppliChem, Darmstadt, Germany
	NaCl	10 mM	AppliChem, Darmstadt, Germany
	$MgCl_2$	1.1 mM	AppliChem, Darmstadt, Germany
	EDTA	0.1 mM	AppliChem, Darmstadt, Germany
	NaN_3	1 mM	AppliChem, Darmstadt, Germany
	DTT	1 mM	AppliChem, Darmstadt, Germany
	ATP	2 mM	Roche Diagnostics, Mannheim, Germany
	Glycerol 87%	10% (v/v)	AppliChem, Darmstadt, Germany
	cOmplete® protease inhibitor	1x	Roche Diagnostics, Mannheim, Germany

Western blot (WB); Native gel (NG); All buffers and solutions were prepared with Milli-Q water.

Table 2.4. Buffers and solutions for Native-PAGE (Native polyacrylamide gel electrophoresis)

Buffer	Reagent	Concentration	Manufacturer
5x Loading buffer:	Tris/HCl pH 7.5	250 mM	AppliChem, Darmstadt, Germany
	Glycerol 87%	50% (v/v)	AppliChem, Darmstadt, Germany
	Bromphenol blue	0.01% (w/v)	AppliChem, Darmstadt, Germany
Native-PAGE resolving gel (10%):	Tris/HCl pH 8.3	90 mM	AppliChem, Darmstadt, Germany
	Boric acid	1.6 mM	AppliChem, Darmstadt, Germany
	EDTA	0.08 mM	AppliChem, Darmstadt, Germany
	Acrylamide 30%	10% (v/v)	Carl Roth, Karlsruhe, Germany
	APS	0.125% (w/v)	AppliChem, Darmstadt, Germany
	TEMED	0.15% (v/v)	AppliChem, Darmstadt, Germany
Native-PAGE stacking gel (3.5%):	Tris/HCl pH 6.8	125 mM	AppliChem, Darmstadt, Germany
	Acrylamide 30%	3.5% (v/v)	Carl Roth, Karlsruhe, Germany
	APS	0.125% (w/v)	AppliChem, Darmstadt, Germany
	TEMED	0.3 % (v/v)	AppliChem, Darmstadt, Germany

Native-PAGE running buffer (TBE):	Tris/HCl pH 8.3	89 mM	AppliChem, Darmstadt, Germany
	Boric acid	89 mM	AppliChem, Darmstadt, Germany
	EDTA	2 mM	AppliChem, Darmstadt, Germany
	DTT	0.5 mM	AppliChem, Darmstadt, Germany
	ATP	0.5 mM	Roche Diagnostics, Mannheim, Germany
	$MgCl_2$	2 mM	AppliChem, Darmstadt, Germany
Proteasome activity reaction buffer:	Tris pH 7.5	50 mM	AppliChem, Darmstadt, Germany
	SLLVY-AMC (I-1395)	50 mM	Bachem, Bubendorf, Switzerland
	$MgCl_2$	10 mM	AppliChem, Darmstadt, Germany
	ATP	1 mM	Roche Diagnostics, Mannheim, Germany
	DTT	0.5 mM	AppliChem, Darmstadt, Germany
Luciferase reaction buffer:	Glycylglycine pH 7.8	25 mM	Sigma-Aldrich, St. Louis, USA
	Potassium phosphate pH 7.8	15 mM	Sigma-Aldrich, St. Louis, USA
	$MgSO_4$	15 mM	Sigma-Aldrich, St. Louis, USA
	EGTA	4 mM	AppliChem, Darmstadt, Germany
	ATP	2 mM	Roche Diagnostics, Mannheim, Germany
	DTT	1 mM	AppliChem, Darmstadt, Germany
Luciferin stock:	Beetle luciferin	1 mM	Promega, Fitchburg, USA
	Glycylglycine pH 7.8	25 mM	Sigma-Aldrich, St. Louis, USA
	DTT	10 mM	AppliChem, Darmstadt, Germany
Solubilization buffer:	SDS	2% (w/v)	AppliChem, Darmstadt, Germany
	Na_2CO_3	66 mM	AppliChem, Darmstadt, Germany
	β-Mercaptoethanol	1.5% (v/v)	AppliChem, Darmstadt, Germany
Native-PAGE transfer buffer:	Tris	25 mM	AppliChem, Darmstadt, Germany
	Glycine	0.192 M	AppliChem, Darmstadt, Germany
	Methanol	10% (v/v)	AppliChem, Darmstadt, Germany
ABP labeling buffer:	MV151	0.5 µM	(Cravatt et al., 2008)
	HEPES pH 7.4	50 nM	AppliChem, Darmstadt, Germany
	KCl	100 mM	AppliChem, Darmstadt, Germany
	$MgCl_2$	10 mM	AppliChem, Darmstadt, Germany

All buffers were prepared with Milli-Q water.

Table 2.5. Buffers and solutions for SDS-PAGE (Sodium dodecyl sulfate polyacrylamide gel electrophoresis)

Buffer	Reagent	Concentration	Manufacturer
6x loading buffer (Lämmli buffer):	Tris/HCl pH 6.8	300 mM	AppliChem, Darmstadt, Germany
	Glycerol 87%	60% (v/v)	AppliChem, Darmstadt, Germany
	SDS	6% (w/v)	AppliChem, Darmstadt, Germany
	Bromphenol blue	0.01% (w/v)	AppliChem, Darmstadt, Germany
	DTT	600 mM	AppliChem, Darmstadt, Germany
SDS-PAGE resolving gel (10%):	Tris/HCl pH 8.8	375 mM	AppliChem, Darmstadt, Germany
	Acrylamide 30%	10% (v/v)	Carl Roth, Karlsruhe, Germany
	SDS	0.06% (w/v)	AppliChem, Darmstadt, Germany
	APS	0.125% (w/v)	AppliChem, Darmstadt, Germany
	TEMED	0.15% (v/v)	AppliChem, Darmstadt, Germany
SDS-PAGE stacking gel (3.6%):	Tris/HCl pH 6.8	125 mM	AppliChem, Darmstadt, Germany
	Acrylamide 30%	3.6% (v/v)	Carl Roth, Karlsruhe, Germany
	SDS	0.1% (w/v)	AppliChem, Darmstadt, Germany
	APS	0.125% (w/v)	AppliChem, Darmstadt, Germany
	TEMED	0.3 % (v/v)	AppliChem, Darmstadt, Germany
SDS-PAGE running buffer:	Tris	25 mM	AppliChem, Darmstadt, Germany
	Glycine	0.192 M	AppliChem, Darmstadt, Germany
	SDS	0.1% (w/v)	AppliChem, Darmstadt, Germany
SDS-PAGE transfer buffer:	Tris	25 mM	AppliChem, Darmstadt, Germany
	Glycine	0.192 M	AppliChem, Darmstadt, Germany
	Methanol	10% (v/v)	AppliChem, Darmstadt, Germany
PBST washing buffer:	NaCl	137 mM	AppliChem, Darmstadt, Germany
	KCl	2.7 mM	AppliChem, Darmstadt, Germany
	Na_2HPO_4	10 mM	AppliChem, Darmstadt, Germany
	KH_2PO_4	2 mM	AppliChem, Darmstadt, Germany
	Tween 20	1% (v/v)	AppliChem, Darmstadt, Germany

All buffers were prepared with Milli-Q water.

Table 2.6. Buffers and solutions IF and IHC

Buffer	Reagent	Concentration	Manufacturer
Citrate buffer pH 6.0:	Citric acid monohydrate	1.8 mM	AppliChem, Darmstadt, Germany
	Sodium citrate tribasic	8.2 mM	AppliChem, Darmstadt, Germany

All buffers and solutions were prepared with Milli-Q water.

Table 2.7. Chemicals

Product	Manufacturer
5x First Strand Buffer	Life Technologies, Carlsbad, USA
Atipamezole	Orion Pharma, Hamburg, Germany
Bleomycin	Sigma-Aldrich, St. Louis, USA
Bortezomib (Velcade®)	Millennium, Cambridge, USA
Bovine serum albumin (BSA)	AppliChem, Darmstadt, Germany
Carboxymethylecelllulose (CMC)	AppliChem, Darmstadt, Germany
Citric acid monohydrate	AppliChem, Darmstadt, Germany
DAPI staining	Sigma-Aldrich, St. Louis, USA
DTT 0.1 M	Life Technologies, Carlsbad, USA
ECL Prime Western Blotting Reagent	GE Healthcare, Cölbe, Germany
Entellan	Merck Millipore, Darmstadt, Germany
Eosin G 0.5% in water	Carl Roth, Karlsruhe, Germany
Fentanyl	Janssen-Cilag, Neuss, Germany
Flumazenil	Hexal, Holzkirchen, Germany
Fluorescent Mounting Medium	Dako, Hamburg, Germany
Giemsa Azur-Eosin_Methylenblue Solution	Merck Millipore, Darmstadt, Germany
Glo-Lysis Buffer	Promega, Fitchburg, USA
Hemalaun	Carl Roth, Karlsruhe, Germany
Isopropanol (p.A.)	AppliChem, Darmstadt, Germany
Ketamine	Bela Pharm, Vechta, Germany
Lipofectamine RNAiMAX	Life Technologies, Carlsbad, USA
May-Grünwalds Eosin-Methylenblue solution	Merck Millipore, Darmstadt, Germany
Medetomin	Orion Pharma, Hamburg, Germany
Midazolam	Roche Pharma, Mannheim, Germany
MV151 ABP	(Cravatt et al., 2008)
Naloxone	Actavis, Munich, Germany
Nucleotide mix 10 mM (dNTP's)	Promega, Fitchburg, USA
Oprozomib (ONX012)	Onyx Pharmaceuticals, South San Francisco, USA
Opti-MEM Reduced-Serum Medium	Life Technologies, Carlsbad, USA
PageBlue Protein Staining solution	Fermentas, Thermo Fisher Scientific, Waltham, USA
Phalloidin Alexa Fluor 568	Life Technologies, Carlsbad, USA
Pluronic F-127	Calbiochem, Billerica, USA
Random Hexamers 250 µM	Promega, Fitchburg, USA
Recombinant human EGF protein	R&D Systems, Minneapolis, USA
Recombinant human TGF-β1 protein	R&D Systems, Minneapolis, USA
RNAsin, RNAse inhibitor 40 U/µl	Promega, Fitchburg, USA
Rompun	Bela Pharm, Vechta, Germany
Roti-Block	Carl Roth, Karlsruhe, Germany
Roti-Immunoblock	Carl Roth, Karlsruhe, Germany
Sodium citrate tribasic dihydrate	AppliChem, Darmstadt, Germany
SuperSignal West FEMTO Max. Sensitivity Substrate, 200 mL	Thermo Fisher Scientific, Waltham, USA
Thiazolyl blue tetrazolium Bromide (MTT)	Sigma-Aldrich, St. Louis, USA

Triton X-100	Life Technologies, Carlsbad, USA
Trypan blue solution (0,4%)	Sigma-Aldrich, St. Louis, USA
Trypsin EDTA 0,25%	Life Technologies, Carlsbad, USA
Xylene	AppliChem, Darmstadt, Germany

2.1.3 Cell lines and primary cells

Table 2.8. Cell culture media

Cell type	Culture medium	Manufacturer
phLF	MCDB 131 medium	PAN-Biotech, Aidenbach, Germany
	FBS 10%	PAA Laboratories, Cölbe, Germany
	Penicillin/Streptomycin 100 U/ml	Life Technologies, Carlsbad, USA
	L-glutamine 2 mM	Life Technologies, Carlsbad, USA
	basic-FGF 2 ng/ml	Life Technologies, Carlsbad, USA
	EGF 0.5 ng/ml	Sigma-Aldrich, St. Louis, USA
	Insulin 5 µg/ml	Life Technologies, Carlsbad, USA
pmLF	DMEM-F12	Life Technologies, Carlsbad, USA
	Penicillin/Streptomycin 100 U/ml	Life Technologies, Carlsbad, USA
	FBS 20%	PAA Laboratories, Cölbe, Germany
A459	DMEM	Life Technologies, Carlsbad, USA
	FBS 10%	PAA Laboratories, Cölbe, Germany
	Penicillin/Streptomycin 100 U/ml	Life Technologies, Carlsbad, USA
CCL-206	DMEM-F12	Life Technologies, Carlsbad, USA
	FBS 10%	PAA Laboratories, Cölbe, Germany
	Penicillin/Streptomycin 100 U/ml	Life Technologies, Carlsbad, USA

Table 2.9. Cell lines

Name	Organism/Age/Tissue/Cell type	Supplier
CCL-206	Mouse/New-born/Lung/ Lung fibroblast	ATCC, Manassas, USA
A549	Human/58 years/Lung/Alveolar basal epithelial cell	ATCC, Manassas, USA

Table 2.10. Primary human lung fibroblast lines

ID	Patient data
Gi-151	Female, 60 years, histologically normal areas of lung specimens obtained after resective surgery for benign or malignant tumors
Gi-152	Female, 72 years, histologically normal areas of lung specimens obtained after resective surgery for benign or malignant tumors
406	Female, 50 years, peripheral normal lung tissue, organ donor
409sp	Male, 51 years, peripheral normal lung tissue, organ donor
411a	Female, 44 years, peripheral normal lung tissue, organ donor
423G	Female, 41 years, peripheral normal lung tissue, organ donor

Primary human lung fibroblast lines were provided by the group of Prof. Dr. Andreas Günther of the "Universities of Giessen and Marburg Lung Center" (UGMLC), Giessen, Germany.

2.1.4 Consumables

Table 2.11. Consumables

Product	Manufacturer
6/24/96 well plates	TPP, Trasadingen, Switzerland
96 well plates, white, for luminescence detection	Berthold Technologies, Bad Wildbad, Germany
Cell culture dishes	Nunc, Wiesbaden, Germany
Cell culture flasks	Nunc, Wiesbaden, Germany
Cell strainer, nylon 70 µm	BD Bioscience, Heidelberg, Germany
Cryovials 1.5 ml	Greiner Bio-One, Frickenhausen, Germany
Dismembrator Tubes (Nalgene Cryogenic Tubes)	Thermo Fisher Scientific, Waltham, USA
Falcon tubes (15 ml, 50 ml)	BD Bioscience, Heidelberg, Germany
Film X-Omat LS, Kodak	Carestream Health, Rochester, USA
Filter pipet tips	Biozym Scientific, Hessisch Oldendorf, Germany
Glass pasteur pipettes	VWR International, Darmstadt, Germany
NuPAGE Novex 3-8% Tris-Acetate Gel 1.5 mm, 10 well	Life Technologies, Carlsbad, USA
PCR plates, white, 96 well	Biozym Scientific, Hessisch Oldendorf, Germany
Pipet tips	Eppendorf, Hamburg, Germany
PVDF membrane	Bio-Rad, Hercules, USA
Reaction tubes (0.5 ml, 1.5 ml)	Eppendorf, Hamburg, Germany
Sealing foil, qPCR	Kisker Biotech, Steinfurt, Germany
Sterican cannulas	BD Bioscience, Heidelberg, Germany
Syringes (10 ml, 20 ml, 50 ml)	Neolab, Heidelberg, Germany
Whatman blotting paper 3 mm	GE Healthcare, Freiburg, Germany

2.1.5 Enzymes

Table 2.12. Enzymes

Product	Manufacturer
Collagenase type I	Biochrom, Berlin, Germany
DNAse 2 U/µl	Peqlab, Erlangen, Germany
Luciferase, recombinant	Promega, Fitchburg, USA
Purified 20S proteasome	Enzo Life Sciences, Lörrach, Germany
M-MLV Reverse Transcriptase	Sigma-Aldrich, St. Louis, USA

2.1.6   Human lung tissue

Table 2.13. Human lung tissue

ID	Patient data
198	Male, 61 years, peripheral normal lung tissue, organ donor
2B	Male, 29 years, peripheral normal lung tissue, organ donor
22	Unknown, peripheral normal lung tissue, organ donor
46	Unknown, peripheral normal lung tissue, organ donor
58	Male, 53 years, peripheral normal lung tissue, organ donor
Gi-151	Female, 60 years, histologically normal areas of lung specimens obtained after resective surgery for benign or malignant tumors
200	Male, 42 years, peripheral normal lung tissue, organ donor
406	Female, 50 years, peripheral normal lung tissue, organ donor
409sp	Male, 51 years, peripheral normal lung tissue, organ donor
411a	Female, 44 years, peripheral normal lung tissue, organ donor
146	Male, 60 years, IPF patient
190	Female, 44 years, IPF patient
207	Male, 47 years, IPF patient
302	Male, 54 years, IPF patient
324	Male, 34 years, IPF patient
325	Female, 51 years, IPF patient
327	Male, 61 years, IPF patient
330	Female, 46 years, IPF patient
331	Male, 57 years, IPF patient
334	Female, 42 years, IPF patient
335	Female, 57 years, IPF patient

Human lung tissue samples were provided by the group of Prof. Dr. Andreas Günther of the "Universities of Giessen and Marburg Lung Center" (UGMLC), Giessen, Germany.

2.1.7   Laboratory equipment and software

Table 2.14. Laboratory equipment

Product	Manufacturer
-20°C freezer MediLine LGex 410	Liebherr, Biberach, Germany
-80°C freezer U570 HEF	New Brunswick, Hamburg, Germany
Analytical scale XS20S Dual Range	Mettler-Toledo, Gießen, Germany
Autoclave DX-45	Systec, Wettenberg, Germany
Autoclave VX-120	Systec, Wettenberg, Germany
Cell culture work bench Herasafe KS180	Thermo Fisher Scientific, Waltham, USA
Centrifuge MiniSpin plus	Eppendorf, Hamburg, Germany
Centrifuge Rotina 420R	Hettich, Tuttlingen, Germany
Centrifuge with cooling, Micro200R	Hettich, Tuttlingen, Germany
CO2 cell Incubator BBD6620	Thermo Fisher Scientific, Waltham, USA
Cytospin 2 centrifuge	Shandon Life Science, Cheshire, UK

Demineralized water	Thermo Fisher Scientific, Waltham, USA
Dismembrator S	Sartorius, Göttingen, Germany
Dry ice container Forma 8600 Series, 8701	Thermo Fisher Scientific, Waltham, USA
Electronic pipet filler	Eppendorf, Hamburg, Germany
Electrophoretic Transfer Cell, Mini Protean Tetra Cell	Bio-Rad, Hercules, USA
Film developer Curix 60	AGFA, Morsel, Belgium
Flexivent system	Scireq, Montreal, Canada
Fluorescent scanner Typhoon TRIO+	Amersham Biosciences, Amersham, UK
Gel imaging system ChemiDoc XRS+	Bio-Rad, Hercules, USA
Hemocytometer	Brand, Wertheim, Germany
Hyrax M55 microtome	Zeiss, Jena, Germany
Ice machine ZBE 110-35	Ziegra, Hannover, Germany
Intelli-Mixer RM-2	Schubert & Weiss Omnilab, Munich, Germany
Light Cycler LC480II	Roche Diagnostics, Mannheim, Germany
Liquid nitrogen cell tank BioSafe 420SC	Cryotherm, Kirchen/Sieg, Germany
Liquid nitrogen tank Apollo 200	Cryotherm, Kirchen/Sieg, Germany
Magnetic stirrer KMO 2 basic	IKA, Staufen, Germany
Mastercycler gradient	Eppendorf, Hamburg, Germany
Mastercycler Nexus	Eppendorf, Hamburg, Germany
Microm HMS 740 Robot-Stainer	Thermo Fisher Scientific, Waltham, USA
Microm STP 420D Tissue Processor	Thermo Fisher Scientific, Waltham, USA
Microscope LSM 710 (confocal)	Zeiss, Jena, Germany
MicroSprayer Aerosolizer, Model IA-1C	Penn-Century, Wyndmoor, USA
Milli-Q Advantage A10 Ultrapure Water Purification System (Milli-Q water)	Merck Millipore, Darmstadt, Germany
Mini Centrifuge MCF-2360	Schubert & Weiss Omnilab, Munich, Germany
MIRAX SCAN	Zeiss, Jena, Germany
Multipette stream	Eppendorf, Hamburg, Germany
Nalgene Freezing Container (Mister Frosty)	Omnilab, Munich, Germany
NanoDrop 1000	PeqLab, Erlangen, Germany
pH meter InoLab pH 720	WTW, Weilheim, Germany
Pipettes Research Plus	Eppendorf, Hamburg, Germany
Plate centrifuge 5430	Eppendorf, Hamburg, Germany
Plate reader TriStar LB941	Berthold Technologies, Bad Wildbach, Germany
Plate reader Sunrise	Tecan, Crailsheim, Germany
Roll mixer	VWR International, Darmstadt, Germany
Power Supply Power Pac HC Power Supply	Bio-Rad, Hercules, USA
Sartorius Micro-Dismembrator S	Thermo Fisher Scientific, Waltham, USA
Scale XS400 2S	Mettler-Toledo; Gießen, Germany
Shaker Duomax 1030	Heidolph, Schwabach, Germany
Thermomixer compact	Eppendorf, Hamburg, Germany
Vortex Mixer	IKA, Staufen, Germany
Vacuum pump NO22AN.18 with switch 2410	KNF, Freiburg, Germany
Water bath Aqua Line AL 12	Lauda, Lauda-Königshofen, Germany

Xcell SureLock Mini Cell	Life Technologies, Carlsbad, USA

Table 2.15. Software

Product	Manufacturer
GraphPad Prism 5	GraphPad Software, La Jolla, USA
Image Lab Version	Bio-Rad, Hercules, USA
LightCycler® 480 SW 1.5	Roche Diagnostics, Mannheim, Germany
Magelan Software	Tecan, Crailsheim, Germany
Microsoft Office Professional Plus 2010	Microsoft, Redmond, USA
Tristar MicroWin 2000	Berthold Technologies, Bad Wildbach, Germany

2.1.8   Oligonucleotides

Table 2.16. Primer for qPCR

Gene	Species		Sequence 5'-3'
ACTA (αSMA)	human	fw	CGAGATCTCACTGACTACCTCATGA
		rev	AGAGCTACATAACACAGTTTCTCCTTGA
Col1A1	human	fw	CAAGAGGAAGGCCAAGTCGAG
		rev	TTGTCGCAGACGCAGATCC
Fibronectin1	human	fw	CCGACCAGAAGTTTGGGTTCT
		rev	CAATGCGGTACATGACCCCT
PSMA3	human	fw	AGATGGTGTTGTCTTTGGGG
		rev	AACGAGCATCTGCCAACAA
PSMB5	human	fw	TCAGTGATGGTCTGAGCCTG
		rev	CCATGGTGCCTAGCAGGTAT
PSMB6	human	fw	CAGAACAACCACTGGGTCCT
		rev	CCCGGTATCGGTAACACATC
PSMB7	human	fw	TCGCTGGGGTGGTCTATAAG
		rev	TCCCAGCACCACAACAATAA
PSMC3	human	fw	GTGAAGGCCATGGAGGTAGA
		rev	GTTGGATCCCCAAGTTCTCA
PSMD11	human	fw	GCTCAACACCCCAGAAGATGT
		rev	AGCCTGAGCCACGCATTTTA
Vimentin	human	fw	CTTTTCCTCCCTGAACCTGAG
		rev	AGAAGTTTCGTTGATAACCTGTCC
RPL19	human	fw	TGTACCTGAAGGTGAAGGGG
		rev	GCGTGCTTCCTTGGTCTTAG
mCollagen	mouse	fw	CCAAGAAGACATCCCTGAAGTCA
		rev	TGCACGTCATCGCACACA
mFibronectin	mouse	fw	GTGTAGCACAACTTCCAATTACGAA
		rev	GGAATTTCCGCCTCGAGTCT
mPSMA3	mouse	fw	TGAAGAAGGCTCCAATAAACGTCT
		rev	AACGAGCATCTGCCAGCAA

mPSMB5	mouse	fw	TGCTCGCTAACATGGTGTATCAGTA
		rev	GGCCTCTCTTATCCCAGCCA
mPSMB6	mouse	fw	AGACGCTGTCACTTACCAACTTGG
		rev	AAGAGACTGGCGGCTGTGTG
mPSMB7	mouse	fw	TGCCTTATGTCACCATGGGTTC
		rev	TTCCTCCTCCATATCTGGCCTAA
mPSMC3	mouse	fw	AAGCTGAGCAAGATGGCATT
		rev	TTCATGGGTGACTCGCAATA
mPSMD11	mouse	fw	GAATGGGCCAAATCAGAGAA
		rev	TGTACTTCCACCAAAAGGGC
mRPL19	mouse	fw	CGGGAATCCAAGAAGATTGA
		rev	TTCAGCTTGTGGATGTGCTC

Table 2.17. siRNA for gene knockdown

siRNA	Species	Supplier
Silencer Select PSMD11 s11413	human	Life Technologies, Carlsbad, USA
Silencer Select PSMD11 s11414	human	Life Technologies, Carlsbad, USA
Silencer Select PSMD11 s11415	human	Life Technologies, Carlsbad, USA
Silencer Select PSMD11 s87417	mouse	Life Technologies, Carlsbad, USA
Silencer Select Negative Control #1	human, mouse	Life Technologies, Carlsbad, USA
Silencer Select Negative Control #2	human, mouse	Life Technologies, Carlsbad, USA

All siRNAs were diluted with purified water to a stock solution of 10 µM.

2.1.9 Standards and kits

Table 2.18. Kits

Product	Manufacturer
Bright-Glo Luciferase Assay System	Promega, Fitchburg, USA
Cell Proliferation ELISA, BrdU (colorimetric)	Roche Diagnostics, Mannheim, Germany
Proteasome-Glo 3-Substrate System	Promega, Fitchburg, USA
LightCycler 480 SYBR Green I Master	Roche Diagnostics, Mannheim, Germany
PeqGOLD Total RNA-Kit	Peqlab, Erlangen, Germany
Pierce BCA Protein Assay Kit	Thermo Fisher Scientific, Waltham, USA
Roti-Quick-Kit	Carl Roth, Karlsruhe, Germany

Table 2.19. Standards

Product	Manufacturer
Protein marker V (10-175 kDa)	AppliChem, Darmstadt, Germany
Protein marker VI (10-245 kDa)	AppliChem, Darmstadt, Germany

2.2 Methods

2.2.1 *Cell culture*

2.2.1.1 *Cell culture of mammalian cell lines*

The A549 human alveolar epithelial cell line and the CCL-206 mouse lung fibroblast cell line were obtained from ATCC (American Type Culture Collection, Manassas, USA).

A549 cells were cultured in DMEM medium supplemented with 10% FBS and 100 U/ml penicillin/streptomycin. Treatment with proteasome inhibitors (bortezomib and oprozomib) was performed in whole culture medium.

CCL-206 fibroblasts were cultured in DMEM-F12 medium supplemented with 10% FBS and 100 U/ml penicillin/streptomycin. Before TGF-β treatment, fibroblasts were starved in reduced culture medium containing 1% FBS for 24 hours. TGF-β then was added to the starvation medium to a final concentration of 5 ng/ml.

All cells were kept at 37°C under humidified atmosphere containing 5% CO_2.

2.2.1.2 *Isolation and cell culture of primary human lung fibroblasts*

Primary human lung fibroblasts (phLF) were provided by the "Universities of Giessen and Marburg Lung Center" (UGMLC) and isolated in the laboratory of Prof. Dr. Andreas Günther.

All experiments were carried out with normal phLF in passages 2 and 3. Prior TGF-β treatment, phLF were starved for 24 hours in reduced culture medium containing 1% FBS.

2.2.1.3 *Isolation and cell culture of primary murine lung fibroblasts*

Primary murine lung fibroblasts (pmLF) were isolated from whole lungs of female FVB.129S6-Gt(ROSA)26Sor[tm2(HIF1A/luc)Kael]/J mice (ODD-luc mice), which contain the ODD-luc transgene. Animals were sacrificed by cervical dislocation and lungs were dissected. Isolated lungs were collected in pre-warmed pmLF culture medium containing DMEM-12 medium supplemented with 20% FBS and 100 U/ml penicillin/streptomycin and chopped into small pieces. Lung pieces were placed into falcon tubes and digested at 37°C for 2 hours, using collagenase type I. Digested tissue then was pressed through a 70 µm nylon filter for further mincing. After washing and pelleting minced tissue was resuspended in culture medium and incubated at 37°C in humidified atmosphere and 5% CO_2 to allow fibroblast outgrowth off the tissue. Media was exchanged every three days. Primary murine lung fibroblasts were split for the first time after

reaching confluency of 80-90% and used up to passage 3. Cells were treated with oprozomib in whole culture medium.

2.2.1.4 Isolation and cell culture of primary murine alveolar epithelial type II cells

Primary murine alveolar epithelial type II cells (pmATII) were isolated by Dr. Kathrin Mutze in collaboration with the lab of Melanie Königshoff at the Comprehensive Pneumology Center. Isolation was performed as described before (Königshoff et al., 2009).

2.2.1.5 Subculturing and cryopreservation of mammalian cells

In general, all cell lines and primary cells were subcultured after reaching confluency of about 80-90%. In the meantime, culture medium was exchanged every 3-4 days. For subculturing, adherent cells were washed with pre-warmed PBS and incubated with Trypsin-EDTA (0.25%) at 37°C under humidified atmosphere containing 5% CO_2 for 2-4 minutes. After incubation, detachment of cells by trypsin digestion was monitored under the light microscope. Digestion was stopped by adding culture medium and the cell suspension then was split in a ratio of five to ten, depending on the cell type and individual growth.

For cryopreservation, cells were harvested by trypsin digestion as described above and collected in cell specific culture medium. Cell pellets were obtained by centrifugation and resuspended in culture medium containing 20% FBS and 10% DMSO at a concentration of $1-2 \times 10^6$ cells/ml. Cryovials were filled, each with 1 ml of cell suspension and slowly frozen in a Nalgene freezing container at -80°C for 24 hours. For long-term storage, cells were kept in liquid nitrogen.

2.2.1.6 Gene silencing of lung fibroblasts

Partial gene knockdown experiments of murine Rpn6 in CCL-206 mouse lung fibroblasts and of human Rpn6 in phLF were performed by reverse liposomal transfection of small interfering RNA (siRNA) using the Lipofectamine RNAiMAX system. For that, CCL-206 and phLF cells were seeded in transfection medium at a density of $4-5 \times 10^5$ cells per 10 cm dish and cultured overnight. Transfection of CCl-206 fibroblasts was performed by using the Silencer Select s87417 siRNA for knockdown of murine Rpn6 in a final concentration of 0.1 nM. Silencer Select s11413 siRNA alone or a pool of Silencer Select siRNAs s11413, s11414, and s11415 was used for knocking down human Rpn6 in phLF at a final concentration of 0.5 nM siRNA. The control siRNA Silencer Select Control#2 was used as a control for mouse and human single

siRNA knockdown and a pool of Silencer Select Control#1 and #2 was used as a control for pooled Rpn6 siRNA experiments.

Rpn6 siRNA and Control siRNA were diluted with Opti-MEM, taking into account the final siRNA concentration of 0.1 nM for mouse and 0.5 nM for human Rpn6 siRNA, gently mixed with Lipofectamine RNAiMAX (10 µl/ml), and incubated for 15 minutes at room temperature to allow formation or siRNA-liposome complexes. Cells were trypsinized and resuspended in culture medium without penicillin/streptomycin and cell suspension was transferred to 10 cm culture dishes at a concentration of 4-5x10^5 cells per dish. The siRNA-Lipofectamine RNAiMAX-mix was added to every dish and gently mixed with the cell suspension. Cells were incubated for 24 hours.

For investigation of Rpn6 knockdown effects in phLF, transfection medium was exchanged with culture medium after 24 hours and phLF were incubated for additional 48 hours. Then they were harvested by trypsinization and cell pellets were snap frozen in liquid nitrogen until further investigation.

To examine TGF-β effects upon Rpn6 knockdown, transfection medium of CCl-206 and phLF was removed after 24 hours and replaced with reduced culture medium, containing 1% FBS and 5 ng/ml TGF-β. Cells were harvested 48 hours after TGF-β treatment.

2.2.1.7 MTT assay

Cell viability in response to proteasome inhibitors was analyzed applying the 3-(4,5-Dimethyl-2-thiazolyl)-2,5-diphenyl-2H-tetrazolium bromide (MTT) assay. In this colorimetric assay, the water soluble yellow tetrazolium salt is taken up by viable cells and reduced to its purple insoluble formazan by mitochondrial dehydrogenases. Formazan crystals are soluble in acidified isopropanol and light absorbance of the solution can be measured colorimetrically. The extension of tetrazolium-formazan reduction can be used as indirect indicator for the amount of viable cells.

Here, 5×10^4 cells (pmLF, A549) per well were seeded in 24-well plates or 25x10^4 cells (pmATII) were seeded in 48-well plates. The next day, cells were incubated with different concentrations of oprozomib or bortezomib for up to 72 hours (pmLF, A549) or up to 52 hours (pmATII). Then, 100 µl 5 mg/ml MTT dissolved in PBS was added to each well and cells were incubated at 37°C for 1 hour to allow reduction of the tetrazolium dye to its formazan within the cell. After aspiration of the supernatant, the purple formazan crystals were dissolved in isopropanol

containing 0.1% Triton X-100 and solution was transferred to transparent 96 well plates. Absorbance was measured at 570 nm in a Tristar LB 941 plate reader.

2.2.1.8   Immunofluorescence staining

Primary murine lung fibroblasts were cultured at a density of 5000 cells per 0.32 cm^2 (96 well plate) in culture medium. The next day, cells were incubated for 72 hours with 50 nM or 100 nM of oprozomib or DMSO as control. For growth factor treatment cells were incubated with 5 ng/ml of TGF-β for 24 hours in starvation medium containing 1% FBS. 50 nM of oprozomib was added and immunofluorescence staining was performed 24 hours later. Cells were then washed with PBS and fixed with 4% paraformaldehyde (PFA), washed again and permeabilized with 0.25% Triton X-100. After further washing, primary antibody for collagen I was added for 1 hour. Secondary antibody Alexa Fluor 488 was added after washing and incubated for additional 45 minutes in darkness. Phalloidin Alexa Fluor 568 and DAPI staining was performed and finally cells were fixed with 4% PFA and stored at 4°C in the dark. Imaging was performed by fluorescent microscopy (LSM710 System).

2.2.1.9   BrdU cell proliferation assay

A colorimetric BrdU cell proliferation assay (Roche) was performed according to the manufacturer's protocol. For that, pmLF or CCL206 fibroblasts were plated at a density of 5000 cells or 2000 cells per 0.32 cm^2 (96 well plate) in their culture medium, respectively. Treatment with oprozomib, siRNA or TGF-β was performed as described in chapters 2.2.1.6 and 2.2.1.7. To assay changes in proliferation, cells were then labeled by adding BrdU at a final concentration of 10 µM to the medium and incubated for 2-4 hours to allow BrdU incorporation into the DNA. Then the medium was removed, cells were dried at room temperature, and stored at 4°C overnight. The next day, cells were fixed and DNA was denatured by adding the FixDenat solution of the kit and incubated with anti-BrdU-POD antibody for 90 minutes at room temperature. Cells were washed and the substrate solution was added and converted by the anti-BrdU antibody conjugated peroxidase. The reaction was stopped after 30 minutes by adding H$_2$SO$_4$ at a final concentration of 0.2 M. Absorbance measurement was performed within 5 minutes at 450 nm using the Tristar LB 941 plate reader.

2.2.2   Animal experiments

All animal experiments were conducted according to international guidelines and were approved by the local government for the administrative region of Upper Bavaria.

Pathogen-free female C57BL/6 mice (10-12 weeks old) were obtained from Charles River and pathogen-free female FVB wild type and FVB.129S6-Gt(ROSA)26Sor$^{tm2(HIF1A/luc)Kael}$/J reporter mice were obtained from Jackson Laboratory. All animals were housed in rooms maintained at constant temperature and humidity with a 12 hours light cycle. Animals were allowed food and water ad libitum.

Prior sacrifice, mice were narcotised by i.p. administration of 100 mg/ml ketamine and 0.7 mg/ml rompun per kg body weight and lung function measurement was performed in some animals using the Flexivent system. Subsequently, animals were sacrificed by exsanguination and lungs and trachea were exposed. Bronchoalveolar lavage (BAL) was performed by inserting a cannula into the trachea and lungs were lavaged four times with 0.5 ml of sterile PBS supplemented with cOmplete® protease inhibitor cocktail. The combined BAL fluid then was centrifuged at 400 x g and the obtained cell pellet was resuspended in RPMI 1640 medium supplemented with 10% FBS. Total cell counts were determined in a hemocytometer via Trypan Blue exclusion. Cell suspension then was subjected to a Cytospin 2 centrifuge to transfer BAL cells on glass slides. May-Grünwald-Giemsa-staining was performed and 200 cells per sample were counted and distinguished using morphological criteria.

Then lungs were perfused with PBS and right lungs were snap frozen in liquid nitrogen for further analysis of mRNA and protein. Left lungs were infused with 4% PFA via the left main bronchus and submerged in 4% PFA for at least 24 hours. Paraffin embedding was performed using the tissue processor Microm STP 420 D. Sections of 3 µm were cut using a Hyrax M55 microtome, mounted on glass slides, and stored at 4°C until further preparation.

Animal experiments were performed in collaboration with the research groups of Prof. Dr. Oliver Eickelberg (OE) and Dr. Tobias Stöger (TS).

Experimental design and organisation: Dr. Silke Meiners, Nora Semren

Bleomycin instillation: David Kutschke (Technician, TS), Isis Fernandez (Postdoc, OE), Nora Semren, Nunja Habel-Ungewitter (PhD student, TS), Constanze Heise (Technician, OE)

Proteasome inhibitor treatment: Nora Semren, David Kutschke, Nunja Habel-Ungewitter, Isis Fernandez

Sacrifice, organ extraction: Nora Semren, Isis Fernandez, Nunja Habel-Ungewitter, David Kutschke, Constanze Heise, Daniela Dietel (Technician, OE)

Sample preparation and analysis: Nora Semren

2.2.2.1   Bleomycin mouse model for pulmonary fibrosis

For bleomycin application, mice were narcotized by i.p. administration of 0.2 mg/ml medetomidin, 2.0 mg/ml midazolam and 0.02 mg/ml fentanyl per kg body weight (MMF narcosis). Then, 50 µl of bleomycin (3 U/kg), dissolved in sterile PBS, were intratracheally instilled into the lungs using the Micro Sprayer Aerosolizer, Model IA-1C as published before (Aumiller et al., 2013). Control mice were instilled with 50 µl of PBS.

MMF narcosis was antagonized by s.c. administration of 0.29 mg/ml atipamezole, 0.059 mg/ml flumazenil and 0.14 mg/ml naloxone per kg body weight.

2.2.2.2   Proteasome inhibitor treatment

For initial dose finding female FVB wild type mice were used. Oprozomib was suspended in a solution of 0.1 % Pluronic F-127 in Milli-Q water and applied once via intratracheal instillation under MMF narcosis and subsequent s.c. administration of antagonist as described for bleomycin application in chapter 2.2.2.1. Mice were sacrificed 24 hours or 96 hours after proteasome inhibitor application.

Validation of antifibrotic effects was performed in FVB.129S6-Gt(ROSA)26Sor$^{tm2(HIF1A/luc)Kael}$/J reporter mice or in C57BL/6 mice. Pulmonary fibrosis was induced as described under 2.2.2.1 and oprozomib was either instilled intratracheally into the lungs as described for FVB wild type mice or applied orally using a gavage needle. For oral application oprozomib was suspended in 1% carboxymethyl cellulose (CMC). Oral application was performed without narcosis. Detailed treatment schemes of different animal experiments are given in the results part.

2.2.2.3   Hematoxylin & Eosin staining

Paraffin embedded lung sections were incubated at 60°C for at least 30 minutes, deparaffinized in xylene twice for 5 minutes, rehydrated in a graded alcohol series (ethanol 99.8% twice 1 minute; 90% 1 minute; 80% 1 minute; 70% 1 minute) and transferred in distilled water by using the robot stainer Microm HMS 740. Subsequently, hematoxylin and eosin (H&E) staining was performed. For that, slices were incubated in Hemalaun for 6 minutes, washed in distilled water and transferred into a solution of 0.5% Eosin G in water containing one drop of acidic acid per 100 ml and incubated for 10 minutes. Sections were washed in distilled water, stepwise dehydrated in ascending ethanol series (ethanol 70% 1 minute; 80% 1 minute; 90% 1 minute; 99.8% twice 1 minute) and transferred in xylene by two incubation steps of 5 minutes each.

Sections were mounted using Entellan. For imaging, sections were scanned in by a MiraxScan and analyzed using the Panoramic Viewer software.

2.2.2.4 Immunofluorescence staining

For immunofluorescence staining, paraffin-embedded lung tissue sections were heated and rehydrated as described in chapter 2.2.2.3. Antigen retrieval was performed in citrate buffer (pH 6.0) for 30 seconds at 125°C and 10 seconds at 90°C. Slides were blocked with 5% BSA to avoid unspecific antibody binding and primary antibodies against Collagen I and αSMA were applied on tissue slides. Slides were washed with Tris buffer and incubated with secondary antibodies Alexa Fluor 568 anti-rabbit (Coll-I) and Alexa Fluor 488 anti-mouse (αSMA) for 1 hour in darkness. Counterstaining with DAPI was performed and slides were covered with Fluorescent Mounting Medium. Imaging was performed by fluorescent microscopy using the LSM710 System.

2.2.2.5 Immunohistochemistry

Immunohistochemistry of bleomycin challenged mouse lungs was performed by Dr. Martina Korfei in collaboration with the group of Prof. Dr. Andreas Günther of the "Universities of Giessen and Marburg Lung Center" (UGMLC).

2.2.3 Human lung tissue

Tissue samples of explanted human lungs were provided by the "Universities of Giessen and Marburg Lung Center" (UGMLC) and processed in the laboratory of Prof. Dr. Andreas Günther. For that, explanted lungs or lobes were obtained from the Department of Thoracic Surgery, Vienna. Tissue samples from the subpleural region of the lungs were used and diagnosis of IPF was retrospectively validated by A. Günther and an expert pathologist using current American Thoracic Society/European Respiratory Society guidelines (Travis et al., 2002). The study protocol was approved by the Ethics Committee of the Justus-Liebig-University School of Medicine (No. 31/93, 84/93, 29/01) and the University of Vienna Hospital ethics committee (EK-Nr 076/2009).

2.2.3.1 Immunohistochemistry

Immunohistochemistry of human and mouse lungs was performed and analyzed by Dr. Martina Korfei in collaboration with the group of Prof. Dr. Andreas Günther of the "Universities of Giessen and Marburg Lung Center" (UGMLC).

IHC was performed for 10 IPF and 6 control lung tissue samples. Furthermore, lungs of 3 PBS treated control animals and 14 bleomycin challenged animals (4 animals after 7 days, 6 animals after 14 days and 4 animals after 56 days of bleomycin instillation) were analyzed.

2.2.4 Proteinbiochemistry

2.2.4.1 Protein extraction from cells and tissue

Prior protein extraction, cells were harvested by trypsin digestion, collected in culture medium, centrifuged, and washed with PBS. Cell pellets were snap-frozen in liquid nitrogen.

For disintegration, frozen mouse or human tissue samples were transferred into dismembrator vials containing a grinding ball and applied to the shaking flask of a Mikro-Dismembrator S. A shaking frequency of 3000 RPM was applied two times for 30 seconds to provide disruption and mixing of the tissue to obtain a homogenous tissue powder. To avoid thawing, samples were frequently submerged in liquid nitrogen.

Hypoosmotic protein extraction or extraction with TSDG buffer (composition of lysis solutions are described in Table 2.3) was performed to maintain native proteasome complexes and preserve their activity as detergents like SDS are known to activate the proteasome by opening of the entry pore (Shibatani & Ward, 1995). Cell pellets or frozen tissue powder were suspended in hypoosmotic lysis solution or TSDG buffer. Lysis was performed by 5-7 freeze and thaw cycles by repeatedly subjecting sample tubes to liquid nitrogen and warm water of 37°C. Cell debris and non-soluble fractions were removed by centrifugation (15000 g, 4°C, 30 minutes) and supernatants were collected for further analysis.

For RIPA lysis, cell pellets or frozen tissue powder were suspended in RIPA buffer (Table 2.3) and incubated on ice for 30 minutes to allow cell lysis. Regular shaking of the tubes during incubation promoted maximal protein extraction. Cell debris and non-soluble fractions were removed by centrifugation (15000 g, 4°C, 30 minutes) and supernatants were collected for further analysis.

2.2.4.2 Protein quantification by bicinchoninic acid assay (BCA)

To quantify protein concentrations in cell and tissue lysates the Pierce BCA kit was used according to the manufacturer's protocol. Lysates were diluted 1:5 in PBS and 25 µl of this dilution was mixed in a 96 well plate with 200 µl working reagent provided by the kit. Bovine serum albumin standards of known concentrations were assayed on the same plate to obtain a standard curve for final protein quantification. Sample plates were incubated for 30 minutes at

37°C for optimal color development and absorbance was measured at a wavelength of 562 nm using the Sunrise Plate Reader.

2.2.4.3 Proteasome activity assay

Chymotrypsin-like, trypsin-like and caspase-like proteasome activities were determined in cell and tissue lysates applying the Proteasome-Glo Assay kit according to the manufacturer's protocol. For that, hypoosmotic lysates were diluted to 0.12-0.2 µg/µl and 25 µl of this dilution was mixed with the same volume of reaction buffer, provided by the kit, in a white 96 well microplate. Three different reaction buffers were provided by the assay to measure chymotrypsin-like, trypsin-like and caspase-like proteasome activities. These buffers contain specific luminogenic substrates (Suc-LLVY-aminoluciferin for CT-L, Z-LLR-aminoluciferin for T-L and Z-nLPnLD-aminoluciferin for C-L activity, respectively) for each active site that are cleaved to release aminoluciferin, which is transformed by luciferase to produce a luminescent signal (Figure 2.1).

Figure 2.1. Proteasome activity assay
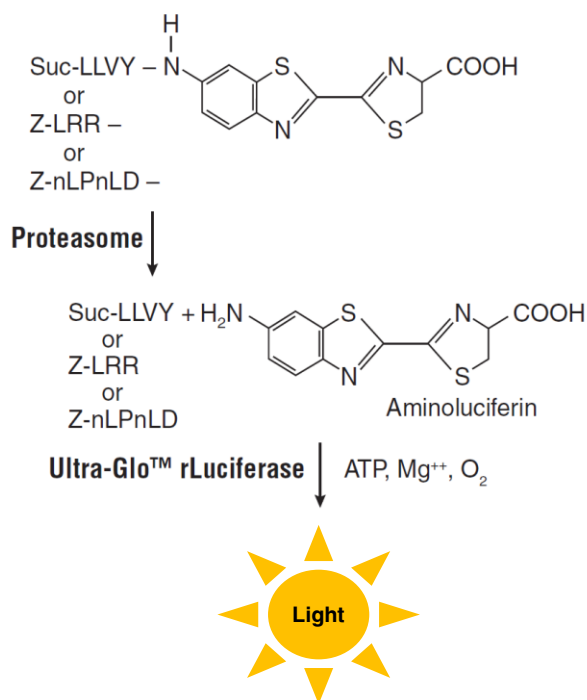Suc-LLVY-, Z-LRR- or Z-nLPnLD-aminoluciferase are specific substrates of the CT-L, T-L or C-L active sites, respectively. Substrate cleavage by the proteasome releases aminoluciferin which is then transformed by luciferase. This reaction leads to light emission which is directly proportional to the rate of substrate cleavage by the proteaseome. (Taken from Moravec et al. 2009)~modified

The microplate was subjected to a Tristar LB941 plate reader immediately after addition of the reaction buffer and luminescent signal was measured every 2 minutes for 30 minutes. For final analysis, values were obtained after 10-20 minutes of reaction, when light emission reached a plateau. Data are shown as relative values to the activity of untreated controls of the same experiment. In cell culture experiments, the control of each experiment and in animal experiments the average value of control groups is set as one.

2.2.4.4   *Native gel analysis*

Native gel electrophoresis was performed using the XCell SureLock Mini-Cell system. 18-40 µg protein per sample from hypoosmotic or TSDG lysates, respectively, were loaded on gradient (3-8% acrylamide) tris-acetate NuPAGE Novex gels and proteasome complexes were separated in running buffer (composition of all buffers are described in Table 2.4) for 4 hours at 150 V and 4°C. Subsequently, native gels were incubated for 30 minutes at 37°C in proteasome activity reaction buffer containing 50 µM Suc-LLVY-AMC, a fluorogenic, synthetic peptide substrate of the chymotrypsin-like activity of the proteasome and gently washed in 50 mM Tris buffer. Gels were imaged at an excitation wavelength of 380 nm and emission wavelength of 460 nm using the ChemiDoc XRS+ system. Subsequently, gels were soaked in solubilisation buffer for 10-15 minutes and blotted onto methanol activated polyvinylidene difluoride (PVDF) membranes for 1.5 hours at 250 mA and 4°C using the Mini Protean Tetra electrophoretic transfer cell. Subsequently, membranes were blocked with Roti®-Block for at least 1 hour and incubated with primary antibody, diluted in Roti®-Block, overnight at 4°C under constant shaking. The next day, membranes were washed three times for 10 minutes with PBST and incubated with HRP-linked secondary antibody for 1 hour at room temperature under constant shaking. Membranes were washed once more and chemiluminescence was generated by applying ECL Plus Detection Reagent for normal or SuperSignal West Femto Maximum Sensitivity Substrate for weak signals followed by exposure of Kodak X-Omat LS films and development of films in a Curix 60 developer or with the ChemiDoc XRS+. Quantification of in-gel proteasome activity and immunoblotted bands were analyzed with the volume tool of Image Lab software and normalized to non-treated controls.

To assay luciferase activity, native gels were soaked in luciferase reaction buffer and luminescence was imaged for 30 minutes using the ChemiDoc XRS+. Afterwards gels were washed with 50 nM Tris and in-gel proteasome activity was assayed as described above. To determine total protein concentrations within the gel, gels were soaked in PageBlue Protein Staining Solution, microwaved for 1 minute and washed several times with deionized water.

ABP labeling experiments were performed by Vanessa Welk (PhD Student, 2015). For labeling of active proteasomes, the pan-reactive proteasome ABP MV151 was used (Verdoes et al., 2006). TSDG buffer lysates of whole human lung tissue were diluted with ABP labeling buffer to a total protein concentration of 0.5 µg/µl. 30 µl of sample were incubated with 0.5 µM MV151 for 1 hour at 37°C and subsequently quenched by the addition of 1x sample buffer. Native gel separation was performed as described above and proteasome activity was visualized using a fluorescent scanner Typhoon TRIO+. Images were taken at 450 PTM and 50 µm pixel resolution with fluorescence Cy3/TAMRA.

2.2.4.5   SDS-PAGE and Western blotting

Protein samples (hypoosmotic, RIPA or TSDG lysates) were mixed with Lämmli loading buffer (compositions of all buffers are described in Table 2.5) and cooked at 95°C for 5 minutes. Samples were cooled down and 15-20 µg of protein per sample were loaded onto 10% SDS-PAGE gels. Electrophoresis was performed at 100-110 V in running buffer and gels were subsequently blotted onto methanol activated PVDF membranes for 90 minutes at 250 mA and 4°C in transfer buffer using the Mini Protean Tetra electrophoretic transfer cell. Proteins of interest were detected by standard immunodetection techniques applying primary and HRP-linked secondary antibodies as described in chapter 2.2.4.4. β-actin was used as loading control. For densitometric analysis protein bands were quantified using the volume tool of Image Lab software and normalized to their β-actin protein bands.

2.2.4.6   Luciferase assay

pmLF, isolated from FVB.129S6-Gt(ROSA)26Sor[tm2(HIF1A/luc)Kael]/J mice as described in 2.2.1.3, were seeded at a density of 5000 cells per 0.32 cm^2 (96 well plate) in culture medium and treated with different concentrations of oprozomib the next day. 24 hours later, luciferase activity was assayed using the Bright-Glo system according to the manufacturer's protocol. For that, cells were lysed in 50 µl of Glo-Lysis buffer per well. 20 µl of cell lysate was then transferred into a white walled 96 well plate and 20 µl of Bright-Glo-Luciferase was added to each well. Luminescence was measured immediately using a Tristar LB 941 plate reader.

2.2.5   RNA analysis

2.2.5.1   mRNA extraction

Total RNA from cells was prepared using the Roti-Quick Kit according to manufacturer's protocol, which is based on the acid guanidinium thiocyanate-phenol-chloroform method for total

RNA extraction (Chomczynski & Sacchi, 1987). Frozen cell pellets were lysed in 500 µl Roti-Quick 1 and 650 µl cold Roti-Quick 2 was added and mixed by vortexing of the sample tube to allow RNA extraction by phase separation. Samples were incubated on ice for 10 minutes and subsequently centrifuged for 15 minutes at 10000 rpm and 4°C to separate RNA. Two phases were clearly separated and the upper water phase, containing RNA, was collected, 500 µl Roti-Quick 3 was added, and gently mixed. Samples were incubated for 40 minutes at -20°C to precipitate RNA, which was finally sedimented via centrifugation for 20 minutes at 13.000 and 4°C. RNA pellets were washed with ethanol 70% three times and ethanol was removed via evaporation. Finally RNA was dissolved in Milli-Q water.

Frozen human or mouse tissue was grinded to powder as described in 2.2.4.1. Tissue powder was suspended in Roti-Quick 1 and incubated on ice as described above to allow cell lysis, Roti-Quick 2 was added, and RNA extraction via phase separation was performed. In a next step, RNA was purified using the Peqlab-Gold Total RNA-Kit according to the manufacturer's protocol starting with loading of the prepared RNA extract onto RNA-binding columns.

RNA concentrations were assessed via absorbance measurement at 260 nm using a NanoDrop 1000.

2.2.5.2 Reverse transcription of mRNA into cDNA

For reverse transcription of RNA into cDNA, 1 µg of sample RNA was mixed with 2 µl of Random Hexamers (250 µM) and Milli-Q water was added to a final volume of 11.5 µl. Samples were incubated at 70°C for 10 minutes and immediately placed on ice. 8.5 µl master mix was added to every preparation to obtain a final concentration of 1x First Strand Buffer, 10 mM DTT, 0.5 mM dNTP's, 1 U/µl RNAsin RNAse Inhibitor, 10 U/µl M-MLV Transcriptase. Reverse transcription was performed using a Mastercycler Nexus applying the following settings: Annealing 5 minutes at 25°C, elongation 60 minutes at 37°C.

Finally, DNAse was added to the cDNA at a final concentration of 0.05 U/µl and genomic DNA was digested by incubation of the samples for 15 minutes at 37°C. Subsequently, DNAse was heat-inactivated for 10 minutes at 75°C and cDNA was diluted 1:5 with Milli-Q water.

2.2.5.3 Quantitative polymerase chain reaction (qPCR)

For quantitative PCR reactions, the SYBR Green LC480 System was used. Per sample, 2.5 µl cDNA solution was mixed with 5 µl of LC480 SYBR Green I Master mix and 2.5 µl primer mix was added, containing forward and reverse primer at a final concentration of 0.5-0.75 µM

(primer sequences are listed in Table 2.16). qPCR was performed in duplicates per sample in a LightCycler 480II applying standard conditions: 95°C for 5 minutes for initial denaturation were followed by 45 cycles of 95°C for 5 seconds (denaturation), 59°C for 5 seconds (annealing), 72°C for 20 seconds (elongation), 60-95°C for 1 minute with continuous acquisition (melting curve). Expression of target genes was normalized to the hypoxanthine phosphoribosyl transferase gene (HPRT) or the 60S ribosomal protein L19 as a housekeeping gene.

2.2.6 Statistics

Data are presented as means ± SEMs as indicated in the figure legends and were considered statistically significant when $p \leq 0.05$ (*$p \leq 0.05$, **$p < 0.01$, ***$p < 0.001$). Data were analyzed using Prism 5 software. Statistical analysis was performed using one-way ANOVA, followed by Post-hoc testing for multiple comparisons (Bonferroni-Holmes or Dunnett's test), Mann-Whitney t-test, two-tailed paired t-test or Spearman correlation as indicated in the figure legends. Dixon outlier test was performed.

3   RESULTS

In this study, proteasome activity and composition was analyzed during myofibroblast differentiation and fibrotic lung remodeling to evaluate a possible role of the proteasome as a trigger of IPF. To further validate the proteasome as a target in lung fibrosis, a novel second-generation inhibitor, oprozomib, was tested for therapeutic effects in the bleomycin mouse model of pulmonary fibrosis.

3.1   The Proteasome as a Trigger of IPF

This chapter is based on the following manuscript:

<u>Nora Semren</u>, Vanessa Welk, Martina Korfei, Ilona E. Keller, Isis E. Fernandez, Heiko Adler, Andreas Günther, Oliver Eickelberg, and Silke Meiners. Regulation of 26S proteasome activity in pulmonary fibrosis. *American Journal of Respiratory and Critical Care Medicine,* 2015 Nov;192(9):1089-1101.

The ubiquitin-proteasome system is critical for maintenance of intracellular homeostasis by degrading proteins in a spatially and timely controlled manner. During fibrotic tissue remodeling, cell and protein homeostasis are altered. A contribution of the proteasome to the development of pulmonary fibrosis, however, is unknown. Therefore it was hypothesized that proteasome function is altered in fibrotic lung remodeling and adds to the pathogenesis of IPF.

To investigate a possible role of the proteasome in profibrotic TGF-β signaling, the murine lung fibroblast line CCL-206 was stimulated with TGF-β to induce myofibroblast differentiation. After serum starvation, fibroblasts were incubated with 5 ng/ml of TGF-β for 6, 24 and 48 hours to analyze short and long-term effects on the proteasome. Proteasome activity was measured in hypoosmotic cell lysates to preserve cellular proteasome function, as detergents such as SDS, which are present in many lysis buffers, are known to activate the proteasome (Coux et al., 1996). The chymotrypsin-like active site was analyzed as it is regarded as the most important proteolytic site of the proteasome (Marques et al., 2009). For that, cell lysates were incubated with the chymotrypsin-like site specific luminogenic substrate Suc-LLVY-aminoluciferin, which generates a luminescent signal via the luciferase reaction after cleavage by the proteasome (Moravec et al., 2009) (Figure 2.1).

A significant elevation of the chymotrypsin-like activity was observed after 24 hours of

TGF-β treatment, which further increased within 48 hours compared to untreated fibroblasts (Figure 3.1A). This activation of the proteasome by TGF-β could be counteracted by subsequent treatment with the proteasome inhibitor bortezomib for 1.5 hours before cell lysis, confirming the specificity of the activity assay for the proteasome (Figure 3.1B).
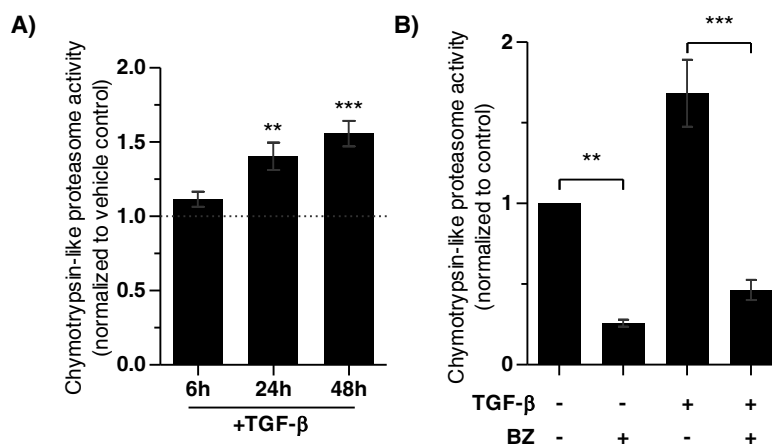

Figure 3.1: TGF-β increases proteasome activity in lung fibroblasts
CT-L activity in cell lysates of CCL-206 fibroblasts treated with TGF-β for (**A**) 6h, 24h and 48h (Mean ± SEM. n=4 for 6h and 24h, n=7 for 48h. One-way ANOVA, Dunnett's Multiple Comparison Test) or for (**B**) 48h and additional incubation with bortezomib (BZ) 10 nM for 1.5h (Mean ± SEM. n=4. One-way ANOVA, Bonferroni's Multiple Comparison Test).

Levels of proteins, which are tagged with K48-linked polyubiquitin chains, were measured by Western blot analysis as their accumulation here can be regarded as an indicator for induced protein degradation in response to elevated protein turnover. Therefore, a significant increase in K48-polyubiquitinated proteins in response to 48 hours of TGF-β treatment here confirmed TGF-β-induced activation of proteasomal substrate turnover (Figure 3.2).

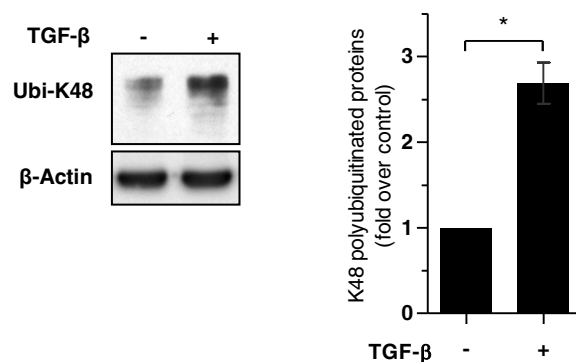**Figure 3.2. TGF-β increases protein turnover in CCL-206 fibroblasts**
Western blot and densitometric analysis of hypoosmotic lysates of CCL-206 fibroblasts treated with TGF-β for 48h (Mean ± SEM. n=3. Paired t-test).

3.1.1 TGF-β increases formation of highly active 26S/30S proteasomes

To dissect different proteasome complexes, native gel analysis was performed. Hypoosmotic lysates were loaded on native gels and electrophoresis was performed at 4°C. In this setup, proteasomes are separated as native, functional, whole complexes and their enzymatic activity can be assayed (Elsasser et al., 2005). In-gel proteasome activity can be assessed by overlay of gels with fluorogenic substrates. Proteasome activity was visualized by enzymatic cleavage of the chymotrypsin-like site-specific substrate Suc-LLVY-AMC, which, upon cleavage, releases the fluorophore 7-amino-4-methylcoumarin in a similar manner as described for the luminogenic substrates before (Figure 2.1). Using this method, different proteasome complexes (30S, 26S and 20S complexes) could be separated. In a next step, gels were immunoblotted for the α1-7 subunits of the 20S CP and 19S ATPase Rpt5. In TGF-β stimulated cells, a significant increase in formation of highly active 26S and 30S complexes was observed, which might contribute to the previously observed elevation of protein degradation rates by the proteasome (Figure 3.3).
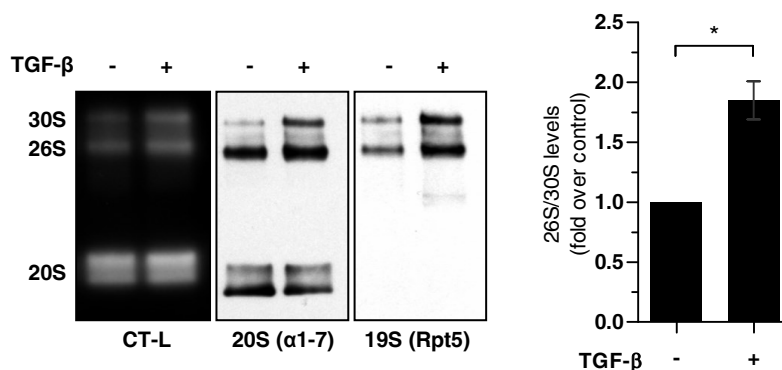

Figure 3.3. TGF-β increases formation of highly active 26S and 30S proteasomes
Native gel analysis and immunoblotting of hypoosmotic cell lysates of CCL-206 fibroblasts after treatment with TGF-β for 48h and densitometric analysis of 26S/30S complexes obtained from α1-7 immunoblots (Mean ± SEM. n=3. Paired t-test).

3.1.2 Formation of 26S/30S proteasomes is regulated by the 19S subunit Rpn6

In a next step, it was analyzed whether Rpn6, a 19S subunit which is rate-limiting for 26S formation (Vilchez, Boyer, et al., 2012; Vilchez, Morantte, et al., 2012), might also mediate TGF-β-induced assembly of 26S and 30S proteasome complexes.

Expression of Rpn6, Rpt5 and α1-7 subunits was analyzed by Western blot. Rpn6 protein levels were clearly increased after 48 hours of TGF-β treatment. This induction was not observed for the 19S ATPase subunit Rpt5 or the 20S subunits α1-7 (Figure 3.4A). Furthermore, immunofluorescence staining showed an increased cytoplasmic distribution of Rpn6 in TGF-β treated lung fibroblasts (Figure 3.4B)
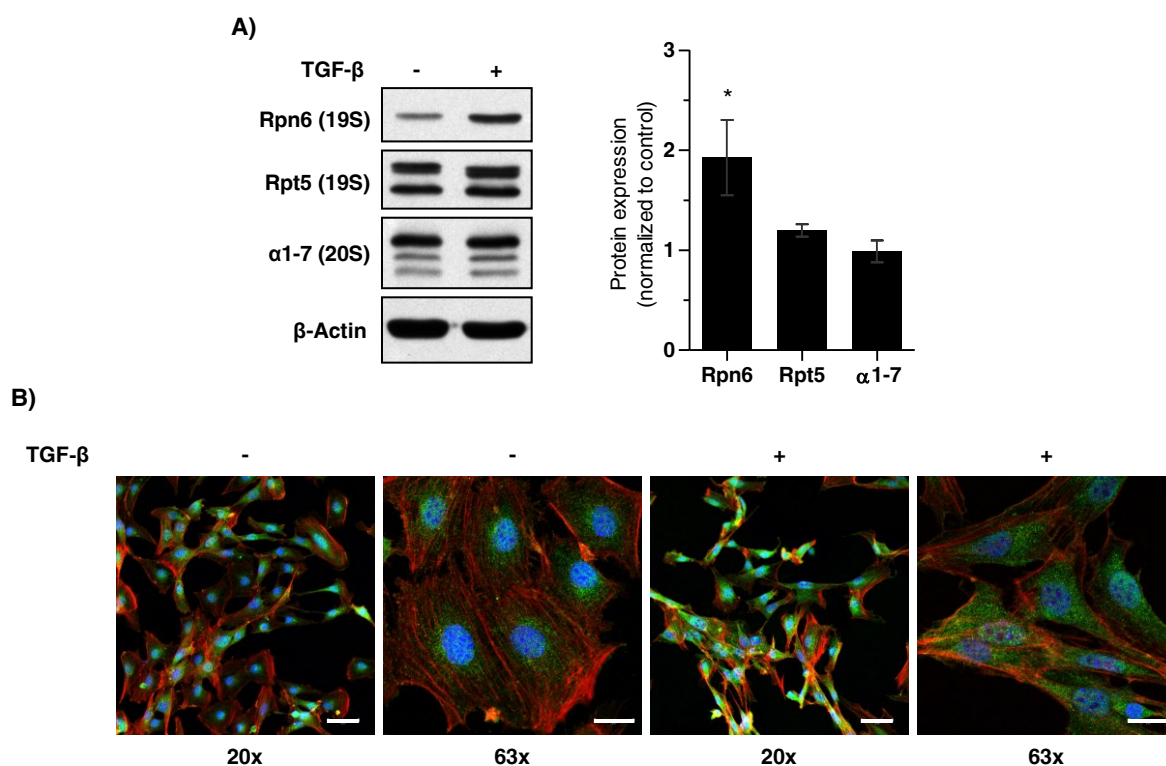
Figure 3.4. TGF-β increases expression of Rpn6
(**A**) Western blot and densitometric analysis of hypoosmotic cell lysates of CCL-206 fibroblasts treated with TGF-β for 48h (Mean ± SEM. n=3. One-way ANOVA, Dunnett's Multiple Comparison Test). (**B**) Immunostaining of CCL-206 fibroblasts after treatment with TGF-β for 48h. Green: Rpn6; red: Phalloidin (F-actin); blue: Dapi (Nucleus) (scale bars for 20x=50 µm and 63x=20 µm).

To validate whether Rpn6 is involved in TGF-β mediated formation of 26S and 30S proteasomes, a partial knockdown of Rpn6 was performed in CCL-206 murine lung fibroblasts and proteasome complexes were analyzed in response to 48 hours of TGF-β treatment. Partial knockdown of approximately 40% of Rpn6 was well tolerated (Figure 3.5A and B) whereas higher knockdown efficiencies resulted in cell death (data not shown), which is probably

triggered by the incapacity of the cell to provide enough 26S/30S proteasomes for protein degradation.

Figure 3.5. Rpn6 mediates formation of 26S and 30S proteasomes
(**A**) Western blot of hypoosmotic cell lysates of CCL-206 fibroblasts after knockdown of Rpn6 followed by treatment with TGF-β for 48h and densitometric analysis of Rpn6 protein expression (Mean ± SEM. n=4. One-way ANOVA Bonferroni's Multiple Comparison Test). (**B**) Morphological changes of CCL-206 fibroblasts after Rpn6 silencing and TGF-β treatment. (**C**) Native gel analysis and immunoblotting of hypoosmotic cell lysates of CCL-206 fibroblasts after Rpn6 knockdown and treatment with TGF-β for 48h.

Partial knockdown of Rpn6 effectively counteracted TGF-β induced upregulation of Rpn6 compared to control cells which had been transfected with scrambled siRNAs (Figure 3.5A). Moreover, Rpn6 silencing neutralized TGF-β-mediated assembly of 26S and 30S proteasome complexes, as determined by native gel activity assay and subsequent immunoblot analysis (Figure 3.5C). These data strongly propose that TGF-β induced upregulation of Rpn6 mediates increased assembly of 26S and 30S proteasome complexes. Higher amounts of 26S/30S proteasomes might be necessary during TGF-β mediated myofibroblast differentiation to adjust rates of ubiquitin-dependent protein degradation for a rapid disposal of unneeded proteins.

3.1.3   26S proteasome activity is reversibly increased during fibrotic remodeling

After verification of Rpn6 as a regulator of TGF-β-stimulated proteasome activation, proteasome activities were assayed in the bleomycin mouse model of lung fibrosis.

In this study, whole lung tissue was assayed at day 7 (inflammatory phase), day 14 (fibrotic phase), and day 56 (physiologic state after resolution of fibrosis) after bleomycin instillation. Lung function was performed to monitor fibrotic remodeling and resolution of fibrosis and showed a significant decline during inflammation and ongoing fibrotic remodeling at day 7 and in fibrotic lungs at day 14 post-bleomycin. Lung function was restored after resolution of fibrosis at day 56 (Figure 3.6A).

To further validate fibrosis development at day 14 after bleomycin challenge, qRT-PCR was performed and significant elevation of mRNA levels of the fibrotic marker collagen I and fibronectin confirmed induction of fibrosis (Figure 3.6B).

Proteasome activities were measured in whole lung lysates and revealed a pronounced increase in substrate cleavage by all three active sites during the early inflammatory phase at day 7 and in fibrotic lungs at day 14. This increase in proteasome activities, however, normalized to levels of control animals at day 56 when fibrosis was resolved (Figure 3.7A, B, and C).

Alterations in proteasome activities thus closely followed the course of adaptive lung damage and lung function decline in bleomycin-induced lung fibrosis. Native gel analysis of fibrotic lungs at day 14 showed that the observed increase in proteasomal activities was due to enhanced formation of 26S/30S proteasome complexes as corroborated by immunoblotting for the catalytic 20S subunit β1 and the 19S subunits Rpt5 and Rpn6 (Figure 3.7D).
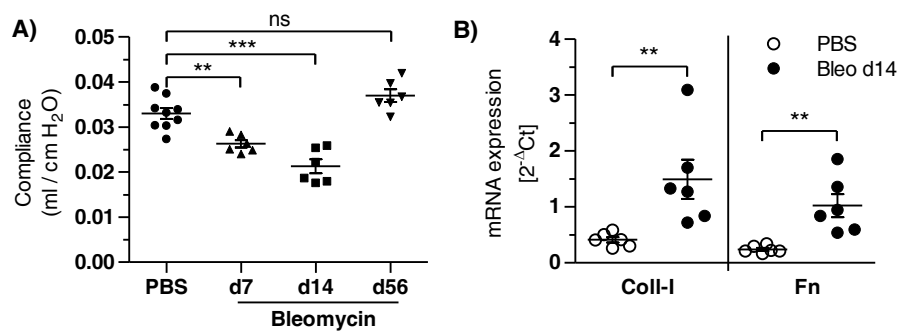
Figure 3.6. Lung function and gene expression of profibrotic markers in the bleomycin mouse model
(**A**) Compliance measurement at day 7, 14 and 56 after bleomycin treatment of C57BL/6N (Mean ± SEM. n=5-9 per group. Two-tailed Mann Whitney Test). (**B**) qRT-PCR analysis of whole lung tissue at day 14 after bleomycin challenge (Mean ± SEM. n=6 per group. Two-tailed Mann Whitney Test). Compliance measurement was performed by Isis Fernandez (Scientist CPC, 2014).
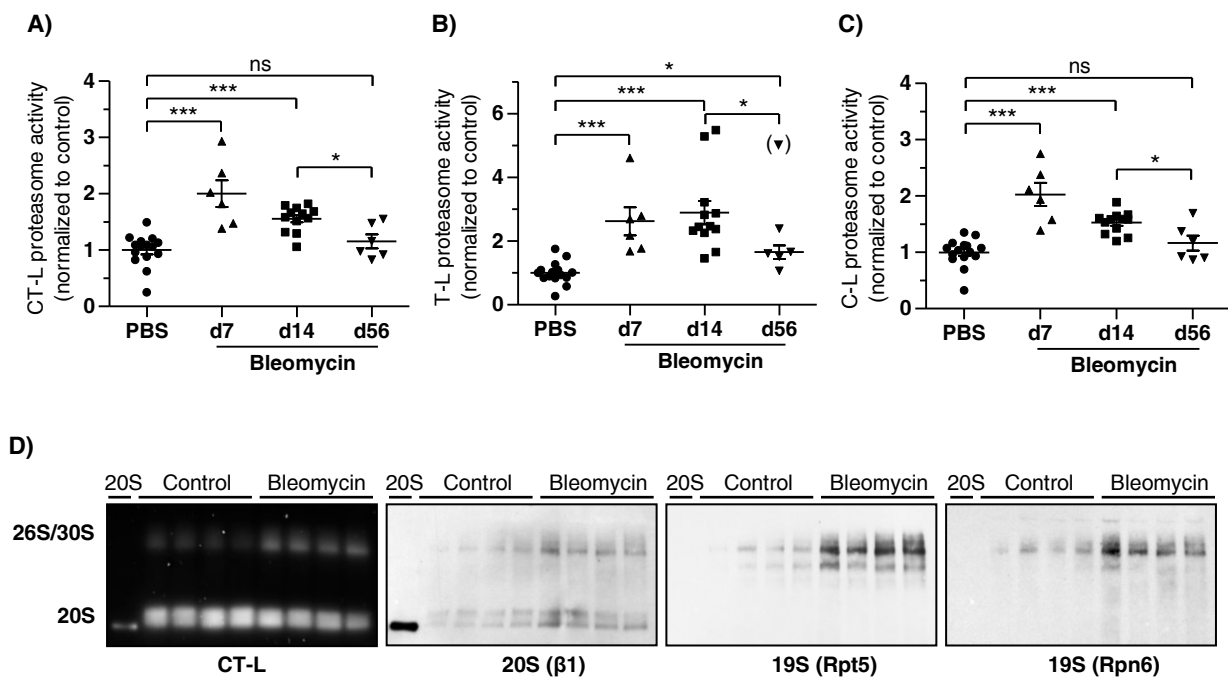
Figure 3.7. Proteasome activities are increased in bleomycin-induced pulmonary fibrosis
Proteasome activities of the (**A**) CT-L, (**B**) T-L and (**C**) C-L active sites in hypoosmotic lysates of whole lung tissues of C57BL/6N mice 7, 14 and 56 days after treatment with bleomycin (Mean ± SEM. n=5-15 per group. Two-tailed Mann Whitney Test, Dixons outlier test was performed and outlier is shown in brackets). (**D**) Native gel analysis and immunoblotting of hypoosmotic lysates of whole lung tissue at day 14 post-bleomycin

Moreover, Western blot analysis of these tissue lysates revealed significant upregulation of only Rpn6 in fibrotic mouse lungs while expression of 20S and other singular 19S subunits was not altered (Figure 3.8).
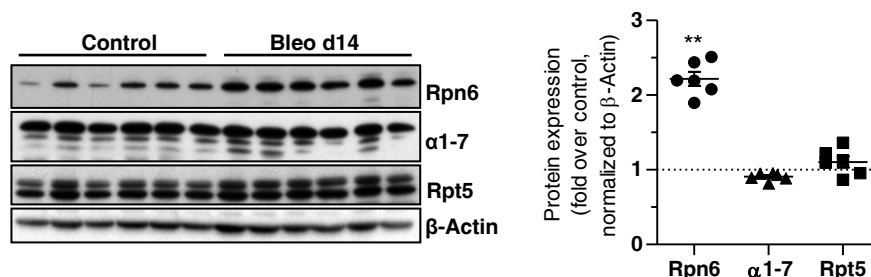
Figure 3.8. Rpn6 expression is increased in fibrotic lungs
Western blot and densitometric analysis of hypoosmotic lysates of whole lung tissue of C57BL/6N mice 14 days after bleomycin instillation (Mean ± SEM. n=6 per group. Two-tailed Mann Whitney Test). Western blot was performed by Vanessa Welk (PhD student CPC, 2014).

To investigate a possible transcriptional regulation of the proteasome, qRT-PCR of several proteasome genes, including Rpn6, was performed in whole lung tissue of fibrotic animals 14 days after bleomycin challenge. None of the investigated mRNAs coding for several 19S or 20S subunits revealed significant elevation in fibrotic mouse lungs suggesting that the increase in Rpn6 protein levels might be induced via protein stabilization rather than transcriptional regulation.

Figure 3.9. mRNA expression of several proteasomal subunits is not altered in bleomycin-induced pulmonary fibrosis
qRT-PCR of whole lung tissue of animals 14 days after bleomycin instillation compared to PBS-treated controls (Mean ± SEM. n=6 per group. Two-tailed Mann Whitney Test).

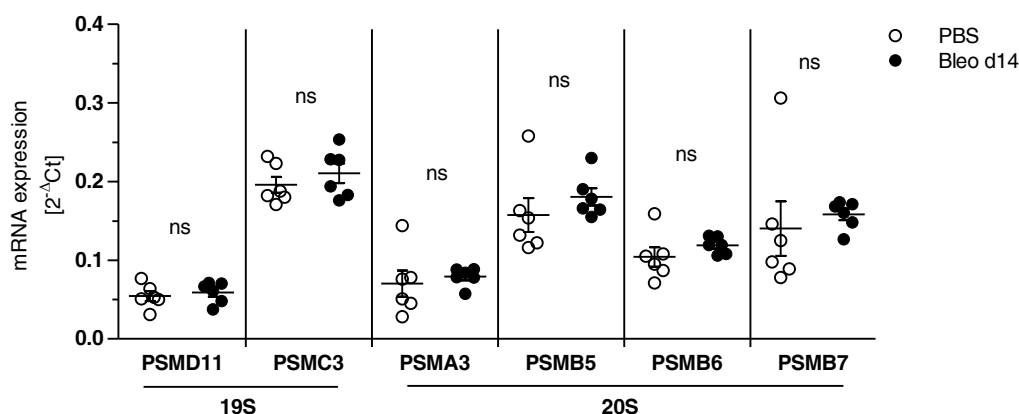To assess the dynamics and cellular source of Rpn6 expression in the course of reversible fibrotic remodeling, cellular composition of the lungs and expression of Rpn6 at days 7, 14 and 56 after bleomycin instillation were analyzed in detail (Figure 3.10).

For that, detailed histological analysis on the cellular composition of the lungs was performed. Serial sections of PBS control lungs and of lungs 7, 14 and 56 days after bleomycin challenge were Masson-Goldner stained for overall collagen deposition and extent of fibrosis, and immunostaining was performed for Rpn6, αSMA (myofibroblast and smooth muscle cell marker), and NK2 homeobox 1 (NKX2-1), also known as thyroid transcription factor 1 TTF1 (marker for AECII and bronchiolar Clara cells). This analysis revealed a strikingly altered cellular composition of mouse lungs at days 7 and 14 after bleomycin challenge, which normalized almost completely to a physiological lung structure at day 56: While the histology of healthy lungs of PBS-treated control animals showed little collagen deposition and very low levels of Rpn6 expression, beginning of fibrotic remodeling, indicated by increased collagen deposition, was observed 7 days after bleomycin challenge. In addition, a pronounced increase in proliferation of AECII cells and bronchial Clara cells, a typical feature of fibrotic remodeling (Korfei et al., 2011), was observed. Interestingly, these highly active proliferating cells also showed pronounced expression of Rpn6 in the nucleus and cytoplasm. Inflammatory cells were also detectable at this time point, but they expressed only moderate levels of Rpn6. These data indicate that increased proteasome activity at day 7 might be mediated by highly proliferating AECII, which are widely regarded as key drivers of fibrotic remodeling in response to lung injury (King et al., 2011; Wynn, 2011). During the fibrotic phase at day 14 after bleomycin challenge, dense fibrosis was observed with strong deposition of collagen in the interstitial area. Hyperplastic AECII were found to be surrounded by dense fibrosis and strongly overexpressed Rpn6. Myofibroblasts were present as well and partially stained positive for Rpn6. Inflammatory lymphocytes showed also some expression of Rpn6.

These data thus demonstrate that Rpn6 expression is upregulated in epithelial and fibroblast effector cells of reversible wound healing in the bleomycin model of lung fibrosis. Expression closely follows the course of proteasome activity suggesting that increased 26S/30S proteasome activity is responsible for the observed activation of the proteasome as shown for fibrotic lungs at day 14.
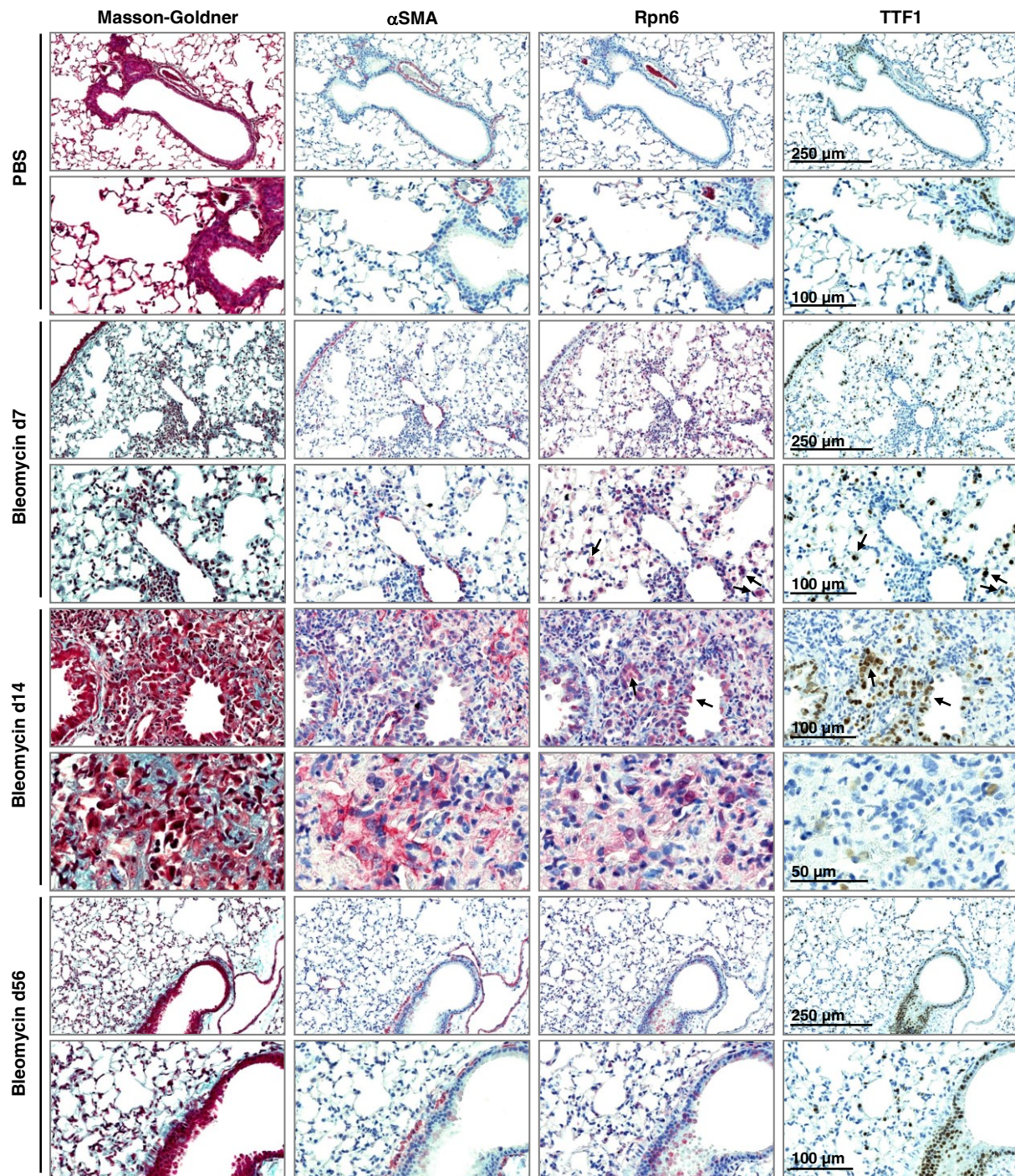
Figure 3.10. Rpn6 expression is upregulated in hyperplastic AECII, Clara cells and myofibroblasts during reversible fibrotic remodeling in bleomycin-induced pulmonary fibrosis

Paraffin embedded lung sections of PBS-treated control animals or animals, which were sacrificed 7, 14 or 56 days post-bleomycin, were analyzed by Masson-Goldner staining for fibrotic remodeling (red: keratin and muscle fibres; blue/green: collagen; pink: cytoplasm; brown/black: nucleus). Expression of αSMA (myofibroblasts and smooth muscle cells) and Rpn6 is indicated in red and expression of TTF1 (AECII and Clara cells) in brown color (arrows indicate Rpn6 positive hyperplastic AECII cells). Pictures show representative stainings from 3-6 animals per group. Staining was performed by Martina Korfei (Scientist UGMLC, 2014).

3.1.4   Rpn6 levels are upregulated in IPF lungs

To investigate whether Rpn6 upregulation might also be relevant in IPF, fibrotic lung tissue samples of IPF patients were analyzed for expression of proteasome subunits. To confirm fibrosis in these samples, qRT-PCR analysis of fibrotic marker Acta (coding for αSMA) and collagen I was performed and showed a significant increase in lung tissue of IPF patients (Figure 3.11).

Figure 3.11. Gene expression of profibrotic marker in IPF lungs
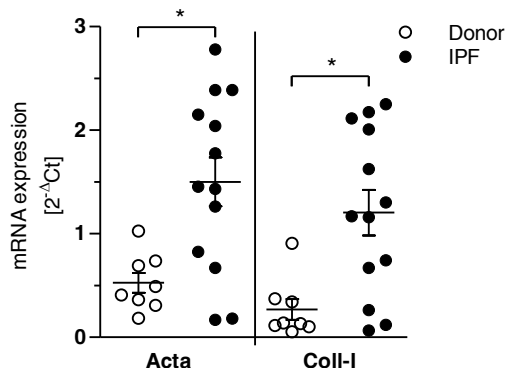qRT-PCR analysis of whole lung tissue samples of 8 donors and 13 IPF patients (Mean ± SEM. n=8 donors and n=13 IPF patients. Two-tailed Mann Whitney Test).

The fibrotic marker αSMA was also used to reconfirm fibrosis in IPF lung tissue on protein level (Figure 3.12A). Indeed, Western blot analysis revealed a significant upregulation of Rpn6 and also Rpt5 in lung tissue of IPF patients compared to donor lungs. Expression of the 20S subunit α3, however, was not altered. Furthermore, levels of K48-ubiquitinated proteins were highly increased in IPF lungs (Figure 3.12A) and positively correlated with Rpn6 expression (Figure 3.12B), indicating an elevated protein turnover in fibrotic lungs, which might be connected to higher expression levels of Rpn6 levels.

To further investigate a possible regulation of proteasome function in fibrotic lungs, proteasome activity was assayed in donor and IPF lung tissues. For that, the proteasome activity-based probe (ABP) MV151 (Cravatt et al., 2008) was used and combined with native gel analysis to resolve the different complexes. ABPs covalently bind to the active sites of the proteasome and can be detected by their attached fluorescent tag, thus allowing quantification of active proteasome complexes. Proteasome activity was neither consistently inhibited nor activated in IPF lungs compared to donor tissue (Figure 3.13A), but in IPF samples, Rpn6 levels positively correlated with formation of 26S/30S proteasomes (Figure 3.13B). This was not evident in donor

samples and suggests some distinct activation of 26S proteasome activity in diseased IPF lungs.
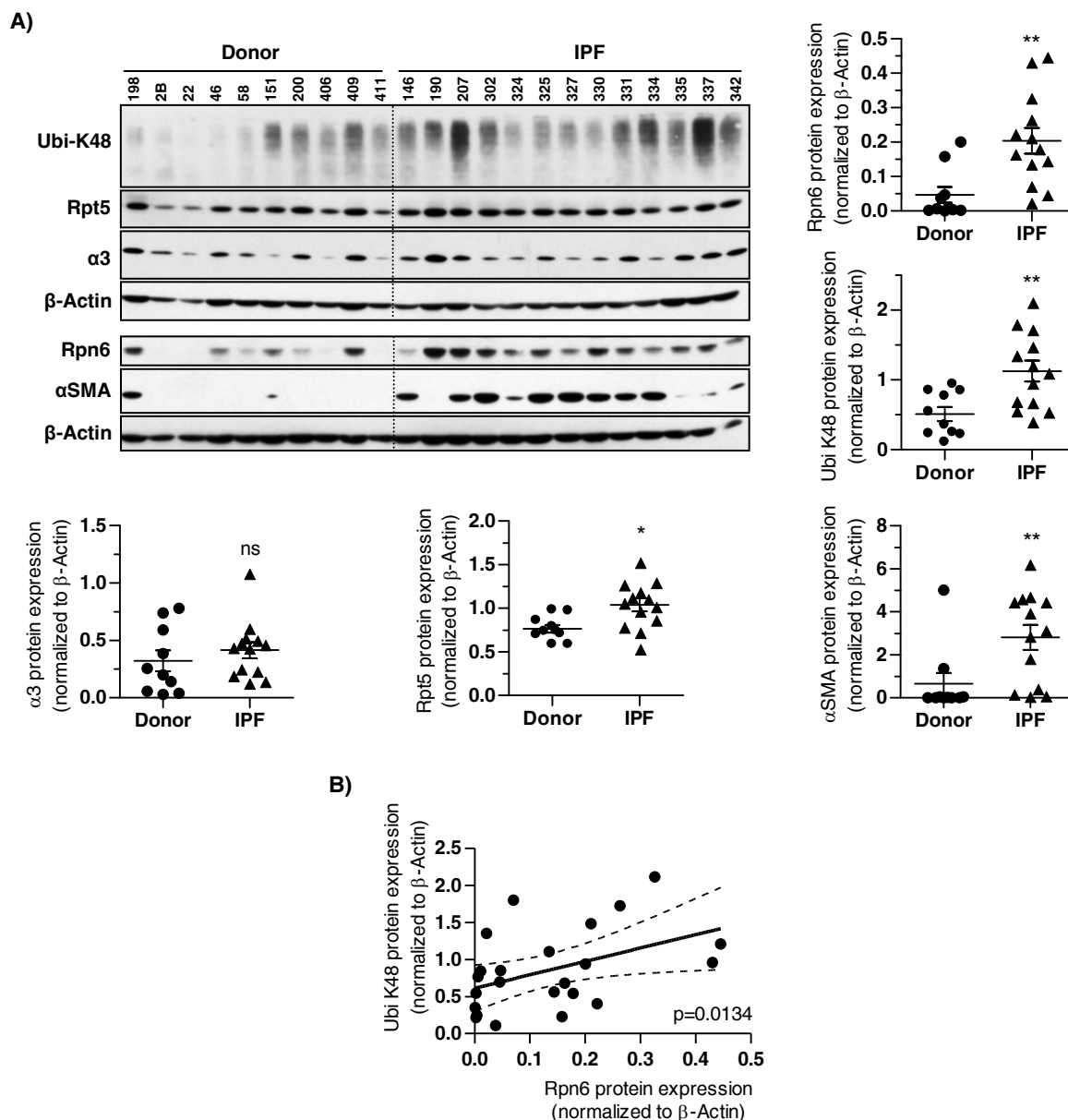
Figure 3.12. Expression of Rpn6 and K48-polyubiquitinated proteins is increased in human IPF lungs
(**A**) Western blot analysis of RIPA lysates of whole lung tissue of donor and IPF lungs. Expression of Rpn6, Rpt5, K48-polyubiquitinated proteins, αSMA, and the α3 subunit of the 20S proteasome was quantified by densitometry after normalization to β-actin (Mean ± SEM. n=11-13 per group. Two-tailed Mann Whitney Test). (**B**) Correlation analysis of normalized expression of K48-polyubiquitinated proteins and Rpn6 obtained from the Western blot data. Donor and IPF values were pooled (Two-tailed Spearman correlation, r=0.5079, p=0.0134). Western blot was performed by Vanessa Welk (PhD student CPC, 2014).
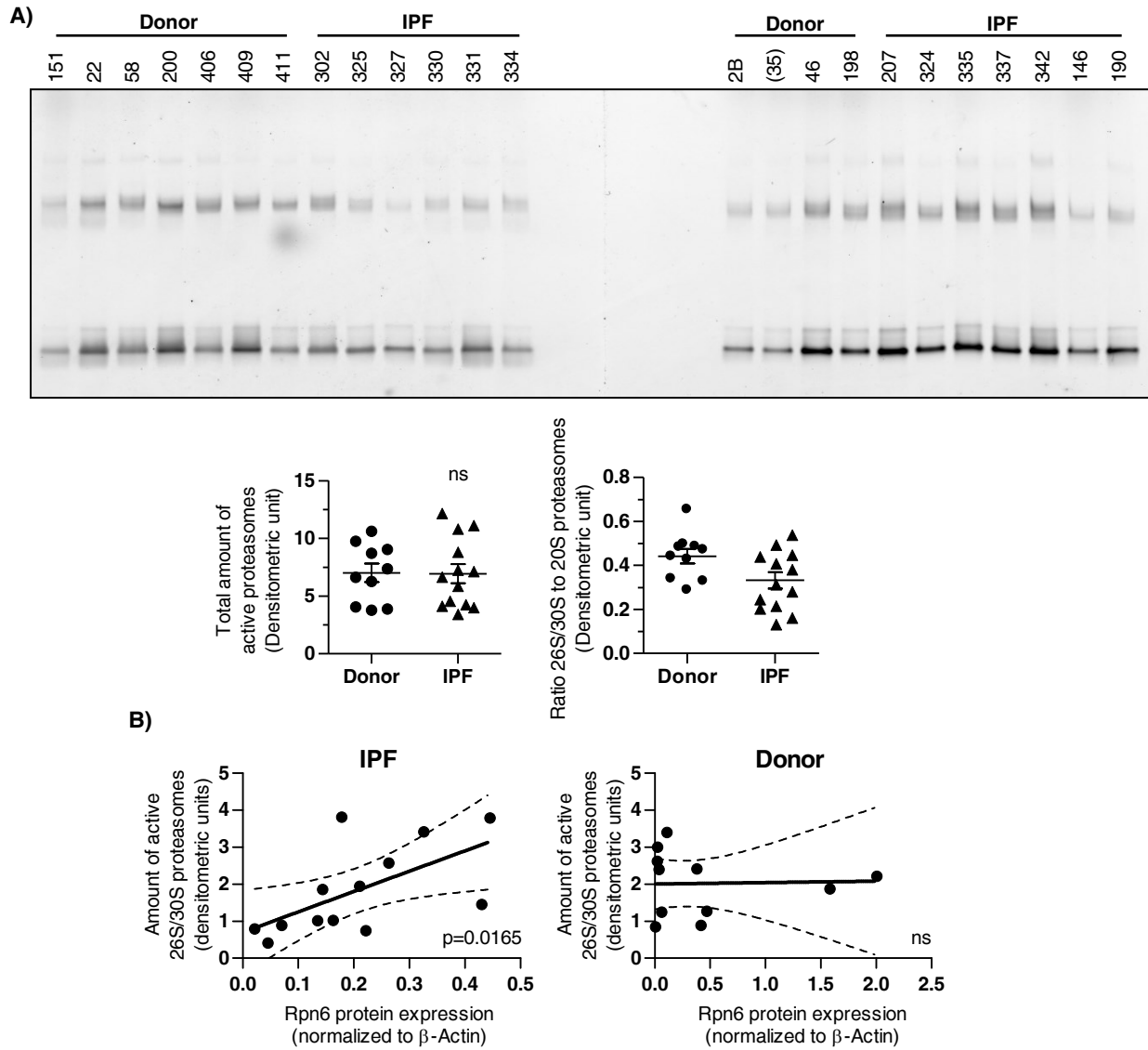
Figure 3.13. Rpn6 expression correlates with formation of active 26S/30S proteasomes in IPF lungs
(**A**) ABP-labeling of proteasomes in whole lung extracts and subsequent native gel analysis (Donor 35 was excluded from analysis as a case of chronic thromboembolic pulmonary hypertonia). Samples were labeled and run in parallel on two gels and imaged at the same time to allow for comparable exposure and densitometric analysis of signals (Mean ± SEM. n=10 donors and n=13 IPF patients. Two-tailed Mann Whitney Test). (**B**) Separate correlation analysis of donor and IPF lungs for the amount of active 26S/30S proteasomes as obtained from densitometric analysis of ABP native gel analysis and β-actin normalized Rpn6 expression levels obtained from the Western blot (Figure 3.12) (Two-tailed Spearman correlation, IPF r=0.6484, p=0.0165; Donor r=-0.1273, p=0.7092). Native gel blot was performed by Vanessa Welk (PhD student CPC, 2014).

Increased Rpn6 expression in IPF lung tissue was further confirmed by histological analysis of donor and IPF lungs. Here, Rpn6 levels were highly elevated in pathologic myofibroblasts, abnormal hyperplastic basal cells, and smooth muscle cells, as revealed by co-staining with αSMA and the basal cell marker keratin 5 (KRT5), respectively (Figure 3.14).
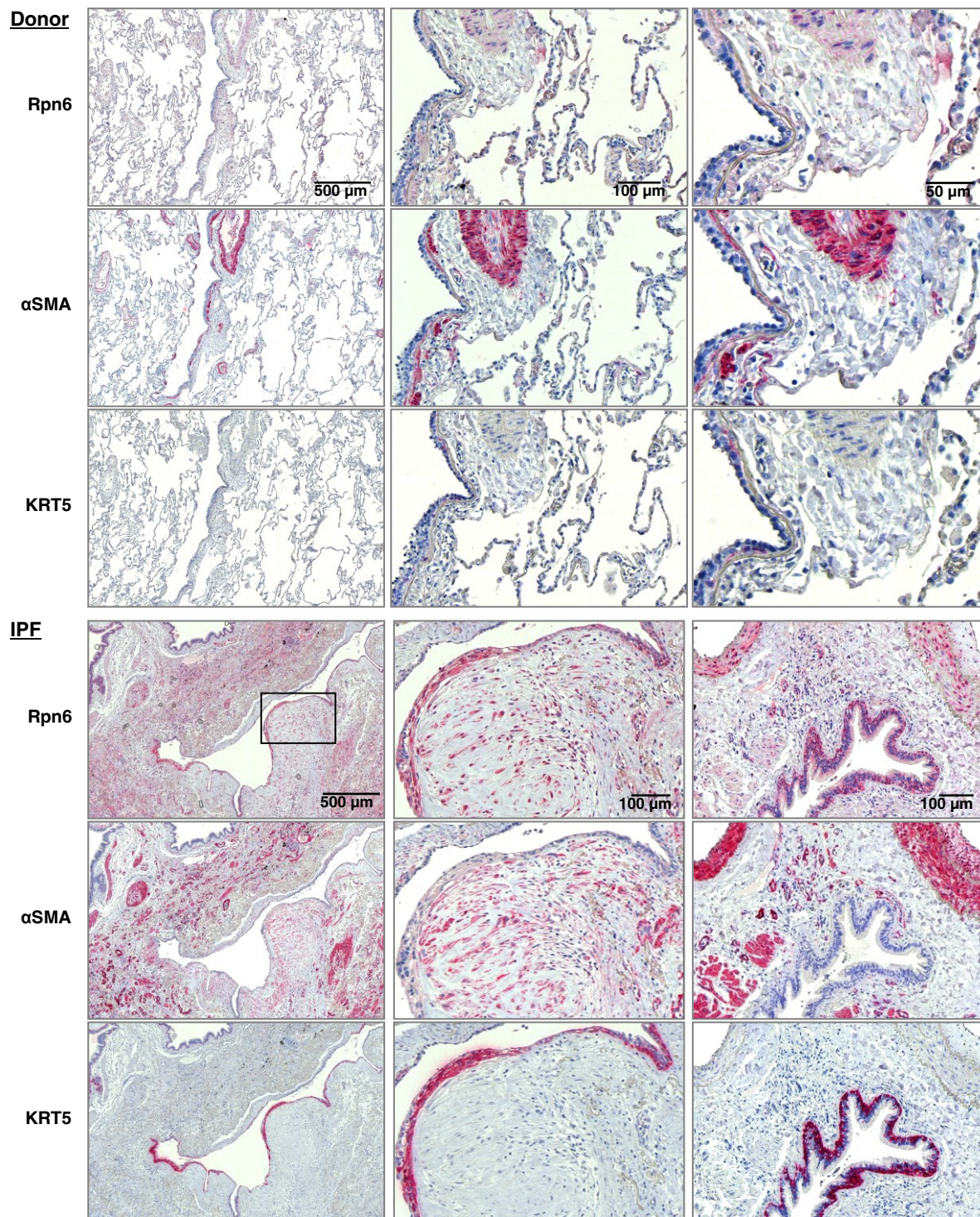
Figure 3.14. Rpn6 is elevated in myofibroblasts and hyperplastic basal cells in human IPF lungs
Immunohistochemistry of paraffin-embedded donor and IPF lung tissues stained for Rpn6, KRT5 (basal cells), or αSMA (smooth muscle cells and myofibroblasts). Pictures show representative stainings of 10 IPF and 6 donor lungs. (red: Rpn6, αSMA, and KRT5; blue: Nuclei). Staining was performed by Martina Korfei (Scientist UGMLC, 2014).

Myofibroblasts and abnormal basal cells are hallmarks of pulmonary remodeling in IPF and not present in healthy donor lungs (Korfei et al., 2011). Therefore, non-fibrotic lungs of organ donors showed an overall weak expression of Rnp6 with higher level mainly in smooth muscle cells (Figure 3.14).

Co-staining for K48-linked polyubiquitin revealed accumulation of polyubiquitinated proteins mainly in myofibroblasts and hyperplastic basal cells of IPF lungs. These cells also showed increased Rpn6 expression suggesting an enhanced turnover of polyubiquitinated proteins in areas of active fibrotic remodeling (Figure 3.15). In contrast to that, K48-linked polyubiquitinated proteins were hardly present in donor lungs.
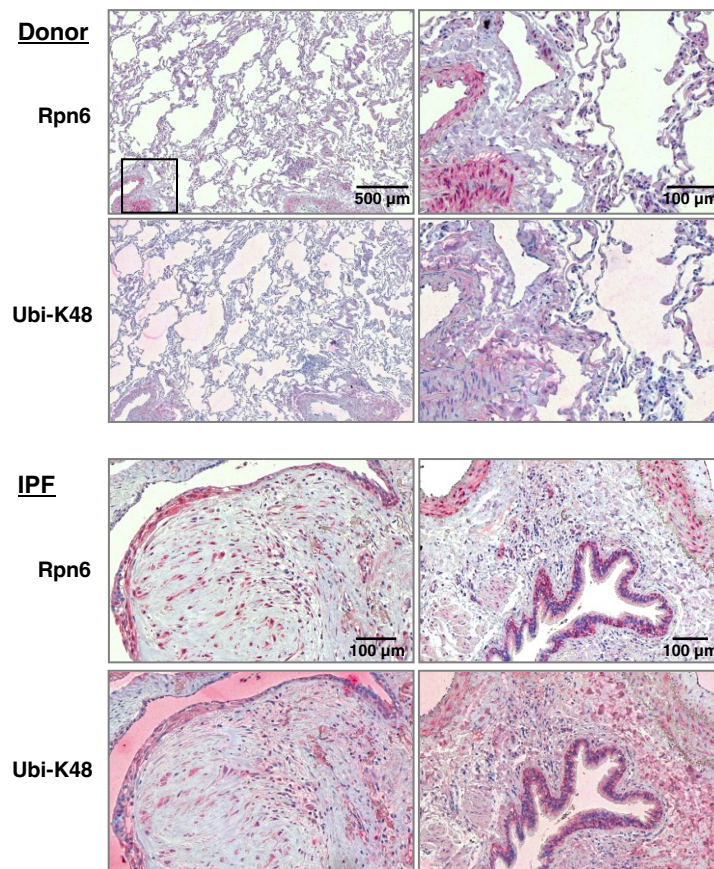
Figure 3.15. Levels of K48-polyubiquitinated proteins are increased and correlate with Rpn6 upregulation in myofibroblasts and hyperplastic basal cells in human IPF lungs
Immunohistochemistry of donor and IPF lungs stained for Rpn6 and K48-polyubiquitinated proteins (Ubi-K48) (red: Rpn6 and Ubi-K48, blue: Nuclei). Staining was performed by Martina Korfei (Scientist UGMLC, 2014).

To validate a possible transcriptional regulation of proteasomal genes in IPF, qRT-PCR analysis was performed for several subunits of the 19S and 20S proteasome (Figure 3.16). Confirming RNA data obtained from the bleomycin mouse model, no significant changes on mRNA level were observed in whole lung tissue samples of donors and IPF patients. This finding again points towards a posttranscriptional regulation of Rpn6.
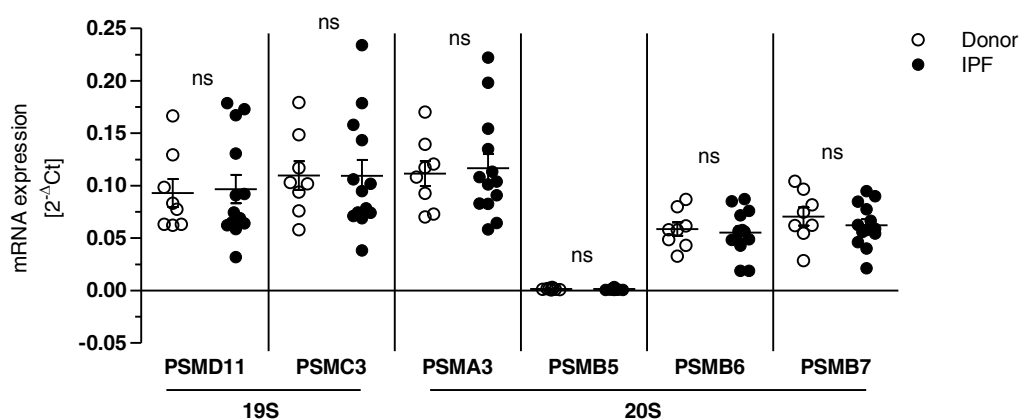
Figure 3.16. mRNA expression of proteasome subunits is not significantly altered in IPF lungs
qRT-PCR analysis of whole lung tissue of donor and IPF lungs (Mean ± SEM. n=8 donors and n=13 IPF patients per group. Two-tailed Mann Whitney Test).

Enhanced levels of Rpn6 together with increased accumulation of polyubiquitinated proteins in tissue samples of IPF patients indicate increased protein turnover along with an overall upregulation of the ubiquitin-proteasome system in fibrotic IPF lungs. Further, elevated levels of Rpn6 and polyubiquitinated proteins in myofibroblasts and hyperplastic basal cells of IPF lungs propose an important role of increased protein turnover in these highly active cells, which might contribute to the pathogenesis of this disease.

3.1.5   Silencing of Rpn6 counteracts profibrotic remodeling of human lung fibroblasts

Next, it was investigated whether Rpn6-mediated induction of 26S/30S proteasome formation and increase in overall proteasome activity is involved in the implementation of TGF-β-mediated profibrotic effects like myofibroblast differentiation and proliferation. Treatment with TGF-β significantly induced proliferation of CCL-206 fibroblasts within 24 hours as shown by increased incorporation of BrdU into the DNA. Knockdown of Rpn6 alone had no effects on cellular growth but efficiently counteracted TGF-β-mediated induction of proliferation (Figure 3.17).
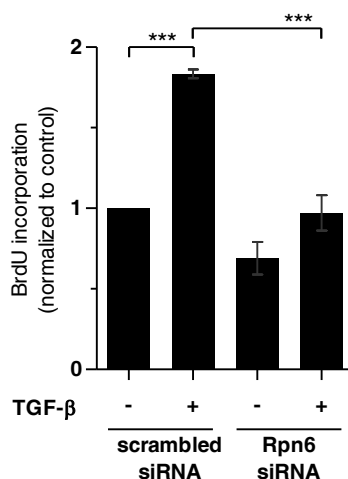
Figure 3.17. Rpn6 knockdown counteracts TGF-β mediated induction in proliferation
BrdU assay of CCL-206 fibroblasts treated for 48h with TGF-β starting 24h after Rpn6 knockdown (Mean ± SEM. n=3. One-way ANOVA, Bonferroni's Multiple Comparison Test).

Further experiments were performed in primary human lung fibroblast lines prepared from six healthy organ donors to perform specific Rpn6 knockdown in the absence and presence of TGF-β. Prior to these experiments Rpn6 siRNA was titrated to find an optimal well tolerated and non-toxic dose as a high knockdown efficiency and therefore extensive destruction of 26S/30S complexes resulted in increased cell death and morphological changes like elongation or formation of stress fibres (Figure 3.18).

Partial Rpn6 knockdown of approximately 40% of physiological protein levels was achieved by transfection with a final concentration 0.5 nM siRNA and well tolerated by the cells as indicated by minor morphological changes (Figure 3.18).

Knockdown experiments in phLF were conducted using a single siRNA and single control siRNA or a pool of three siRNAs and a pool of two control siRNAs at a final concentration of 0.5 nM to counteract Rpn6 expression. Information about the particular siRNA treatment is

given in each figure legend.
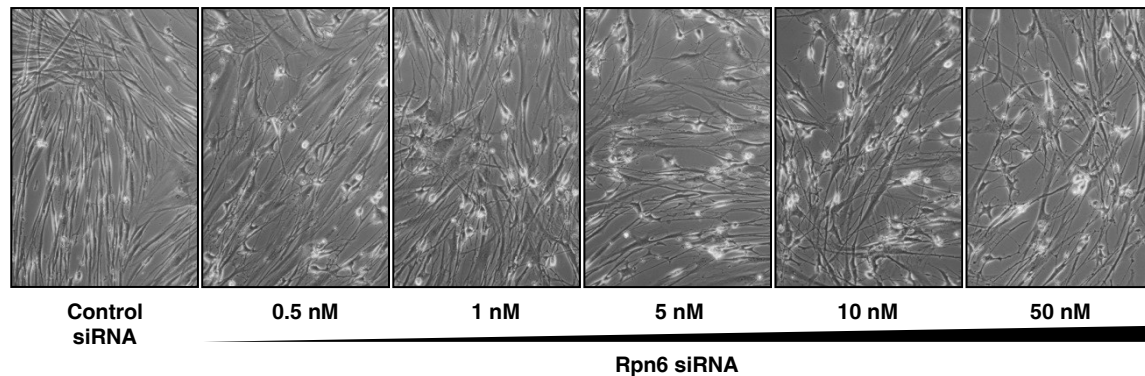
Figure 3.18. Morphological changes of primary human lung fibroblasts in response to Rpn6 knockdown
phLF were transfected with different final concentrations of Rpn6 siRNA (single siRNA) and analyzed 72h after transfection.

40% reduction of Rpn6 already showed impairment of basal expression of the profibrotic marker collagen I and induced G1 cell cycle arrest as indicated by a clear increase in cyclin D1 (Figure 3.19). This is well in accordance with the growth inhibitory effects observed upon silencing of Rpn6 in CCL-206 murine lung fibroblast as detected by BrdU incorporation before (Figure 3.17). Furthermore, accumulation of K48-polyubiquitinated proteins in response to Rpn6 knockdown confirmed reduced 26S/30S proteasome activity as a direct effect of impaired 26S/30S formation (Figure 3.19).
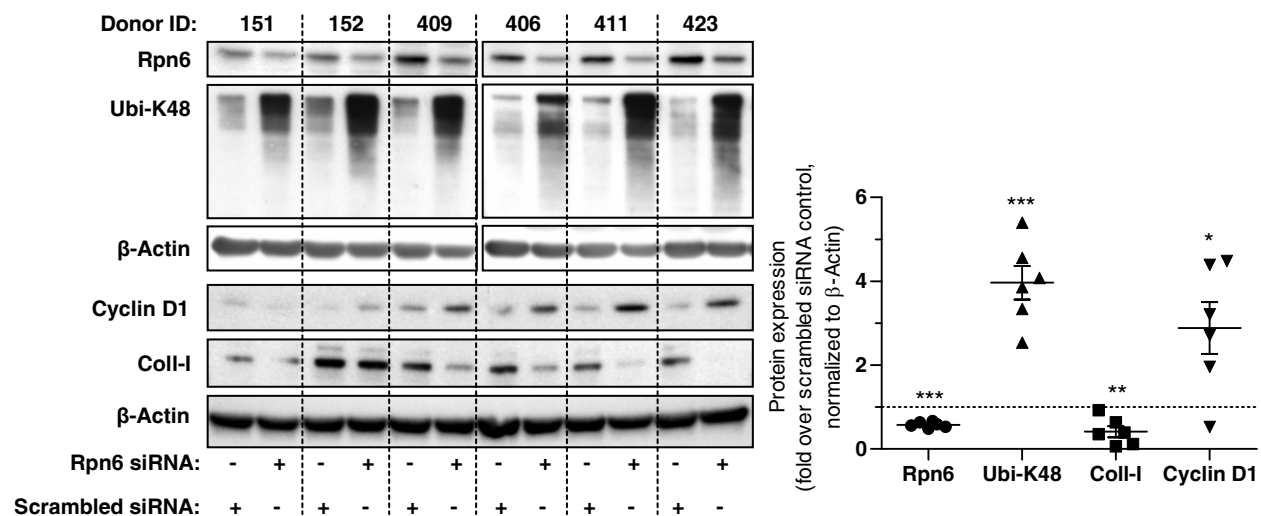
Figure 3.19. Rpn6 silencing reduces basal expression of myogenic marker in phLF
Western blot and densitometric analysis of unstimulated primary human lung fibroblasts after partial knockdown of Rpn6 (single siRNA) (Mean ± SEM. n=6. Paired t-test, two-tailed).

To investigate whether Rpn6 silencing also counteracts TGF-β induced profibrotic effects, phLF were stimulated with TGF-β for 48 hours after Rpn6 knockdown. Knockdown efficiency was controlled on mRNA level. Rpn6 (here named PSMD11 to refer to the gene name) was significantly increased on mRNA level in response to TGF-β and could efficiently be knocked down by siRNAs to about 60% of baseline levels (Figure 3.20).
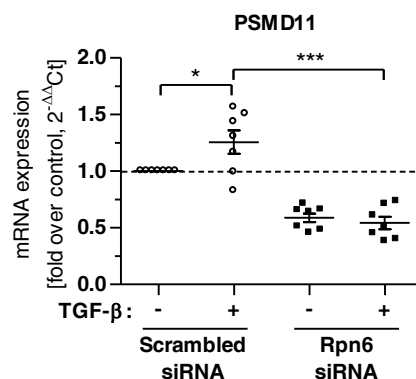
Figure 3.20. TGF-β mediated increase in mRNA levels of Rpn6 can efficiently be counteracted by siRNA knockdown
mRNA expression of Rpn6 (gene name PSMD11) of donor phLF stimulated with TGF-β for 48h starting 24h after Rpn6 knockdown (Mean ± SEM. n=7. One-way ANOVA, Bonferroni's Multiple Comparison Test).

Native gel analysis was performed and confirmed TGF-β-mediated induction of 26S/30S formation in phLF (Figure 3.21). Furthermore, 26S/30S formation could efficiently be counteracted by knockdown of Rpn6.
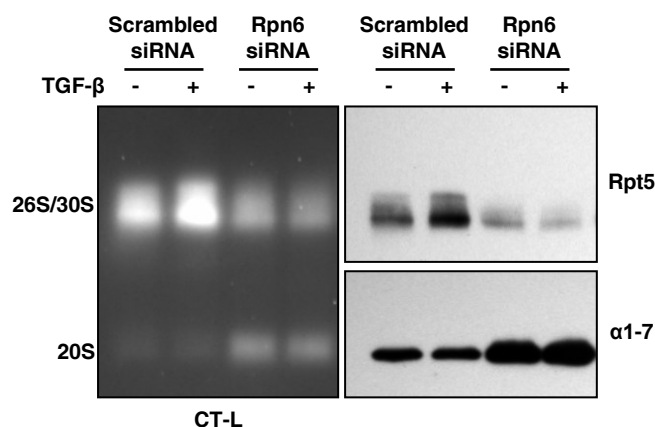
Figure 3.21. Rpn6 knockdown counteracts TGF-β induced formation of 26S/30S proteasomes
Native gel analysis of CT-L proteasome activity and immunoblotting for Rpt5 and α1-7 (pool of three siRNAs) (n=3, representative gel is shown). Native gel was performed by Vanessa Welk (PhD student CPC, 2014).

qRT-PCR analysis for mRNA expression of profibrotic genes was performed to investigate whether Rpn6 knockdown might counteract profibrotic effects of TGF-β in phLF (Figure 3.22A and B). mRNA levels of collagen I and fibronectin were significantly induced by TGF-β. Knockdown of Rpn6 could efficiently antagonize overexpression of these myogenic marker genes. Indeed, collagen I mRNA levels of TGF-β-treated phLF were almost reduced to baseline expression when Rpn6 was silenced. This effect was not as strong for fibronectin but still significant compared to scrambled siRNA treated phLF. Counteraction of TGF-β-mediated expression of collagen I and fibronectin after Rpn6 knockdown could also be confirmed on protein level by Western blot analysis (Figure 3.22 C). Even though reduction here was not significant, a decrease in protein expression was reproducible in four different phLF lines.
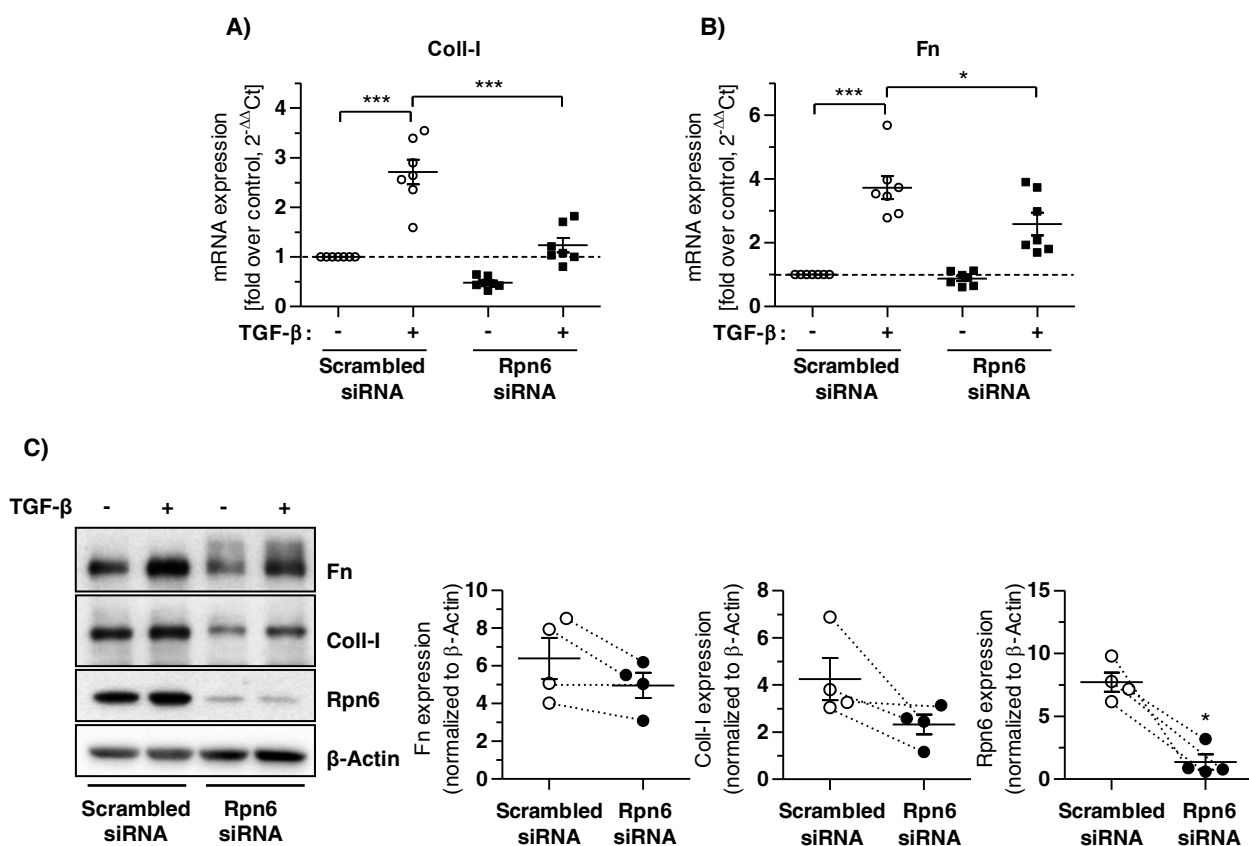
Figure 3.22. Silencing of Rpn6 counteracts TGF-β-induced myofibroblast differentiation in phLF
mRNA expression of fibrotic marker (**A**) collagen I and (**B**) fibronectin in phLF, treated for 48h with TGF-β, starting 24h after Rpn6 knockdown (results are pooled from single siRNA and pool of three siRNA experiments) (Mean ± SEM. n=7. One-way ANOVA, Bonferroni's Multiple Comparison Test). (**C**) Western blot analysis of RIPA lysates for fibronectin, collagen I and Rpn6 in phLF after Rpn6 knockdown and TGF-β treatment and densitometric analysis (single siRNA) (Mean ± SEM. n=4. Two-tailed Mann Whitney Test).

Using a pool of three Rpn6 siRNAs and two control siRNAs, Rpn6 was significantly reduced on protein level up to 25% of basal expression (Figure 3.23). However, in this experiment TGF-β treatment did not significantly induce Rpn6 protein expression, even though increased proteasome activity was observed for the same experiment as shown before in Figure 3.21. This indicates that there might be other factors, besides Rpn6, involved in TGF-β-mediated upregulation of 26S/30S formation. However, Rpn6 silencing induced pronounced accumulation of polyubiquitinated proteins, thereby showing efficient reduction of 26S/30S formation. Furthermore, expression of cyclin D1 was also increased in phLF, which were treated with TGF-β and Rpn6 siRNA and confirmed cell cycle arrest as a consequence of reduced levels of 26S/30S complexes (Figure 3.23).
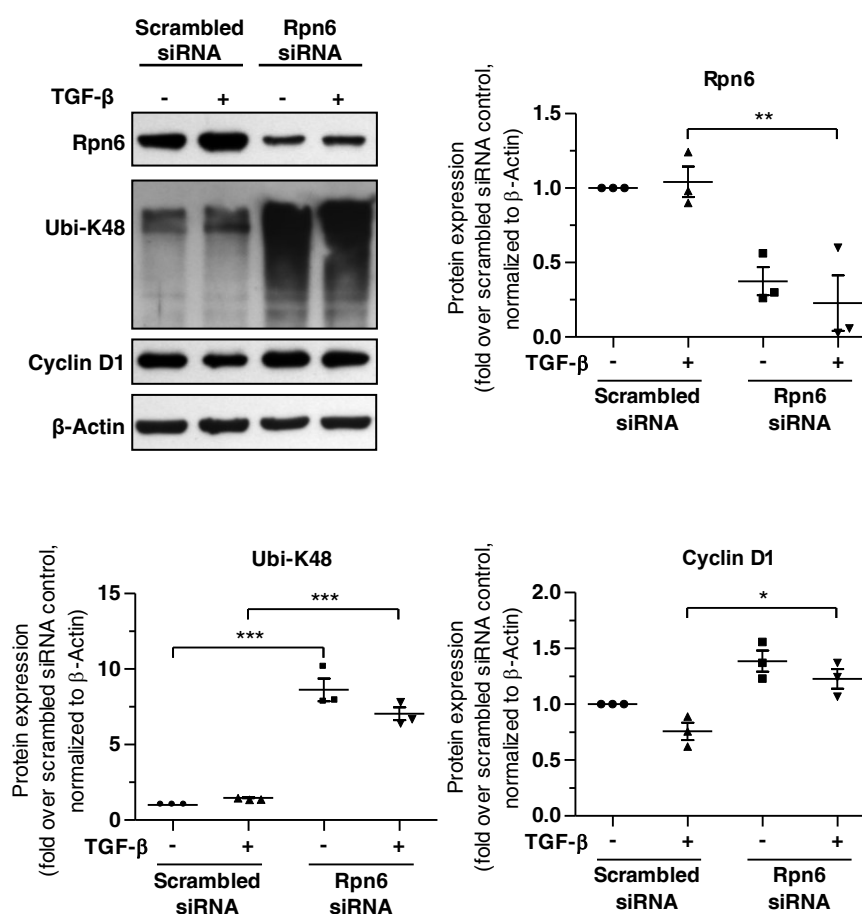
Figure 3.23. Silencing of Rpn6 counteracts TGF-β-induced proliferative effects in phLF
Protein expression of Rpn6, Cyclin D1, K48-polyubiquitinated proteins and β-actin was assessed by Western blot analysis. phLF were treated as described in Figure 3.22 applying a pool of three siRNAs. Densitometric data were first normalized to the respective β-actin loading control and then to the scrambled siRNA/non-TGF-β control (Mean ± SEM. n=3. One-way ANOVA, Bonferroni'sMultiple Comparison Test).

These results thus identify Rpn6-induced formation of 26S/30S proteasome complexes as an essential mediator of myofibroblast differentiation in primary human lung fibroblasts, which can be counteracted by depletion of Rpn6.

Taken together, increased expression of Rpn6 in activated myofibroblasts and pulmonary fibrosis along with elevated 26S/30S formation and accumulation of K48-polyubiquitinated proteins suggests an increased protein turnover in fibrotic remodeling of the lung. Successful counteraction of 26S/30S formation and myofibroblast differentiation by knockdown of Rpn6 further proposes a novel pathomechanism of lung fibrosis, involving Rpn6-mediated proteasome activation upon myofibroblast differentiation.

3.2   The Proteasome as a Target in IPF

This chapter is based on the following manuscript:

Nora Semren, Nunja C. Habel-Ungewitter, Isis E. Fernandez, Melanie Königshoff, Oliver Eickelberg, Tobias Stöger, and Silke Meiners. Validation of the 2nd Generation Proteasome Inhibitor Oprozomib for Local Therapy of Pulmonary Fibrosis. *PloS One,* 10(9), e0136188.

Application of proteasome inhibitors for the treatment of pulmonary fibrosis has been shown to prevent fibrotic lung remodeling in the bleomycin mouse model (Mutlu et al., 2012) but also provided high toxicity leading to excessive mortality in fibrotic animals (Fineschi et al., 2008). These results are controversial and indicate a narrow therapeutic window for the use of proteasome inhibitors in lung fibrosis. Therefore, it was hypothesized that local pulmonary application of a novel site-specific proteasome inhibitor, oprozomib, efficiently reduces lung fibrosis at low doses and provides less systemic side effects.

3.2.1   *Oprozomib is less toxic compared to bortezomib in alveolar epithelial cells*

Local pulmonary drug application exposes lung epithelial cells to high drug concentrations as they constitute the first cellular barrier for the lung towards the environment (Haghi et al., 2014). Any local treatment strategy for lung fibrosis should thus provide antifibrotic effects in lung fibroblasts while maintaining pulmonary epithelial integrity. Therefore, cytotoxicity and proteasome inhibition profile of the novel second generation inhibitor oprozomib was analyzed and compared with the FDA-approved proteasome inhibitor bortezomib in the human alveolar adenocarcinoma cell line A549, which is also widely used as alveolar epithelial-like cell line, and in primary murine alveolar epithelial type II cells.

Treatment of A549 cells with doses of 10 to 100 nM oprozomib for 72 hours was well tolerated, while 250 nM caused pronounced loss of cell viability as assessed by MTT assay (Figure 3.24A). In contrast, bortezomib doses of more than 10 nM induced severe cytotoxicity as demonstrated by cell death of about 60% (for 50 nM) and 75% (for 100 nM), respectively (Figure 3.24B). Reduced toxicity of oprozomib compared to bortezomib correlated well with its high selectivity towards the chymotrypsin-like active site of the proteasome: After 24 hours of inhibitor treatment, 10 and 50 nM of oprozomib specifically inhibited only the chymotrypsin-like active site, while the trypsin-like and caspase-like activities were only marginally affected (Figure 3.24D). A non-toxic dose of 10 nM bortezomib also specifically inhibited the chymotrypsin-like active site only, while higher doses, in addition, significantly blocked trypsin-

like and caspase-like activities (Figure 3.24C). Higher specificity for the chymotrypsin-like active site of oprozomib compared to bortezomib thus provided reduced toxicity in alveolar epithelial-like cells. To confirm lower toxicity of oprozomib compared to bortezomib in a more physiological setting, pmATII were isolated and treated for 52 hours with different doses of these proteasome inhibitors. While 50 nM of oprozomib was well tolerated, 50 nM of bortezomib reduced cell survival by up to 35% (Figure 3.24E and F). These findings were well in accordance with results obtained from A549 cells.
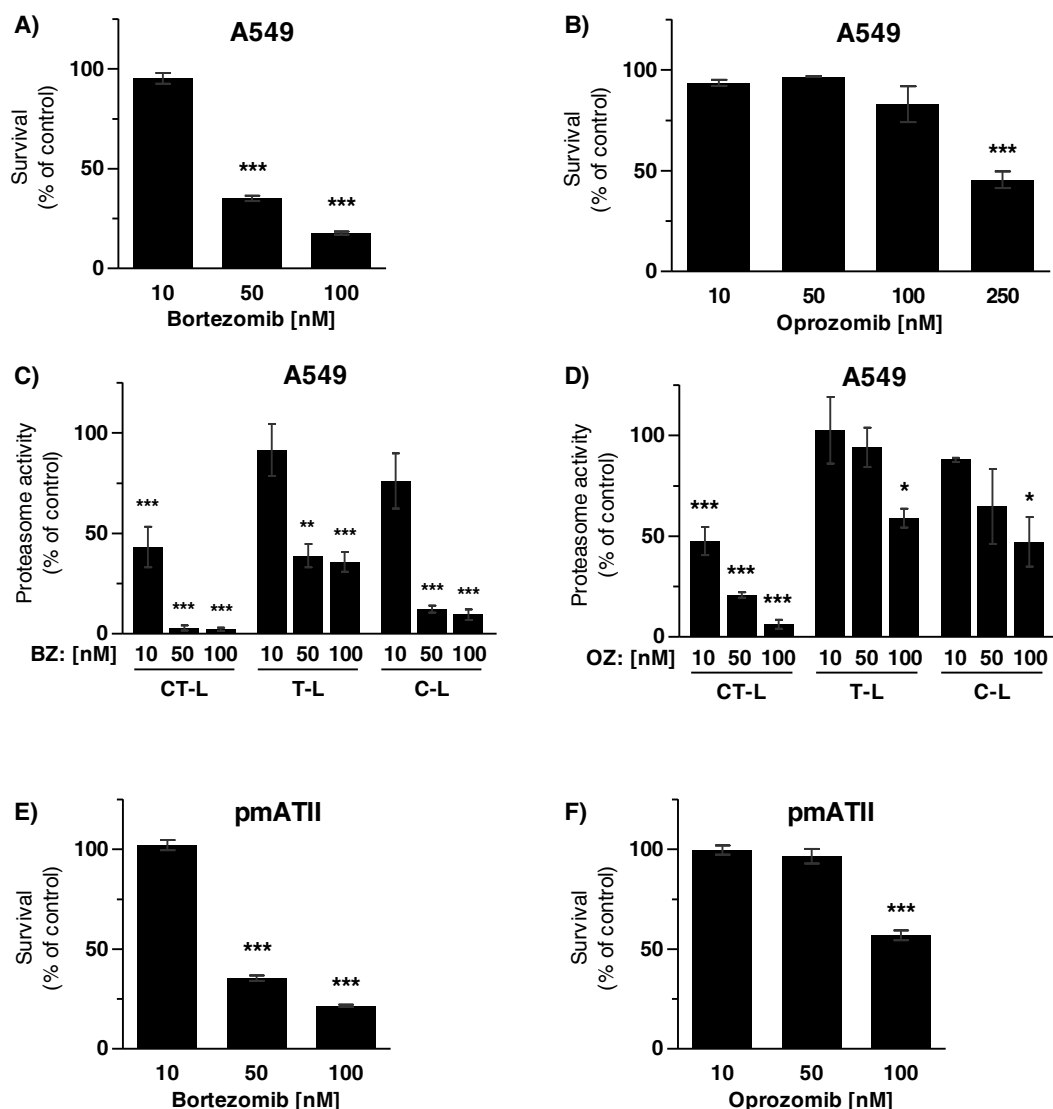
Figure 3.24. Toxicity and inhibitory profile of bortezomib and oprozomib in alveolar epithelial cells
MTT assay after 72h of treatment with (**A**) bortezomib (BZ) or (**B**) oprozomib (OZ) (Mean ± SEM. n=3. One-way ANOVA, Dunnett's Multiple Comparison Test). (**C**) Proteasome activity 24h after treatment with BZ or (**D**) OZ (Mean ± SEM. n=3. One-way ANOVA, Dunnett's Multiple Comparison Test). (**E**) and (**F**) MTT assay of pmATII cells after 52h of treatment with OZ or BZ (Mean ± SEM. n=4. One-way ANOVA, Dunnett's Multiple Comparison Test). pmATII cells were isolated by Dr. Kathrin Mutze (Postdoc CPC, 2015).

3.2.2 Non-toxic doses of oprozomib specifically inhibit the CT-L active site in pmLF

To evaluate the inhibitory profile and toxicity of oprozomib in lung fibroblasts, the main effector cells of pulmonary fibrosis, primary mouse lung fibroblasts were treated with different concentrations of oprozomib for up to 72 hours. These fibroblasts were isolated from mice containing the ODD-luc reporter for proteasome inhibition. In the ODD-luc mouse model, an oxygen-dependent degradation domain (ODD) is fused to luciferase (luc), which serves as a proteasomal degradation signal for the luciferase fusion protein (Goldman et al., 2011; Safran et al., 2006). The ODD domain is derived from the hypoxia inducible factor (HIF)-1α and allows for proteasomal degradation of the HIF-1α transcription factor under physiological oxygen conditions. Under hypoxic conditions, however, ODD is hydroxylated and stabilizes HIF-1α thereby activating a protective gene program to counteract hypoxia (Lee et al., 2004). The ODD-luc reporter thus accumulates at hypoxic conditions but also after inhibition of the proteasome and has been established to quantitatively monitor inhibition of the proteasome in cells and mice (Figure 3.25) (Kimbrel et al., 2009).
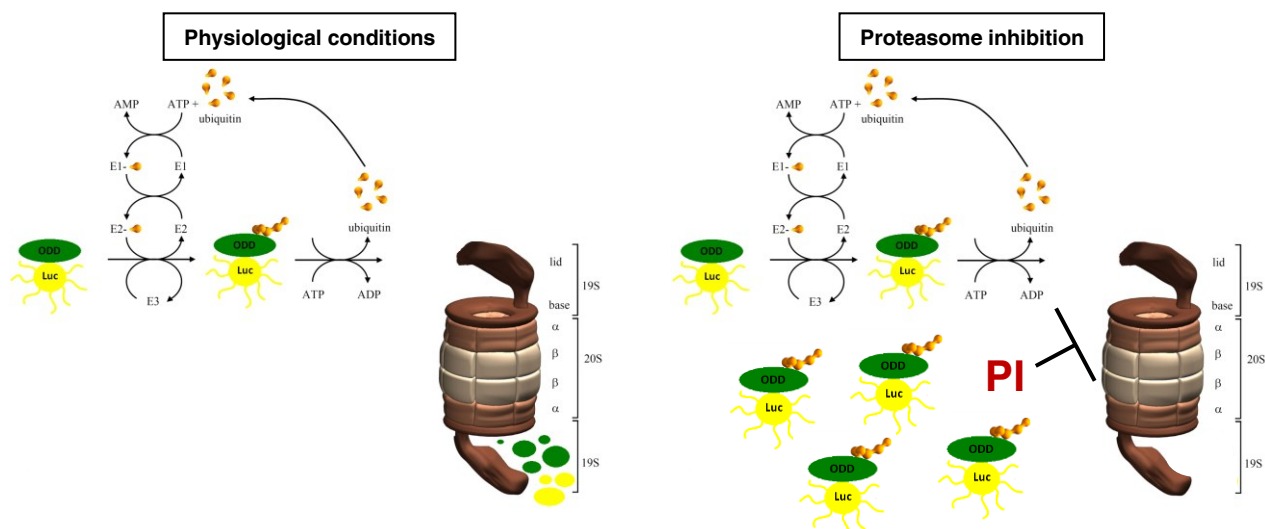
Figure 3.25. The ODD-luc reporter for proteasome inhibition
Under normal conditions, ODD-luc is degraded by the proteasome. After inhibition of the proteasome ODD-luc accumulates and the luciferase reaction can be applied to monitor proteasome activity. (Taken from Meiners, Ludwig, et al., 2008)~modified

In primary lung fibroblasts of ODD-luc reporter mice, significant and specific reduction of the chymotrypsin-like activity of the proteasome was observed already at a concentration of 10 nM after 24 hours of treatment with oprozomib whereas trypsin-like and caspase-like activities were not affected. Higher doses of 100 nM oprozomib inhibited the chymotrypsin-like activity by 85% but only marginally affected the other two active sites (Figure 3.26A). Accumulation of the luciferase reporter was observed only at a dose of 100 nM oprozomib as measured by an increase in luminescence intensity, due to the luciferase reaction, in the same cell extracts

(Figure 3.26B). Native gel analysis was applied to directly visualize the dose-dependent inhibition of the proteasome and accumulation of luciferase in a single experiment (Figure 3.26C). Subsequent overlay of the native gel with the chymotrypsin-like specific fluorogenic substrate Suc-LLVY-AMC and luciferin showed a dose dependent reduction in proteasome activity from 10 to 500 nM oprozomib and a corresponding dose-dependent increase in luciferase levels starting at 50 nM oprozomib and clearly visible from 100 nM onwards (Figure 3.26C). These experiments show that oprozomib-mediated specific inhibition of the proteasomal chymotrypsin-like activity by 70-90% results in the accumulation of a proteasomal reporter protein. Importantly, a dose of 50 nM oprozomib still was in the non-toxic range. However, viability of primary mouse lung fibroblasts was reduced after 72 h treatment with 100 nM oprozomib (Figure 3.26D).
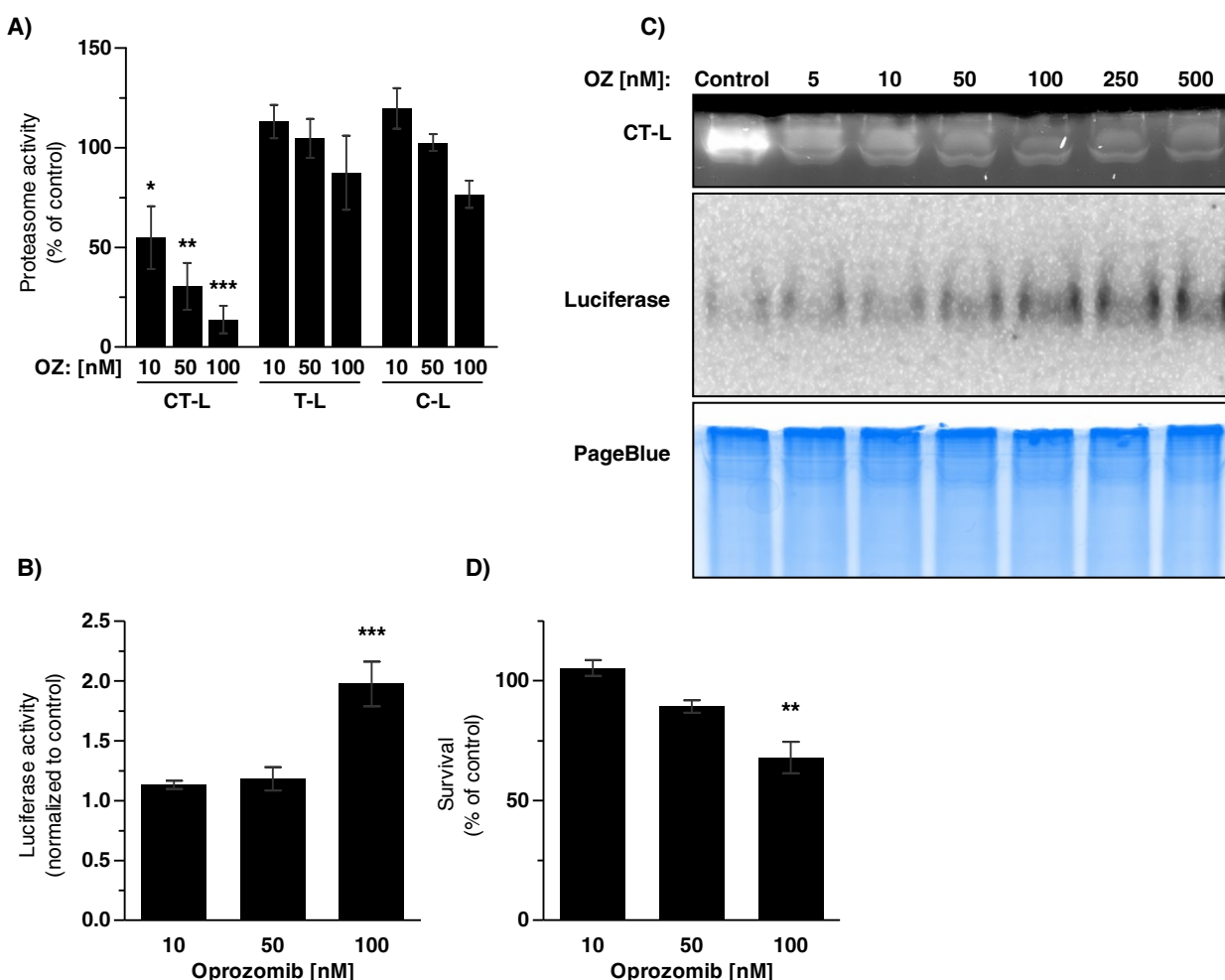
Figure 3.26. Inhibition profile of oprozomib in primary mouse lung fibroblasts
(**A**) Proteasome activity and (**B**) luciferase activity of ODD-luc pmLF 24h after treatment with OZ (Mean ± SEM. n=3. One-way ANOVA, Dunnett's Multiple Comparison Test). (**C**) Native gel of ODD-luc pmLF 24h after OZ treatment. (**D**) MTT assay of ODD-luc pmLF 72h after treatment with OZ (Mean ± SEM. n=3. One-way ANOVA, Dunnett's Multiple Comparison Test).

3.2.3 Oprozomib provides antifibrotic effects in primary lung fibroblasts

To evaluate whether the observed site-specific and non-toxic inhibition of the proteasome by oprozomib also provided antifibrotic effects in lung fibroblasts, pmLF were treated with 50 nM or 100 nM of oprozomib for 72 hours and expression of the profibrotic marker collagen I was determined by immunocytochemistry. Collagen I expression was strongly reduced as shown by immunofluorescence staining of the cells (Figure 3.27A). Furthermore, BrdU incorporation and therefore proliferation was significantly decreased in oprozomib-treated fibroblasts in comparison to DMSO-treated control cells (Figure 3.27B).

A)

| DMSO | 50 nM | 100 nm |
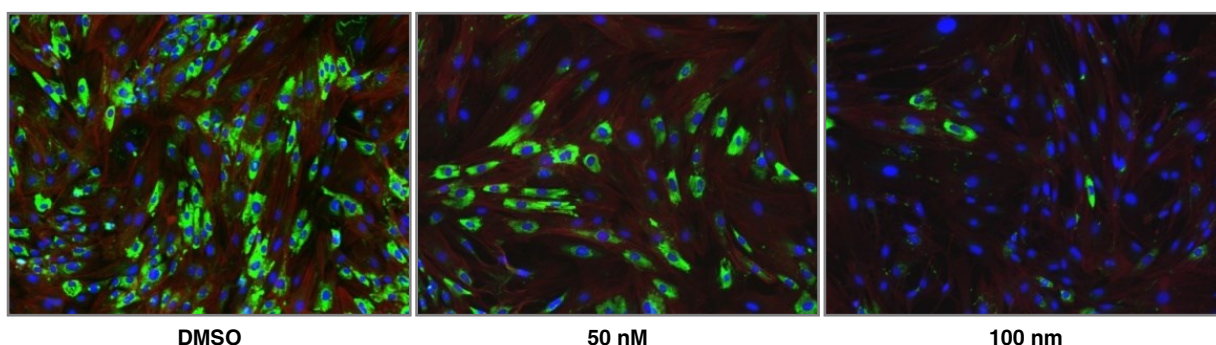
B)
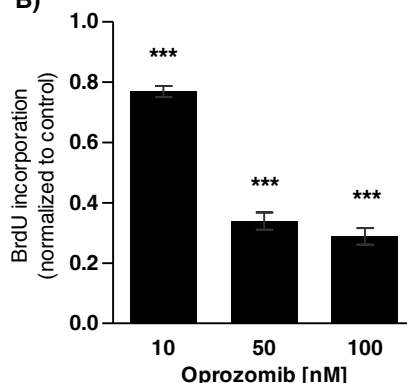
Figure 3.27. Antifibrotic effects of oprozomib in primary mouse lung fibroblasts
(**A**) Immunofluorescence staining for Coll-I (green), F-Actin (red) and nuclei (blue) after 72h of treatment with OZ. (**B**) BrdU proliferation assay of primary lung fibroblasts treated with OZ for 72h (Mean ± SEM. n=4. One-way ANOVA, Dunnett's Multiple Comparison Test).

Several studies identified impaired TGF-β signaling in response to proteasome inhibition as a possible mechanism for the antifibrotic effects of proteasome inhibitors (Mutlu et al., 2012; Sakairi et al., 2011). Therefore, it was tested whether oprozomib also counteracts profibrotic TGF-β signaling. For that, pmLF were pre-treated with TGF-β for 24 hours to induce myofibroblast differentiation, then 50 nM of oprozomib was added and cells were incubated for

another 24 hours for immunofluorescence staining and 72 hours for mRNA expression analysis. Oprozomib treatment of mouse lung fibroblasts efficiently inhibited TGF-β-induced collagen I expression, both on protein and mRNA level (Figure 3.28A and B). In addition, mRNA expression of the myofibroblasts marker αSMA was also significantly reduced in cells incubated with oprozomib. Of note, basal αSMA mRNA levels were already reduced by oprozomib in the absence of TGF-β stimulation (Figure 3.28C). These data indicate that oprozomib efficiently counteracts TGF-β mediated profibrotic responses by transcriptional downregulation of myogenic marker genes.
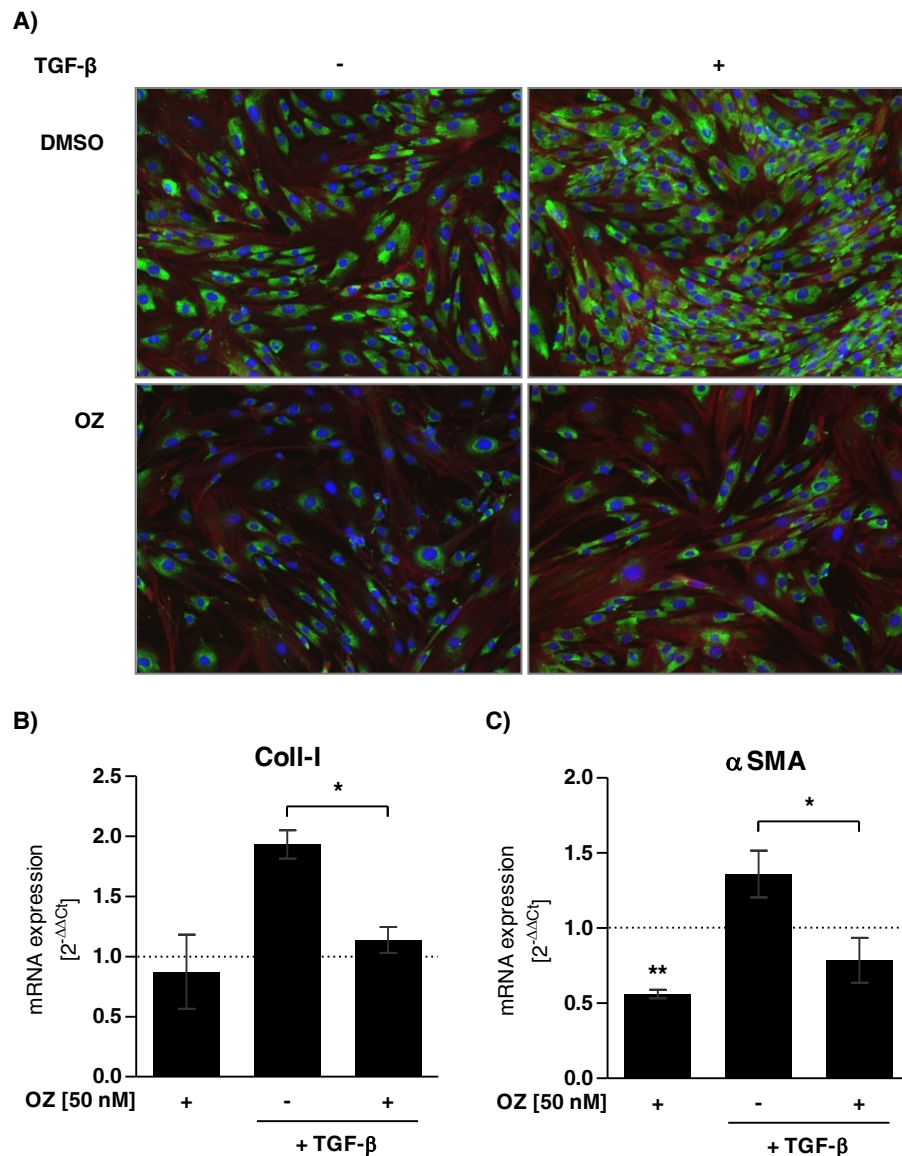
Figure 3.28. Oprozomib impairs TGF-β mediated induction of profibrotic marker
(**A**) Immunofluorescence staining for Coll-I (green), F-Actin (red) and nuclei (blue) after treatment with TGF-β and OZ. (**B**) and (**C**) mRNA expression of Coll-I and αSMA after treatment with TGF-β and OZ (Mean ± SEM. n=3. Paired t-Test).

Results obtained from these *in vitro* studies provide strong evidence that oprozomib represents a novel, chymotrypsin-like-specific, second generation proteasome inhibitor conferring anti-proliferative and antifibrotic effects on lung fibroblasts at low concentrations without major cytotoxic effects on fibroblast and alveolar epithelial cells.

3.2.4 Intratracheal application of oprozomib efficiently inhibits proteasome activity in the lung

To confirm antifibrotic effects of oprozomib in pulmonary fibrosis, an optimal well tolerated but still effective dose had to be determined for local pulmonary application. Therefore, increasing doses of 0.5 mg, 1 mg or 5 mg oprozomib per kg body weight were instilled intratracheally into the lungs of healthy mice. Oprozomib was suspended in 0.1% Pluronic F-127, a well-tolerated, FDA-approved, biodegradable copolymer surfactant, which has been shown to be non-toxic in epithelial cells (Horie et al., 2013; Kabanov & Alakhov, 2000; Malmsten, 2000). Animals were sacrificed 24 or 96 hours after application of oprozomib to analyze the chymotrypsin-like proteasome activity of whole lung tissue as a measure of efficient proteasome inhibition and to determine cell counts in the BAL as a read-out for acute lung injury (Figure 3.29A).

24 hours after instillation, no significant reduction in proteasome activity was observed for any of the applied oprozomib doses (Figure 3.29B) but the amount of polymorphonuclear leukocytes (PMNs) in the BAL increased up to 30% at the highest dose of 5 mg, indicating an acute inflammatory response in the airspace of the lungs (Figure 3.29C). Proteasome activity was, however, significantly decreased in lungs 96 hours after application of 0.5 mg or 1 mg/kg oprozomib (Figure 3.29D). The acute response declined and there was no indication of inflammatory PMN accumulation with these doses after 96 hours of instillation as determined by BAL cell count (Figure 3.29E). For further experiments, a concentration of 1 mg OZ per kg body weight was chosen as an optimal non-harmful dose, thereby providing effective proteasome inhibition in the lungs after local application by intratracheal instillation.
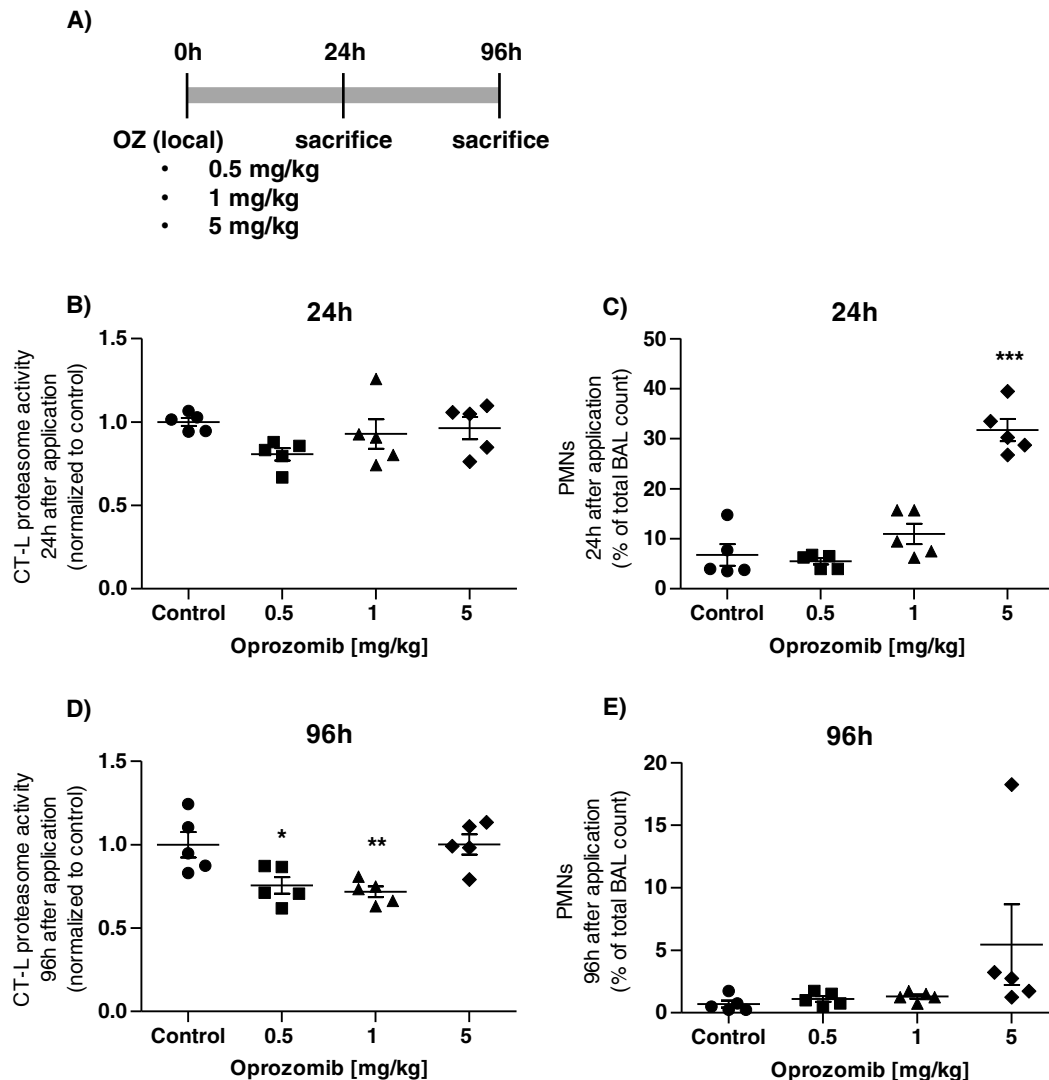
Figure 3.29. Dose response to local pulmonary application of 0.5, 1 and 5 mg/kg oprozomib
(**A**) Treatment scheme: local pulmonary application of OZ, (**B**) CT-L proteasome activity after 24h, (**C**) percent of PMNs to total BAL count after 24h (**D**) CT-L proteasome activity after 96h and (E) percent of PMNs to total BAL count after 96h (Mean ± SEM. n=5 per group. One-way ANOVA, Dunnett's Multiple Comparison Test). Animal experiment was performed together with Nunja Habel-Ungewitter (PhD student CPC, 2012).

3.2.5 Local pulmonary application of oprozomib fails to prevent lung fibrosis

To investigate the therapeutic potential of locally applied oprozomib on lung fibrosis, oprozomib was intratracheally instilled into bleomycin challenged mice. The ODD-luc proteasome reporter mouse model was used to monitor the degree of proteasome inhibition by accumulation of the ODD-luc reporter in mouse lungs. FVB-ODD-luc mice were first challenged with bleomycin (3 U/kg) by intratracheal instillation. Oprozomib was applied 11 and 16 days after bleomycin challenge at a dose of 1 mg/kg of body weight and mice were sacrificed at day 21 (Figure 3.30A). Of note, treatment of bleomycin challenged mice with oprozomib did not

counteract bleomycin induced expression of the fibrotic marker genes collagen I and fibronectin (Figure 3.30B and C). In accordance, H&E staining also did not show any therapeutic effects on lung fibrosis in response to oprozomib (Figure 3.30D).
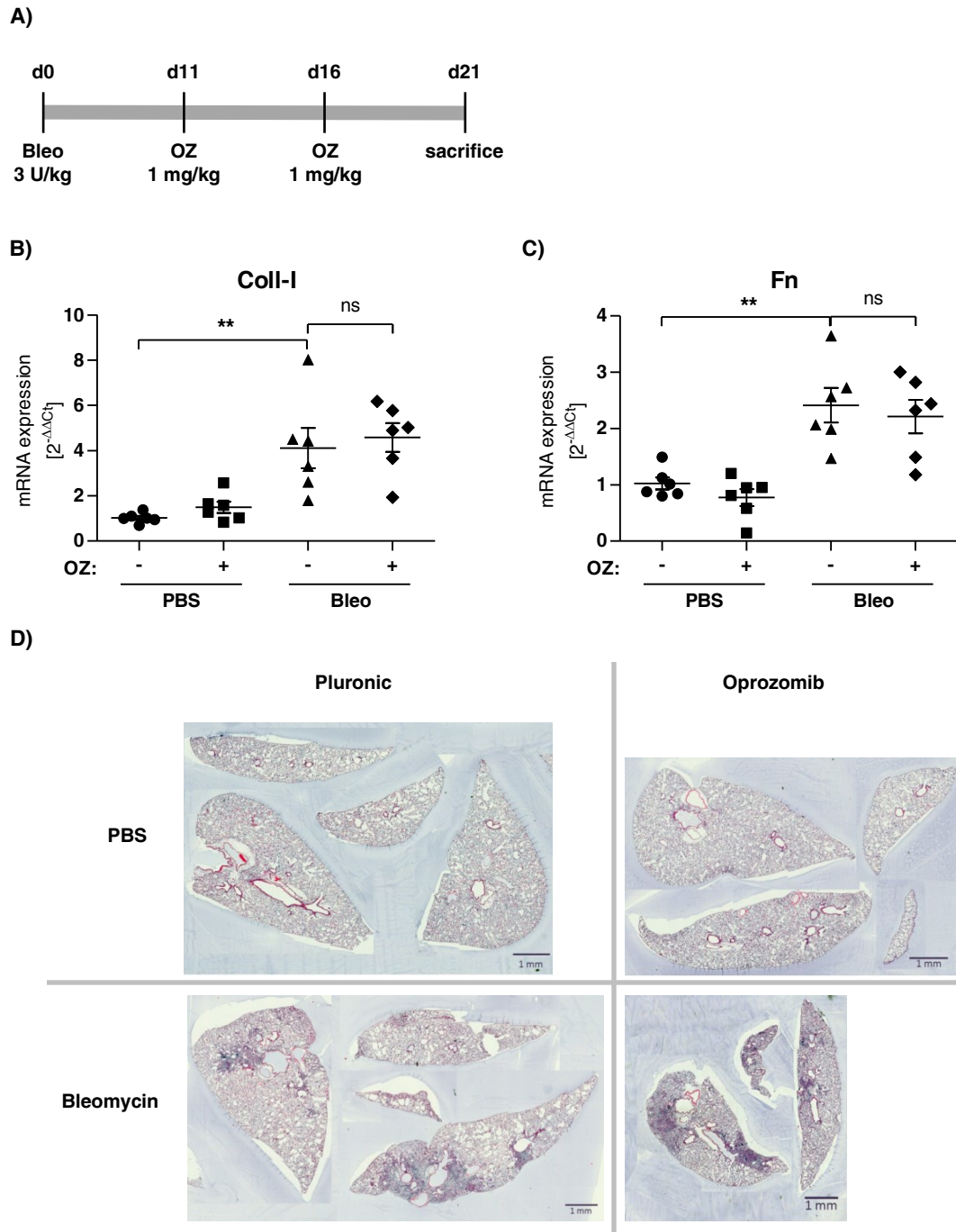
Figure 3.30. Local pulmonary application of oprozomib does not provide antifibrotic effects in the bleomycin mouse model
(**A**) Treatment scheme: local pulmonary application of OZ. (**B**) and (**C**) mRNA levels of Coll-I and Fn (Mean ± SEM. n=6 per group. One-way ANOVA, Bonferroni's Multiple Comparison Test). (**D**) H&E staining of lung slices. Animal experiment was performed together with Nunja Habel-Ungewitter (PhD student CPC, 2012).

Chymotrypsin-like proteasome activity in whole lung tissue of control mice that had been treated with oprozomib was only slightly, but not significantly, decreased. However, inhibition of the proteasome was not detected in bleomycin-treated animals, but proteasome activity was rather slightly increased in fibrotic lungs (Figure 3.31A). This is well in accordance with previous findings showing activation of the proteasome during fibrotic lung remodeling (Chapter 3.1.3). The luciferase reporter, supposed to accumulate upon reduction of proteasome activity, did not give any indication of reduced proteasomal cleavage rates. Rather, a significant increase in luciferase activity was observed in lungs of bleomycin-challenged mice compared to controls indicating an unexpected accumulation of the luciferase reporter in fibrotic lungs (Figure 3.31B).
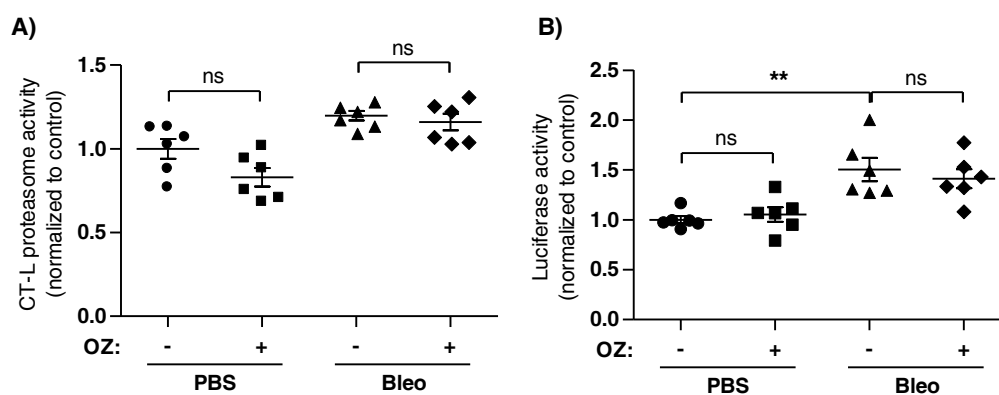
Figure 3.31. Oprozomib fails to inhibit proteasome activity after local pulmonary application in the bleomycin mouse model
(**A**) CT-L proteasome activity and (**B**) luciferase activity of whole lung tissue (Mean ± SEM. n=6 per group. One-way ANOVA, Bonferroni's Multiple Comparison Test).

Collectively, these results indicate that the ODD-luc reporter mouse model is not suitable for assessment of proteasome inhibition in bleomycin-induced pulmonary fibrosis as the reporter accumulated independently of any proteasome inhibition upon fibrotic lung remodeling. In addition, the applied oprozomib treatment scheme did not effectively inhibit proteasomal activity in the lungs and no protective effects with regard to lung fibrosis were observed. For these reasons and in view of the described resistance of FVB mice to develop liver fibrosis (Hillebrandt et al., 2002), the mouse strain was changed to C57BL/6 mice in subsequent animal experiments and a 14 days bleomycin mouse model was applied which is well established at the institute (Aumiller et al., 2013). In addition, the number of local oprozomib instillations was increased to obtain more sustained local proteasome inhibition in the lung. In the next set of experiments, animals were treated at day 6, 8 and 12 after bleomycin challenge and sacrificed at day 14 (Figure 3.32A). While bleomycin or oprozomib treatment alone was well tolerated, the

double challenge resulted in severe weight loss of all animals of this group, therefore the experiment had to be aborted for ethical reasons at this point (Figure 3.32B).
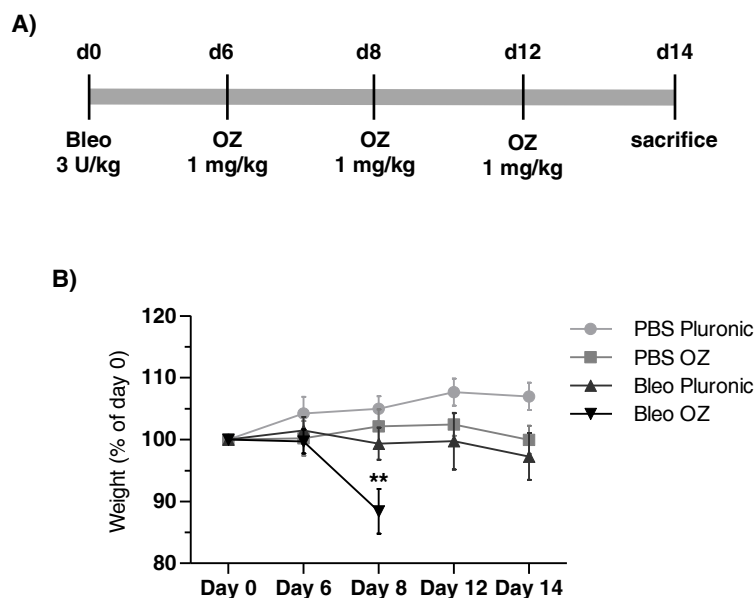
Figure 3.32. Local application of oprozomib provides high toxicity in fibrotic mouse lungs
(**A**) Treatment scheme: repeated local pulmonary application of OZ. (**B**) Weight loss of animals at different time points (Mean ± SEM. n=6 per group. One-way ANOVA Bonferroni's Multiple Comparison Test). Animal experiment was performed together with Isis Fernandez (Scientist CPC, 2012).

These data suggest that local application of oprozomib to diseased and fibrotic lungs may even be fatal as proper proteasome function might be essential during tissue remodeling. This proposes a very narrow therapeutic window for antifibrotic therapy with proteasome inhibitors.

3.2.6 Systemic application of oprozomib fails to prevent lung fibrosis

In a final approach, it was tested whether oprozomib might be better tolerated in the diseased lung after systemic application rather than after local delivery. An initial dose-finding experiment identified a concentration of 10 mg/kg body weight as an optimal dose of oprozomib that was well tolerated after repeated oral application in bleomycin challenged animals (data not shown). For oral application, oprozomib was suspended in 1% carboxymethylcellulose (CMC) and applied via a gavage needle 7 and 12 days after bleomycin treatment in female C57BL/6 mice. Animals were then sacrificed at day 14 (Figure 3.33A). Oprozomib significantly reduced the chymotrypsin-like proteasome activity in healthy mouse lungs. This reduction was, however, not observed in fibrotic lungs (Figure 3.33B). Oral oprozomib treatment alone did not show any toxic effects but co-treatment with bleomycin resulted in significant reduction of body weight (Figure 3.33C) similar to previous results after local application.
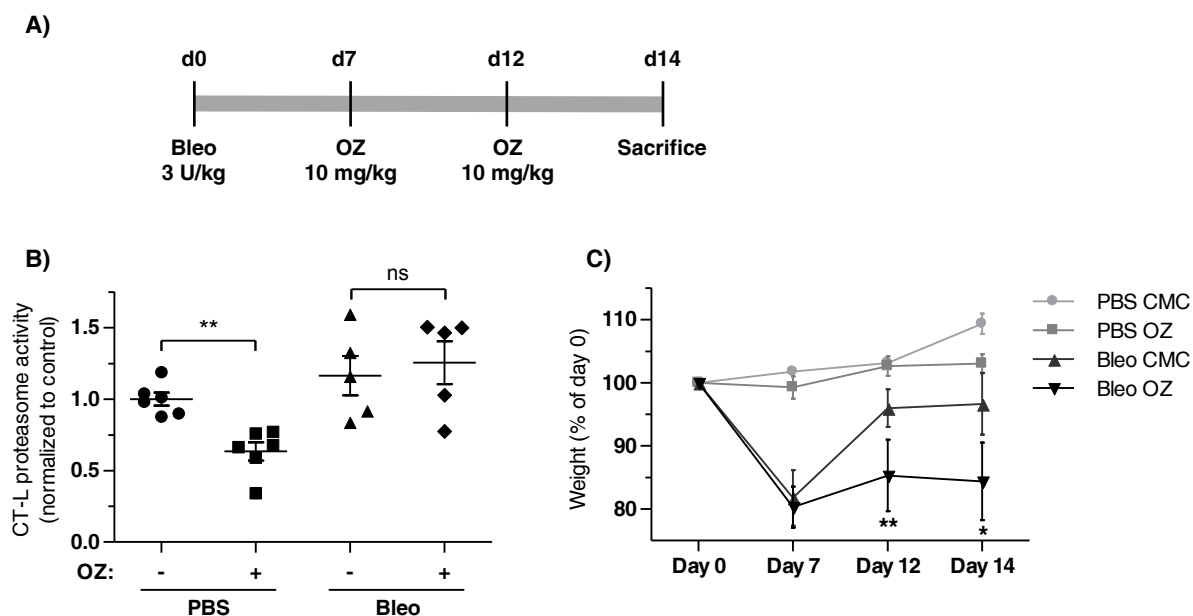
Figure 3.33. Oral application of oprozomib does not reduce proteasome activity in fibrotic lungs and is not well tolerated in bleomycin challenged animals
(**A**) Treatment scheme: repeated oral application of OZ. (**B**) CT-L proteasome activity (Mean ± SEM. n=5-6 per group. Mann Whitney t-test) and (**C**) weight loss of animals at different time points (Mean ± SEM. n=5-6 per group. One-way ANOVA, Bonferroni's Multiple Comparison Test). Animal experiment was performed together with Nunja Habel-Ungewitter and Isis Fernandez (PhD student and scientist CPC, 2013).

mRNA expression of collagen I and fibronectin was not altered by therapeutic oprozomib treatment compared to the bleomycin control group. Indeed, fibronectin mRNA was even increased in oprozomib-treated fibrotic lungs (Figure 3.34A and B). H&E staining was performed to compare structural changes of the lung and sections were immunofluorescence stained to

assess expression of fibrotic markers collagen I and αSMA (Figure 3.34C). However, no antifibrotic effects of oprozomib were observed in bleomycin challenged animals confirming mRNA data of this experiment.
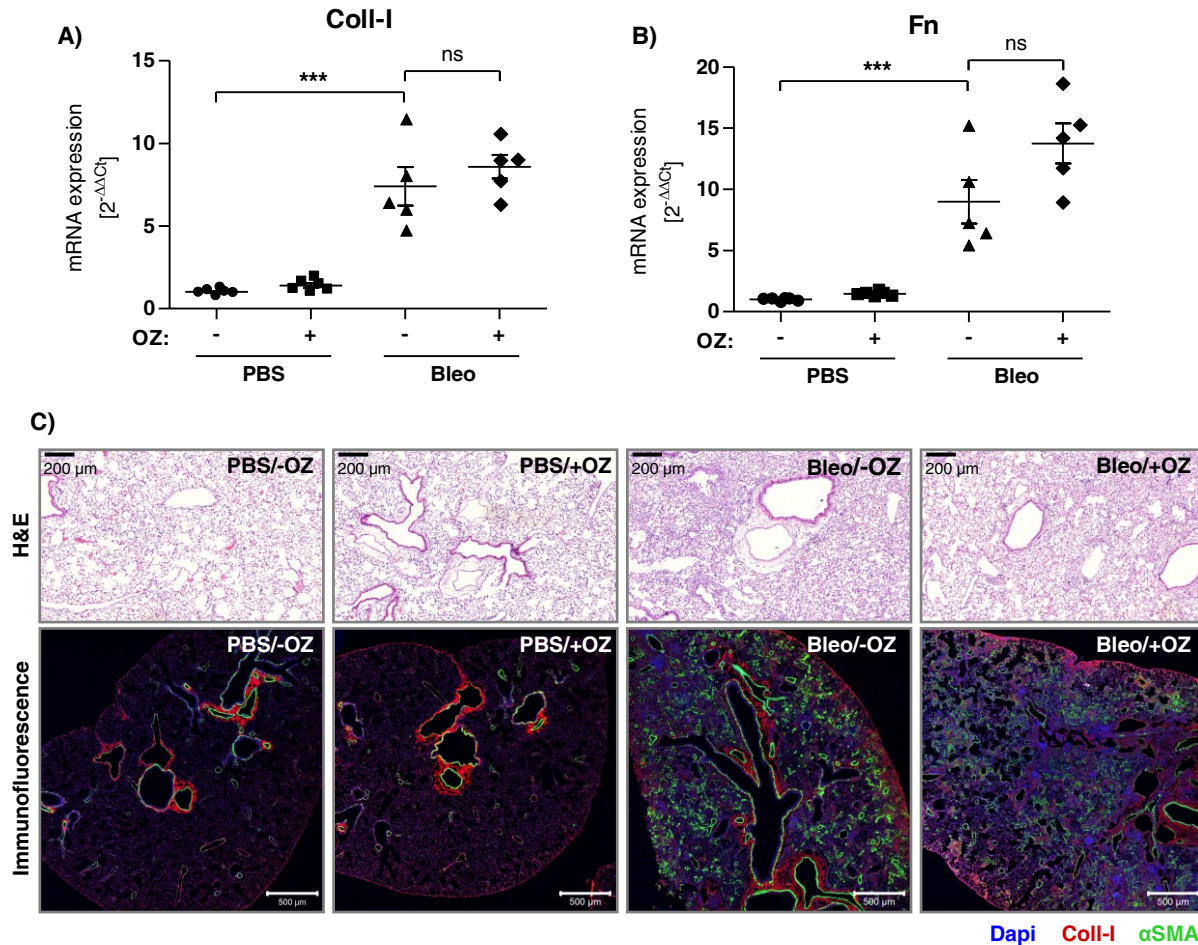
Figure 3.34. Oral application of oprozomib provides no antifibrotic therapeutic effects
(**A**) and (**B**) mRNA levels of Coll-I and Fn (Mean ± SEM. n=5-6 per group. One-way ANOVA, Bonferroni's Multiple Comparison Test). (**C**) H&E staining of mouse lung slices and immunofluorescence staining for Coll-I (red), αSMA (green), and nuclei (blue).

Taken together, reduced toxicity of oprozomib in alveolar epithelial cells and promising antifibrotic effects in lung fibroblasts could not be confirmed in the bleomycin mouse model for pulmonary fibrosis. Indeed, local or oral application of oprozomib rather seemed to accelerate damage in fibrotic lungs. This study therefore provides evidence for a crucial role of the proteasome during fibrotic lung remodeling and a very narrow therapeutic window for proteasome inhibitors in this disease.

4 DISCUSSION

4.1 The Proteasome as a Trigger of IPF

IPF is a fast progressive and lethal lung disease with very limited treatment options. It is characterized by excessive deposition of ECM and destruction of the delicate alveolar architecture, leading to severe impairment of respiration and gas exchange, which finally results in organ failure and death.

IPF can also be regarded as a disease of impaired proteostasis as shown for UPR and ER-stress in familial and sporadic cases and reduced autophagy (Balch et al., 2014; Meiners et al., 2015). Therefore a possible contribution of the ubiquitin-proteasome system, as a key regulator of proteostasis (Balch et al., 2014), seems to be obvious. However, no study so far comprehensively analyzed a possible role of dysregulated proteasome function during fibrotic tissue remodeling and myofibroblast differentiation.

The present study shows for the first time that proteasome function is indeed regulated during fibrotic remodeling and proposes a TGF-β-dependent mechanism. Here, TGF-β upregulated proteasome activity and ubiquitin-mediated protein turnover in the process of myofibroblast differentiation. Proteasome activation involved increased formation of highly active 26S/30S proteasomes via the 19S regulatory subunit Rpn6, which was required for myodifferentiation of lung fibroblasts. Moreover, enhanced 26S/30S proteasome activity and upregulation of Rpn6 in activated parenchymal lung cells closely followed the course of reversible fibrotic tissue remodeling in bleomycin challenged mice. In IPF lungs, Rpn6 levels were increased particularly in myofibroblasts and hyperplastic basal cells of fibroblast foci. Accumulation of K48-polyubiquitin protein conjugates in these cells and the positive correlation of whole lung Rpn6 protein levels with K48-polyubiquitinated proteins suggest activation of ubiquitin-dependent protein degradation by the 26S proteasome as a pathologic feature of profibrotic remodeling in IPF. This study thus identified a novel pathomechanism involving proteasome activation upon TGF-β mediated myofibroblast differentiation and pulmonary fibrosis which might represent a common feature for fibrotic tissue remodeling in general.

4.1.1 TGF-β mediates activation of the 26S proteasome via Rpn6

In this study, TGF-β-dependent increase in protein degradation was mediated by induced formation of 26S/30S proteasome complexes in mouse and human pulmonary fibroblasts. 26S/30S proteasomes can be regarded as the active form of the proteasome as 20S

proteasomes are quite ineffective in protein degradation due to the narrow entry pore formed by by the α-ring (Dahlmann, 2005; Y. Saeki & Tanaka, 2012). *In vitro* measurement of proteasome activity for example showed a 3-20 fold higher peptide cleavage of fluorogenic substrates in the presence of 26S proteasomes in comparison to 20S proteasomes (Hoffman et al., 1992; Rechsteiner, 2008). Furthermore, only proteasome complexes containing 19S particles are able to degrade polyubiquitinated proteins and thus to conduct controlled proteolysis. It is not clear if the 20S CP itself is actually able to degrade proteins *in vivo* therefore free 20S pools might be necessary to provide fast assembly of active proteasomes to deal with an increased requirement of protein degradation in the cell (Savulescu & Glickman, 2011).

Here, TGF-β induced elevation of the 19S subunit Rpn6 was identified to promote assembly of 26S/30S proteasomes as Rpn6 knockdown counteracted TGF-β-mediated formation of 26S/30S complexes in lung fibroblasts. Of note, no changes in expression levels were observed for Rpt5, another 19S subunit, or the 20S subunits α1-7, indicating an exclusive role of Rpn6 as rate limiting subunit for 26S/30S formation. De facto, first cryo-EM structures of the 26S proteasome revealed that Rpn6 indeed serves as a clamp, which stabilizes the interaction between 19S RPs and the 20S CP. Here, Rpn6 interacts with α2 of the 20S α-ring and Rpt6 of the 19S ATPase ring (Pathare et al., 2012). In accordance with this structural finding, Rpn6 has also been proposed to serve as a rate limiting subunit to promote assembly of 19S regulators with the 20S catalytic core in yeast cells: Depletion of Rpn6 impaired assembly of 26S proteasomes and suggests an essential role for their integrity and formation (Isono et al., 2005; Santamaria et al., 2003). These results are also supported by recent studies in ES cells and *Caenorhabditis elegans* (*C. elegans*). ES cells have been shown to maintain high levels of 26S/30S proteasomes together with high degradation rates, which is lost upon differentiation into NPCs and neurons (Vilchez, Boyer, et al., 2012). Similarly, long-lived mutants of *C. elegans* displayed elevated levels of active 26S/30S proteasome complexes compared to wild type animals leading to increased proteasome activity (Vilchez, Morantte, et al., 2012). In both studies, increased formation of 26S/30S complexes was critically and specifically dependent on the 19S subunit Rpn6 as shown by overexpression, knockdown and genetic deletion analysis, respectively (Vilchez, Boyer, et al., 2012; Vilchez, Morantte, et al., 2012).

Assuming that a pool of free 20S and 19S particles exists in the cell, upregulation of a single subunit such as Rpn6, which then mediates formation of 26S/30S proteasomes, provides a fast, flexible and economic mechanism to adapt cellular degradation capacities to intrinsic and extrinsic changes, rather than time and energy consuming synthesis of new, whole proteasomes.

Enhanced formation of 26S/30S complexes along with increased proteasome activity has also been observed by Rodriguez et al. in the exceptionally long-lived naked mole rat when compared to C57BL/6 mice. This study revealed higher expression levels of the 19S subunits Rpn10 and Rpt5 and some subunits of the immunoproteasome (Rodriguez et al., 2012). However, these findings were not confirmed by mechanistic data to actually increase proteasome activity and may be controversial as animals of two different species were compared.

Furthermore, increased 26S-dependent proteasome activity has been observed in endothelial cells which were challenged with high glucose and confirmed in hyperglycaemic mice. This increase in 26S activity was found to be mediated by augmented tyrosine nitration of the 19S RP (H. Liu et al., 2012). Another study identified ATP levels as regulatory factor for proteasome activity within the cell. Here, high proteasomal degradation rates were only observed in a certain concentration range of intracellular ATP, whereas higher or lower ATP levels decreased 26S activity (Huang et al., 2010). ATP-dependent regulation of proteasome activity is also supported by a study from Liu et al, who showed that ATP is required during various steps of 26S formation and activation (C.-W. Liu et al., 2006). Furthermore, a recent study unravelled a previously unknown link between the induction of mechanistic target of rapamycin complex 1 (mTORC1) and 26S proteasome activation. Here, induced protein synthesis by mTORC1 activation in response to growth signals coincided with increased expression of proteasomes, transcriptionally regulated by nuclear factor (erythroid-derived 2)-like 1 (Nrf1) (Zhang et al., 2014).

Activation of proteasomal protein degradation indeed seems to be a general mechanism to maintain protein homeostasis in the cell. Similar to the present findings on TGF-β mediated upregulation of proteasome activity, Liu et al. observed induction of genes, which are part of the ubiquitin-proteasome system, in response to EGF signaling in *C. elegans*, leading to increased proteasome activity and polyubiquitination in these animals. In this study, fertile adult *C. elegans*, which upregulate EGF, were assayed for proteasome activity and showed EGF-dependent augmentation of proteasomal degradation rates as observed by a reduced signal of their GFP reporter. This reporter is polyubiquitinated and subsequently degraded by the proteasome, resulting in a decreased fluorescence signal at higher degradation rates and therefore specifically identifies 26S/30S-mediated protein degradation. However, the underlying mechanism for EGF-dependent increase in proteasomal degradation rates was not studied in detail by Liu et al., but they proposed enhanced activity of ubiquitin ligases, which might drive this process (G. Liu et al., 2011).

Various studies, as described here, show adjustment of proteasome activity in response to certain stimuli. Regulation of the 19S regulatory subunit Rpn6, however, has either not been investigated or not been found to be affected in these studies, suggesting that multiple mechanisms can promote upregulation of 26S proteasome activity including post-translational modifications, assembly or half-life of proteasomes, or association of 26S proteasomes with additional activators such as PA200 or PA28γ (Meiners et al., 2014)

In lung fibroblasts, the extent of TGF-β-mediated Rpn6 induction was stronger on protein than on mRNA level and was only observed on the protein level in mouse and human fibrotic lung tissue. Here, upregulation of Rpn6 appears to involve both, transcriptional activation and posttranscriptional stabilization of Rpn6. Rpn6 induction was also a quite slow process, as pronounced increase was observed in CCL206 lung fibroblasts after 24 to 48 hours. Therefore, it might even be possible that accumulation of polyubiquitinated proteins itself could mediate a feedback loop leading to higher degradation rates.

In phLF, Rpn6 was slightly induced on mRNA but not on protein level, however, 26S/30S formation was clearly increased by TGF-β and could be counteracted by Rpn6 knockdown, as shown by native gel analysis. These findings are indeed controversial, as 26S/30S formation here cannot solely be explained by overexpression of Rpn6. Therefore, it can be assumed that other mechanisms than Rpn6 induction are involved in TGF-β-mediated activation of the proteasome, which might also depend on the particular cell type.

These findings are in contrast to Rpn6 regulation in ES cells or *C. elegans*. In both studies, Vilchez et al. report transcriptional regulation via the forkhead box O (FOXO) transcription factor 4 (FOXO4) in ES cells or DAF-16 in *C. elegans*. However, they also did not find FOXO4 regulation of Rpn6 in other cells like BJ human foreskin fibroblasts or the human embryonic kidney cell line HEK293T (Vilchez, Boyer, et al., 2012; Vilchez, Morantte, et al., 2012). Even though transcriptional changes of proteasomal genes are moderate, some transcription factors have been identified to regulate expression of proteasome genes. Nrf1 and Nrf2, for example, upregulate expression of proteasome subunits in response to oxidative stress (Koch et al., 2011; Meiners et al., 2014). The molecular pathways regulating TGF-β-induced upregulation of Rpn6, however, remain to be elucidated.

4.1.2 TGF-β-mediated induction of 26S-dependent protein turnover is necessary for myofibroblast differentiation

A tight interaction between the ubiquitin-proteasome system and TGF-β signaling has been implicated in several studies. Ubiquitin-dependent degradation of TGF-β receptors, SMADs and

their interacting proteins up- or downregulate TGF-β signaling. Hereby, E3 ligases like Smurfs or Arkadia promote ubiquitination and proteasomal degradation of mediators, thereby influencing signaling within the TGF-β pathway (David et al., 2013; Imamura et al., 2013; Soond & Chantry, 2011). However, a possible regulation of the ubiquitin-proteasome system by TGF-β signaling has not been studied so far. This study therefore shows for the first time that TGF-β activates the ubiquitin-proteasome system during myofibroblast differentiation of lung fibroblasts.

In addition to increased proteasome activity by 26S formation, CCL206 lung fibroblasts also showed accumulation of polyubiquitinated proteins in response to TGF-β as an indicator of enhanced protein turnover. Levels of polyubiquitinated proteins were also elevated in response to Rpn6 knockdown in phLF and confirmed impairment of ubiquitin-mediated protein degradation by the 26S proteasome. As shown here, accumulation of K48-polyubiquitinated proteins is widely used as an indicator not only for proteasome inhibition but also for increased protein turnover and is supported by several publications (D'Arcy et al., 2011; G. Liu et al., 2011; van Rijt et al., 2012). Therefore additional monitoring of proteasome activity is essential to draw conclusions about the initial reason for elevated levels of K48-polyubiquitinated proteins. However, accumulation of polyubiquitinated proteins was less pronounced in TGF-β-stimulated phLF than in CCL206 fibroblasts, it therefore seems that the extent of such activation of protein turnover depends very much on the cell type and *in vitro* cell culture conditions.

Indeed, a special need for elevated proteolysis seems to be quite reasonable during TGF-β-mediated myofibroblast differentiation, which is induced by binding of TGF-β to its receptors, thereby starting a signal transduction within the cell through the SMAD family of transcription activators. SMADs then translocate into the nucleus and induce massive biogenesis of profibrotic proteins in fibroblasts, finally resulting in their transformation into myofibroblasts (Leask & Abraham, 2004). This also leads to a strong cellular need for deposition of such pre-existing proteins, which are no longer required. In addition, protein quality control also plays an important role during biosynthesis of proteins to ensure their correct biological actions (Amm et al., 2014). Misfolded proteins, which fail this control, can be toxic and might impair proper cellular functions (Sontag et al., 2014). Therefore, they have to be degraded to avoid damage as shown for a variety of neurodegenerative maladies such as Alzheimer's, Huntington's or Parkinson's disease (Ciechanover & Kwon, 2015; Dennissen et al., 2012). Protein quality control in the cell is mainly conducted by chaperones, which maintain solubility of misfolded proteins and facilitate their refolding or degradation (Sontag et al., 2014). Indeed, dysregulated management of misfolded proteins has been implicated to contribute to a variety

of lung related diseases such as cystic fibrosis, chronic obstructive pulmonary disease, and also IPF (Balch et al., 2014). Therefore, upregulation of protein degradation during differentiation seems to be a reasonable mechanism to rapidly dispose needless or damaged proteins.

In contrast to that, Vilchez et al. observed decreased proteasome activity upon differentiation of ES cells into neuronal cells as shown by cleavage of chymotrypsin-like-specific substrates and accumulation of polyubiquitinated proteins as a read-out for reduced proteasome activity (Vilchez, Boyer, et al., 2012). Here, increased protein turnover together with high proteasomal cleavage rates might be important to assure survival and function of ES cells (Vilchez et al., 2014). The importance of the ubiquitin-proteasome system for maintenance of proliferation, three germ layer differentiation, and cellular reprogramming of self-renewing human ES cells has been supported by the identification of nuclear factor (erythroid-derived 2)-like 2 (Nrf2) as a novel pluripotency gene, which regulates proteasome maturation via the assembly factor POMP (Jang et al., 2014). Similar to this, normal function of hematopoietic stem cells, which generate mature blood cells, has been shown to critically depend on protein regulation via the ubiquitin-proteasome system (Moran-Crusio et al., 2012). The importance of the ubiquitin-proteasome system during differentiation has also been described for a variety of cell types besides stem cells, including plasma cells (Cenci, 2012) or during spermatogenesis (Bose et al., 2014). Still, there is only little known about the regulation of the proteasome to adapt its activity and controlled degradation to the need of the cell within different processes.

In this study, partial knockdown of Rpn6 not only prevented TGF-β-mediated formation of 26S/30S proteasomes but also counteracted expression of profibrotic marker and impaired myofibroblast differentiation of phLF. This indicates that Rpn6-induced formation of 26S/30S proteasomes is important for ubiquitin-mediated protein degradation in the process of myofibroblast differentiation.

Very similar to these findings, hypertrophic growth of cardiomyocytes involved activation of ubiquitin-mediated protein turnover via the 26S proteasome (Mearini et al., 2008). Collectively, these data fit well into the previously proposed concept that signal-induced formation of 26S proteasomes represents a novel regulatory mechanism that allows the cell to rapidly adjust ubiquitin-mediated protein degradation in order to maintain protein homeostasis during differentiation and remodeling (Bhattacharyya et al., 2014; Meiners et al., 2014; Schmidt & Finley, 2014).

While activation of proteasome function in myofibroblast differentiation is a novel observation of this study, the overall importance of proteasome activity for this process has been noted before

by the use of proteasome inhibitors and has also been confirmed by treatment of pmLF with oprozomib in this study. Interestingly, knockdown of Rpn6 provided similar antifibrotic effects as treatment of fibroblasts, obtained from different organs, with specific inhibitors of the 20S catalytic activities. Here, myofibroblast differentiation was uniformly impaired as indicated by reduced expression of matrix metalloproteases, collagens or other profibrotic factors (Koca et al., 2012; Meiners et al., 2002; Mutlu et al., 2012). While the use of proteasome inhibitors indiscriminately inhibits all 20S containing proteasomal complexes, knockdown of Rpn6 (as applied here) impairs the formation of 26S/30S complexes and thus specifically affects ubiquitin-dependent degradation of proteins. These results therefore indicate that myofibroblast differentiation requires enhanced ubiquitin-mediated turnover of proteins by 26S proteasomes and that ubiquitin-independent protein degradation by 20S proteasomes, here, is unable to complement for this activity.

4.1.3 The ubiquitin-proteasome system is regulated in pulmonary fibrosis

Confirming *in vitro* data, proteasome activity, formation of 26S/30S proteasomes and Rpn6 expression were also upregulated in fibrotic lung tissue of bleomycin challenged mice. Only few studies, so far, show increased proteasome activities *in vivo* in response to certain stimuli. Furthermore, Rpn6 levels and polyubiquitinated proteins were significantly increased in human lungs of IPF patients.

EGF-upregulating *C. elegans* or hyperglycaemic mice are two examples, which have been discussed in chapter 4.1.1 (G. Liu et al., 2011; H. Liu et al., 2012). But no study so far also showed normalization of proteasome activity after switchback to physiologic conditions as observed at day 56 post-bleomycin challenge, when proteasome activity returned to control levels. This finding again highlights the ability of the ubiquitin-proteasome system to rapidly adapt its degradation capacity to changing cellular conditions.

In fibrotic mouse lungs, only Rpn6 was increased, whereas Rpt5 and α1-7 did not change. Together with increased 26S/30S formation, this leads to the assumption that Rpn6 indeed might also regulate 26S/30S formation in lung fibrosis. However, to finally prove this hypothesis, transgenic animals with reduced Rpn6 expression might be necessary.

Interestingly, in fibrotic mouse lungs Rpn6 levels were highly elevated in proliferating AECII and bronchial Clara cells, which are hallmarks of fibrotic remodeling (Korfei et al., 2011). Indeed, AECs are discussed to be the primary source of profibrotic mediators to attract resident mesenchymal cells to induce their proliferation and differentiation (King et al., 2011). This raises the hypothesis that Rpn6-mediated induction of proteasomal degradation might be a common

mechanism in activated cells. In contrast to *in vitro* experiments, myofibroblasts here only partially stained positive for Rpn6. However, in human IPF lungs, myofibroblasts are one of the predominant cell types and arranged in foci. Myofibroblast foci are not present in bleomycin induced lung fibrosis and therefore represent one critical limitation of this model (Moore & Hogaboam, 2008). This also explains why Rpn6 in this model is not found to be highly expressed in myofibroblasts. Furthermore, expression of several proteasomal subunits of the 20S CP and 19S RP, including Rpn6, was not changed on mRNA level as obtained by qRT-PCR, again indicating a non-transcriptional regulation of Rpn6.

Similarly, Rpn6 was also specifically increased in IPF lungs compared to donor tissue. Here, a second 19S subunit, Rpt5, was also significantly elevated while the α3 subunit of the 20S proteasome was unaffected. mRNA expression of several 19S and 20S proteasomal subunits, including Rpn6, was not significantly altered in IPF tissue, which is well in agreement with publicly available array data. Here, no genes coding for proteasomal subunits were regulated but changes in mRNA expression of E3 ubiquitin protein ligases were observed, indicating that protein turnover indeed is changed in IPF (Bauer et al., 2014). mRNA data of the present study propose a posttranscriptional regulation of Rpn6 as also suggested by *in vitro* and mouse data.

It can be assumed that Rpn6-mediated increase of 26S/30S proteasome formation adapts proteasomal degradation rates to cope with activated protein turnover in fibrotic lung tissue. In line with this study, it has recently been shown that 26S proteasome content and activity is increased in human IPF lungs compared to donor lungs (Baker et al., 2014). The authors also observed an increased 20S content in IPF tissue compared to donor lungs, which was determined by a proteasome ELISA that was developed by the same group. In contrast to that, here no changes in 20S subunits were observed by direct Western blot analysis. However, in this publication, the authors calculate 20S and 26S ratios assuming a specific molecular weight for all proteasomes without taking into account the existence of other 20S containing complexes such as PA200- and PA28-associated or doubly capped 30S complexes, which are also present in human lungs (Korfei et al., 2013). This might influence the results on actual 20S to 26S ratios.

Levels of polyubiquitinated proteins were significantly increased in IPF patients and positively correlated with protein expression of Rpn6. This finding is interesting, as it clearly shows that Rpn6 levels increase together with ubiquitinated proteins to cope with a higher demand for protein degradation. Increased expression of Rpn6 was also observed in myofibroblasts of fibrotic foci in human IPF lungs and, as well, associated with augmented staining for polyubiquitinated proteins. These data indicate that increased protein turnover and activation of ubiquitin-dependent degradation by the proteasome via Rpn6 induced 26S formation is also a

feature of aberrant myofibroblast differentiation in IPF pathogenesis. Of interest, prominent staining of Rpn6 and polyubiquitin in hyperplastic bronchiolar basal cells of IPF patients was observed. Bronchiolar basal cells have been discussed to serve as progenitor cells for the bronchial epithelium with stem cell-like characteristics (Rock et al., 2009), which is in line with the findings of Vilchez et al. (Vilchez, Boyer, et al., 2012). It is tempting to speculate that overexpression of Rpn6 and activation of proteasomal degradation might be related to aberrant stem cell properties or hypertrophic growth of these cells.

High levels of Rpn6 in myofibroblasts of IPF lungs are in contrast to stainings of fibrotic mouse lung sections, which mainly showed overexpression of Rpn6 in hyperplastic alveolar epithelial cells and Clara cells. However, the bleomycin model for fibrosis reflects the reversible wound healing response to acute lung injury and not the slow and irreversible progression of tissue remodeling as seen in IPF. This is also indicated by the absence of some characteristic hallmarks of IPF like fibroblast foci in bleomycin induced pulmonary fibrosis (Moeller et al., 2008; Moore et al., 2013; Mouratis & Aidinis, 2011). But still, a common feature of these mouse and human data is that activated parenchymal cells had highly increased levels of Rpn6, indicative of elevated 26S/30S proteasome activity, which supports the idea that increased protein turnover in highly active cells indeed depends on increased proteasomal degradation rates.

To investigate whether the observed increase in K48-polyubiquitinated proteins in IPF lung tissue related to proteasome activation, comprehensive analysis of proteasome activity in lung homogenates was performed using activity-based probes (ABPs) and native gel analysis. Of note, activity profiles for the different donor and IPF tissues were quite heterogeneous. This finding most probably reflects the well-known problem of cellular heterogeneity between healthy donor and diseased IPF tissue. In addition, as activity of intact enzymatic complexes that are highly sensitive to prolonged transport and storage conditions was analyzed, it cannot fully be ruled out that some activity was lost in these tissue samples. In contrast, expression analysis by Western blotting was very robust as also seen by the stable expression of the housekeeping protein β-actin. Comparing Rpn6 protein levels with amounts of active 26S/30S proteasomes, which were obtained from APB labeled proteasomes, a significant positive correlation was only observed in IPF samples but not in donor tissue. This indicates that 26S/30S formation indeed might be highly regulated during fibrotic remodeling in IPF lungs in contrast to healthy lungs.

4.2   The Proteasome as a Target in IPF

Various reports propose the proteasome as a possible target for antifibrotic therapies based on the observation that treatment with proteasome inhibitors provides antifibrotic effects in several organs such as lung, skin, liver or heart (Fineschi et al., 2008; Meiners, Dreger, et al., 2008; Mutlu et al., 2012; I. Saeki et al., 2013). However, therapeutic application of first generation proteasome inhibitors in lung fibrosis showed controversial results in the bleomycin mouse model, providing both, high toxicity and beneficial antifibrotic effects (Fineschi et al., 2008; Mutlu et al., 2012). Therefore, inhibition profiles and antifibrotic effects of the novel, more specific and possibly less toxic second generation proteasome inhibitor oprozomib was comprehensively analyzed. Indeed, oprozomib showed higher specificity towards the chymotrypsin-like active site of the proteasome and provided less toxicity in alveolar epithelial cells. Furthermore, *in vitro* studies showed antifibrotic effects of low dose oprozomib treatment in pmLF. Oprozomib was applied locally into the lungs of bleomycin challenged animals to reduce inhibitor doses and systemic side effects. Indeed, as shown before, proteasome inhibitor treatment of fibrotic lungs was not tolerated and did not provide antifibrotic effects. Similar results were obtained after oral application of oprozomib. This study therefore provides strong evidence that proteasome inhibitors of the 20S core particle may be too toxic for application in pulmonary fibrosis.

4.2.1   Toxicity and inhibition profile of oprozomib

To compare cytotoxicity and inhibition profile of bortezomib, a well-studied FDA-approved proteasome inhibitor, and the second generation proteasome inhibitor oprozomib concerning toxicity and inhibition profile, inhibitors were applied to A549 and pmATII cells. In both cell types, oprozomib showed less toxicity than bortezomib. The "No Observed Adverse Effect Level" (NOAEL) of oprozomib exceeded that of bortezomib by a factor of 10 and oprozomib provided high selectivity for the chymotrypsin-like active site, whereas bortezomib inhibited also the caspase-like active site. It has been shown before that toxicities of proteasome inhibitors strongly depend on their inhibition profile (Meiners, Ludwig, et al., 2008). Inhibition studies with selective inhibitors of the chymotrypsin-like active site revealed that maximal toxicity in myeloma cells was only achieved by co-inhibition of the chymotrypsin-like activity with one of the other two catalytic sites of the proteasome (Britton et al., 2009; Mirabella et al., 2011). These data indicate that efficient inhibition of more than one active site is required for inducing cell death (Meiners, Ludwig, et al., 2008). Although oprozomib has been shown to cause apoptosis in different multiple myeloma and cancer cell lines at doses similar to the ones applied here,

unselective co-inhibition of the trypsin-like and caspase-like active sites at toxic doses cannot be ruled out in these studies (Chauhan et al., 2010; Roccaro et al., 2010; Zang et al., 2012).

Inhibition profile and cytotoxicity of oprozomib were very similar in pmLF compared to A549 cells. These fibroblasts were isolated from FVB-ODD-luc reporter mice, in which the ODD-luc reporter is supposed to accumulate upon proteasome inhibition. Therefore, inhibition of the proteasome can also be monitored by the increase of luciferase activity. In this study, only efficient inhibition of about 90% of the chymotrypsin-like proteasome activity showed an effect on the reporter, which was rather weak with an increase of about twofold only. In contrast, previous studies reported a pronounced increase of luciferase activity of more than 14 fold after proteasome inhibition with bortezomib or MG132, another proteasome inhibitor of the 20S CP, in ODD-luc-transfected HCT116 or Hela cells (Chou & Deshaies, 2011; Kimbrel et al., 2009). As both MG132 and bortezomib inhibit two active sites of the proteasome, it might be possible that proteasomal degradation of ODD-luc is not solely dependent on an active chymotrypsin-like activity but also might depend on the trypsin-like and/or caspase-like activities of the proteasome. Such active site specific effects on substrate degradation have been shown before *in vitro* (Kisselev et al., 2006). Furthermore, direct transfection of cells with the reporter construct might lead to higher expression levels of the reporter than in cells of transgenic animals as used here.

4.2.2 Oprozomib provides antifibrotic effects in lung fibroblasts

Oprozomib treatment of primary lung fibroblasts showed antifibrotic effects as indicated by dose dependent reduction in proliferation and collagen I expression. In addition, oprozomib counteracted TGF-β-induced expression of collagen I and αSMA. Similar effects on lung fibroblasts have been shown by Mutlu et al. after treatment with a comparable dose of 200 nM bortezomib (Mutlu et al., 2012). Further, these results are in line with several studies that used fibroblasts of different tissue origins such as skin (Fineschi et al., 2006), heart (Meiners et al., 2004), or kidney (Sakairi et al., 2011), and observed antifibrotic effects after treatment with inhibitors of the 20S CP. Therefore, it can be assume that partial and non-toxic inhibition of the 20S CP in fibroblasts generally results in reduced proliferation and expression of profibrotic markers.

The underlying mechanisms of these antifibrotic actions are not well understood, but several studies highlight the interaction with the TGF-β pathway (Soond & Chantry, 2011; Weiss et al., 2010). Fineschi et al. report a dose- and time-dependent reduction of collagen I and tissue inhibitor of metalloproteinase-1 (TIMP-1) and increase of MMP-1 on mRNA and protein level,

which mediates increased collagenolytic activity on collagen I after application of different proteasome inhibitors on dermal fibroblasts. These antifibrotic effects of proteasome inhibitors were still dominant after profibrotic TGF-β stimulation of fibroblasts. They further observed induction of c-Jun phosphorylation and accumulation upon inhibition of the proteasome, which acts as part of the transcription factor AP-1, upregulating MMP-1 and therefore decreasing collagen I levels, which may here in part explain antifibrotic effects of proteasome inhibitors (Fineschi et al., 2006).

Increased MMP-1 expression by alteration of the binding of c-Jun and SP1 transcription factors upon proteasome inhibition has further been observed by Goffin et al. to result in decreased synthesis of collagen I in dermal fibroblasts, confirming findings by Fineschi et al. (Goffin et al., 2010).

Contradictory to these studies, proteasome inhibition with MG132 in rat cardiac fibroblasts effectively counteracted IL-1β-mediated induction of MMP-2 and -9 expressions. This was associated with downregulation of collagen Iα1, Iα2 and IIIα1 (Meiners et al., 2004).

Another mechanism contributing to proteasome inhibitor-mediated antifibrotic effects has been investigated by Mutlu at al. in human lung and dermal fibroblasts. Treatment with bortezomib after TGF-β stimulation showed significant reduction of αSMA and connective tissue growth factor (CTGF) on mRNA and protein level. Here, bortezomib counteracted TGF-β mediated target gene expression by inhibition of SMAD activation. The nuclear hormone receptor PPARγ, which acts as repressor of SMAD-mediated transcription, was upregulated upon inhibition of the proteasome (Mutlu et al., 2012).

Treatment of renal fibroblasts using the proteasome inhibitors MG132 or lactacystin provided inhibition of TGF-β-induced αSMA expression on protein and mRNA level. MG132 did not counteract TGF-β-induced upregulation of phosphorylated SMAD2 or nuclear translocation of SMAD2/3 but attenuated the activity of the R-SMAD/SMAD4 complex as a transcriptional regulator as indicated by a luciferase assay for SMAD response elements. The transcriptional repressor SnoN was upregulated by proteasome inhibition, which may be responsible for decreased transcriptional activity of the R-SMAD/SMAD4 complex (Sakairi et al., 2011)

Furthermore, Pujols et al. applied non-toxic doses of the proteasome inhibitor MG262 to nasal fibroblasts and observed growth arrest, inhibited DNA replication and retinoblastoma phosphorylation, and increased expression of the cell cycle inhibitors p21 and p27. They confirmed decrease in basal and TGF-β-induced collagen mRNA expression and IL-1β-induced

production of IL-6, IL-8, monocyte chemoattractant protein-1, and granulocyte/macrophage colony-stimulating factor in MG262 treated fibroblasts (Pujols et al., 2012).

Antifibrotic effects of proteasome inhibitors as observed in the present study is not a novel finding, but it should be highlighted that all previous studies used multicatalytic-site inhibitors of the proteasome, (Fineschi et al., 2006; Koca et al., 2012; Meiners et al., 2004; Mutlu et al., 2012) whereas oprozomib only inhibits the chymotrypsin-like active site. Therefore, this study shows for the first time that inhibition of one active site only is sufficient to provide antifibrotic effects in fibroblasts and to counteract TGF-β signaling.

However, given the pleiotropic effects of proteasome inhibition on cellular signaling molecules and transcriptional activators, narrowing the antifibrotic effects of proteasome inhibitors down to a single signaling pathway might be oversimplified. Non-toxic inhibition of the proteasome further has been shown to induce a protective stress response in cells irrespective of the tissue origin, which confers cell cycle arrest, overall attenuation of transcriptional regulation, and protection from stress (Bieler et al., 2009; Meiners et al., 2006). To provide a more comprehensive view on the cellular changes that mediate the observed antifibrotic effects application of high-throughput techniques might be necessary.

4.2.3 *Oprozomib fails to provide antifibrotic effects in vivo*

In this study, oprozomib was initially applied locally into the lungs of mice to reduce systemic side effects and to increase local drug absorption. Indeed, oprozomib reduced proteasome activity in the lungs of healthy mice after local application in a well-tolerated dose range. Pulmonary application of oprozomib in bleomycin-challenged mice, however, was not well tolerated, especially when animals were treated three times within 7 days. Moreover, decreased pulmonary proteasome activities in response to oprozomib treatment was not observed, suggesting that proteasome inhibitors are either not effectively inhibiting the proteasome in fibrotic lungs or that a compensatory increase in proteasome activity counteracts this inhibition as shown by Rpn6-mediated induction of 26S/30S proteasomes. Any attempt to obtain a more efficient inhibition of the proteasome in the lung by repeated oprozomib treatment even worsened lung damage. This observation is in line with studies by Fineschi et al., where treatment with proteasome inhibitors did not attenuate bleomycin induced lung fibrosis. Instead, bleomycin-challenged animals, which were systemically treated every 3-4 days with 0.8 mg bortezomib per kg body weight displayed reduced survival (Fineschi et al., 2008). Very similar, no therapeutic effects were observed when oprozomib was applied systemically by oral application to reduce potential local toxicity of oprozomib after direct instillation into the lungs.

Proteasome activity was significantly reduced by oprozomib treatment in lungs of healthy animals but not in damaged and fibrotic lungs. Treatment of bleomycin-challenged animals with oprozomib rather led to increased weight loss and reduced survival. However, Mutlu et al. could prevent lung fibrosis in the bleomycin mouse model by intraperitoneal application of 0.12 mg/kg body weight bortezomib twice at day 7 and 14 with sacrificing of the mice at day 21 after bleomycin challenge (Mutlu et al., 2012). This is in contrast to the present study and the report of Fineschi et al. but highlights the difficulty of a very narrow therapeutic window of proteasome inhibitors for the treatment of pulmonary fibrosis. These data accord well with the established concept that the degree of proteasome inhibition in a given cell determines the biological outcome ranging from beneficial to cytotoxic effects (Fineschi et al., 2008; Meiners, Ludwig, et al., 2008).

It also has to be considered whether the bleomycin mouse model is an appropriate model for IPF-related pulmonary fibrosis and therapeutic testing of drugs such as proteasome inhibitors. Bleomycin initially causes acute lung injury and inflammation followed by fibrotic tissue remodeling in a very short time of about 7 to 9 days after intratracheal instillation. Within the fibrotic phase it resembles some of the histological patterns also seen in IPF such as increased expression of collagen and fibronectin and fibrotic remodeling. However, fibrotic remodeling in the bleomycin mouse model is reversible and therefore does not fully reflect the slow and irreversible progression of fibrosis as seen in IPF (Moeller et al., 2008; Moore et al., 2013; Mouratis & Aidinis, 2011). Therapeutic intervention with proteasome inhibitors in the beginning of the fibrotic remodeling phase might interfere with normal tissue repair and therefore even accelerate the damaging effects of bleomycin in this mouse model. Despite these limitations, the bleomycin mouse model remains the best characterized and probably most convenient model so far to test novel therapeutic compounds for pulmonary fibrosis (Mouratis & Aidinis, 2011).

Together with published data (Fineschi et al., 2008; Mutlu et al., 2012), these results thus strongly point towards a very narrow therapeutic window of proteasome inhibitors for the treatment of pulmonary fibrosis. The therapeutic window might even be narrower for irreversible proteasome inhibitors such as oprozomib. Together with the observation that treatment of bleomycin-challenged mice with proteasome inhibitors during the fibrotic remodeling phase even aggravated lung damage, it is well feasible that functional proteasomes are even required for the fibrotic wound healing response in the lung. This is also supported by previous data on elevated proteasome activities in fibrotic lungs. Indeed, activation of the proteasome, to a certain point, might also be necessary to promote wound healing during fibrotic remodeling.

Therefore irreversible inhibition of 20S CPs might even be detrimental to fibrotic lungs. The challenge then would be to specifically target activated proteasome complexes in the fibrotic lung to the right degree and at the right time point.

Therefore, inhibition of the formation of 26S proteasome complexes, as shown by Rpn6 knockdown, could represent a novel therapeutic approach to interfere with pulmonary myofibroblast differentiation and fibrosis, being more specific than the use of catalytic proteasome inhibitors that inactivate the proteolytic active sites of the 20S. Indeed, some compounds have already been identified to target protein-protein interactions within the 20S and 26S supercomplex (Gaczynska & Osmulski, 2015). The immunosupressor rapamycin, for example, has been identified to compete with the 19S RP for binding sites on the α-ring of the 20S CP, thereby interfering with 26S formation (Osmulski & Gaczynska, 2013). Treatment of bleomycin-induced fibrosis with rapamycin, however, did not show any antifibrotic effects but rather reduced lung function and increased weight loss in fibrotic animals. This effect cannot solely be explained by rapamycin-mediated impairment of 26S formation as the action of this drug is mainly based on antagonizing the mTOR kinase (Ballou & Lin, 2008).

Targeting of Rpn6 therefore might be a promising approach to selectively inhibit 26S formation without direct interaction with other cellular pathways and might in future represent a novel alternative for conventional proteasome inhibitors of the 20S CP.

4.3 Conclusion and Outlook

This study identified altered proteasome function as a possible novel trigger of IPF. Activation of the proteasome was observed in myofibroblasts, in experimental lung fibrosis, and in human IPF lungs. This activation was controlled by the 19S subunit Rpn6, which was required for the formation of highly active 26S/30S proteasomes. Rpn6 expression was further induced by TGF-β, and Rpn6 knockdown in activated myofibroblasts resulted in reduction of 26S/30S proteasomes, profibrotic marker proteins, and proliferation. Rpn6 was significantly elevated in fibrotic mouse and human lung tissue. Further, Rpn6 was predominantly expressed in human myofibroblasts and hyperplastic basal cells. These cells also showed increased levels of polyubiquitinated proteins providing evidence for an overall elevated protein turnover by the ubiquitin-proteasome system.

Rpn6-mediated activation of the proteasome by formation of 26S complexes during myofibroblast differentiation in IPF thus might provide a novel mechanism within the pathogenesis of IPF.

However, targeting of the proteasomal 20S CP failed to reduce lung fibrosis in this study. Although the novel, chymotrypsin-like site-specific inhibitor oprozomib provided antifibrotic effects in pmLF at non-toxic doses, local pulmonary or oral application accelerated bleomycin-induced lung damage. These findings confirm an overall important role of the proteasome in fibrotic lung remodeling. Therefore conventional proteasome inhibitors of the 20S active sites, which actually affect all proteasome complexes, might be too toxic for application in lung fibrosis.

Together with the finding that prevention of 26S formation and thereby inhibition of ubiquitin-dependent protein degradation provides antifibrotic effects without affecting 20S activities, this study strongly proposes the development of novel proteasome inhibitors that interfere with the assembly of the 19S RP to the 20S CP. Hereby, Rpn6 might serve as a novel drug target to impair pathologic formation of 26S/30S proteasomes and therefore ubiquitin-dependent protein degradation in IPF.

5 REFERENCES

Ahluwalia, N., Shea, B. S., and Tager, A. M. (2014). New therapeutic targets in idiopathic pulmonary fibrosis. Aiming to rein in runaway wound-healing responses. *American Journal of Respiratory and Critical Care Medicine*, *190*(8), 867–78.

Akhurst, R. J., and Hata, A. (2012). Targeting the TGFβ signalling pathway in disease. *Nature Reviews. Drug Discovery*, *11*(10), 790–811.

Amm, I., Sommer, T., and Wolf, D. H. (2014). Protein quality control and elimination of protein waste: The role of the ubiquitin-proteasome system. *Biochimica et Biophysica Acta - Molecular Cell Research*, *1843*(1), 182–196.

Araya, J., Kojima, J., Takasaka, N., Ito, S., Fujii, S., Hara, H., Yanagisawa, H., Kobayashi, K., Tsurushige, C., Kawaishi, M., Kamiya, N., Hirano, J., Odaka, M., Morikawa, T., Nishimura, S. L., Kawabata, Y., Hano, H., Nakayama, K., and Kuwano, K. (2012). Insufficient autophagy in idiopathic pulmonary fibrosis. *AJP: Lung Cellular and Molecular Physiology*, *304*(2), 56–69.

Armanios, M. Y., Chen, J. J.-L., Cogan, J. D., Alder, J. K., Ingersoll, R. G., Markin, C., Lawson, W. E., Xie, M., Vulto, I., Phillips, J. A., Lansdorp, P. M., Greider, C. W., and Loyd, J. E. (2007). Telomerase mutations in families with idiopathic pulmonary fibrosis. *The New England Journal of Medicine*, *356*, 1317–1326.

Aumiller, V., Balsara, N., Wilhelm, J., Günther, A., and Königshoff, M. (2013). WNT/β-catenin signaling induces IL-1β expression by alveolar epithelial cells in pulmonary fibrosis. *American Journal of Respiratory Cell and Molecular Biology*, *49*(1), 96–104.

Bagnato, G., and Harari, S. (2015). Cellular interactions in the pathogenesis of interstitial lung diseases. *European Respiratory Review*, *24*(135), 102–114.

Baker, T. A., Bach, H. H., Gamelli, R. L., Love, R. B., Majetschak, M., Bach Iv, H. H., Gamelli, R. L., Love, R. B., Majetschak, M., Bach, H. H., Gamelli, R. L., Love, R. B., and Majetschak, M. (2014). Proteasomes in lungs from organ donors and patients with end-stage pulmonary diseases. *Physiological Research / Academia Scientiarum Bohemoslovaca*, *63*(3), 311–9.

Balch, W. E., Sznajder, J. I., Budinger, S., Finley, D., Laposky, A. D., Cuervo, A. M., Benjamin, I. J., Barreiro, E., Morimoto, R. I., Postow, L., Weissman, A. M., Gail, D., Banks-Schlegel, S., Croxton, T., and Gan, W. (2014). Malfolded protein structure and proteostasis in lung diseases. *American Journal of Respiratory and Critical Care Medicine*, *189*(1), 96–103.

Ballou, L. M., and Lin, R. Z. (2008). Rapamycin and mTOR kinase inhibitors. *Journal of Chemical Biology*, *1*(1-4), 27–36.

Barkauskas, C. E., and Noble, P. W. (2014). Cellular mechanisms of tissue fibrosis. 7. New insights into the cellular mechanisms of pulmonary fibrosis. *American Journal of Physiology. Cell Physiology*, *306*(11), C987–96.

Bauer, Y., Tedrow, J., de Bernard, S., Birker-Robaczewska, M., Gibson, K. F., Juan Guardela, B., Hess, P., Klenk, A., Lindell, K. O., Poirey, S., Renault, B., Rey, M., Weber, E., Nayler, O., and Kaminski, N. (2014). A Novel Genomic Signature with Translational Significance for Human Idiopathic Pulmonary Fibrosis. *American Journal of Respiratory Cell and Molecular Biology*, (41), 1–101.

Baumgartner, K. B., Samet, J. M., Stidley, C. A., Colby, T. V, and Waldron, J. A. (1997). Cigarette smoking: a risk factor for idiopathic pulmonary fibrosis. *American Journal of Respiratory and Critical Care Medicine*, *155*, 242–248.

Beck, P., Dubiella, C., and Groll, M. (2012). Covalent and non-covalent reversible proteasome inhibition. *Biological Chemistry*, *393*(10), 1101–20.

Benanti, J. A. (2012). Coordination of cell growth and division by the ubiquitin-proteasome system. *Seminars in Cell & Developmental Biology*, *23*(5), 492–8.

Besche, H. C., Peth, A., and Goldberg, A. L. (2009). Getting to first base in proteasome assembly. *Cell*, *138*(1), 25–8.

Beug, S. T., Cheung, H. H., LaCasse, E. C., and Korneluk, R. G. (2012). Modulation of immune signalling by inhibitors of apoptosis. *Trends in Immunology*, *33*(11), 535–45.

Bhattacharyya, S., Yu, H., Mim, C., and Matouschek, A. (2014). Regulated protein turnover: snapshots of the proteasome in action. *Nature Reviews. Molecular Cell Biology*, *15*(2), 122–33.

Bieler, S., Meiners, S., Stangl, V., Pohl, T., and Stangl, K. (2009). Comprehensive proteomic and transcriptomic analysis reveals early induction of a protective anti-oxidative stress response by low-dose proteasome inhibition. *Proteomics*, *9*(12), 3257–67.

Borissenko, L., and Groll, M. (2007). 20S proteasome and its inhibitors: crystallographic knowledge for drug development. *Chemical Reviews*, *107*(3), 687–717.

Bose, R., Manku, G., Culty, M., and Wing, S. S. (2014). Ubiquitin-proteasome system in spermatogenesis. *Advances in Experimental Medicine and Biology*, *759*, 181–213.

Braun, B. C., Glickman, M., Kraft, R., Dahlmann, B., Kloetzel, P. M., Finley, D., and Schmidt, M. (1999). The base of the proteasome regulatory particle exhibits chaperone-like activity. *Nature Cell Biology*, *1*(4), 221–6.

Britton, M., Lucas, M. M., Downey, S. L., Screen, M., Pletnev, A. a, Verdoes, M., Tokhunts, R. a, Amir, O., Goddard, A. L., Pelphrey, P. M., Wright, D. L., Overkleeft, H. S., and Kisselev, A. F. (2009). Selective inhibitor of proteasome's caspase-like sites sensitizes cells to specific inhibition of chymotrypsin-like sites. *Chemistry & Biology*, *16*(12), 1278–89.

Cavazza, A., Rossi, G., Carbonelli, C., Spaggiari, L., Paci, M., and Roggeri, A. (2010). The role of histology in idiopathic pulmonary fibrosis: An update. *Respiratory Medicine*, *104*, S11–S22.

Cenci, S. (2012). The Proteasome in Terminal Plasma Cell Differentiation. *Seminars in Hematology*, *49*(3), 215–222.

Chamberlain, P. P., Lopez-Girona, A., Miller, K., Carmel, G., Pagarigan, B., Chie-Leon, B., Rychak, E., Corral, L. G., Ren, Y. J., Wang, M., Riley, M., Delker, S. L., Ito, T., Ando, H., Mori, T., Hirano, Y., Handa, H., Hakoshima, T., Daniel, T. O., and Cathers, B. E. (2014). Structure of the human Cereblon-DDB1-lenalidomide complex reveals basis for responsiveness to thalidomide analogs. *Nature Structural & Molecular Biology*, *21*(August), 1–8.

Chauhan, D., Singh, A. V, Aujay, M., Kirk, C. J., Bandi, M., Ciccarelli, B., Raje, N., Richardson, P., and Anderson, K. C. (2010). A novel orally active proteasome inhibitor ONX 0912 triggers in vitro and in vivo cytotoxicity in multiple myeloma. *Blood*, *116*(23), 4906–4915.

Chomczynski, P., and Sacchi, N. (1987). Single-Step Method of RNA Isolation by Acid Guanidinium Thiocyanate–Phenol–Chloroform Extraction. *Analytical Biochemistry*, *162*(1), 156–159.

Chou, T.-F., and Deshaies, R. J. (2011). Quantitative cell-based protein degradation assays to identify and classify drugs that target the ubiquitin-proteasome system. *The Journal of Biological Chemistry*, *286*(19), 16546–54.

Christianson, J. C., and Ye, Y. (2014). Cleaning up in the endoplasmic reticulum: ubiquitin in charge. *Nature Structural & Molecular Biology*, *21*(4), 325–35.

Ciechanover, A. (2013). Intracellular protein degradation: From a vague idea through the lysosome and the ubiquitin-proteasome system and onto human diseases and drug targeting. *Bioorganic and Medicinal Chemistry*, *21*(12), 3400–3410.

Ciechanover, A. (2015). The unravelling of the ubiquitin system. *Nature Reviews Molecular Cell Biology*, *16*(5), 322–324.

Ciechanover, A., and Kwon, Y. T. (2015). Degradation of misfolded proteins in neurodegenerative diseases: therapeutic targets and strategies. *Experimental & Molecular Medicine*, *47*(3), e147.

Coux, O., Tanaka, K., and Goldberg, A. L. (1996). Structure and functions of the 20S and 26S proteasomes. *Annual Review of Biochemistry*, *65*, 801–847.

Cravatt, B. F., Wright, A. T., and Kozarich, J. W. (2008). Activity-based protein profiling: from enzyme chemistry to proteomic chemistry. *Annual Review of Biochemistry*, *77*, 383–414.

D'Arcy, P., Brnjic, S., Olofsson, M. H., Fryknäs, M., Lindsten, K., De Cesare, M., Perego, P., Sadeghi, B., Hassan, M., Larsson, R., and Linder, S. (2011). Inhibition of proteasome deubiquitinating activity as a new cancer therapy. *Nature Medicine*, *17*(12), 1636–40.

Dahlmann, B. (2005). Proteasomes. *Essays in Biochemistry*, *41*, 31–48.

David, D., Nair, S. A., and Pillai, M. R. (2013). Smurf E3 ubiquitin ligases at the cross roads of oncogenesis and tumor suppression. *Biochimica et Biophysica Acta*, *1835*(1), 119–28.

Dennissen, F. J. A., Kholod, N., and van Leeuwen, F. W. (2012). The ubiquitin proteasome system in neurodegenerative diseases: Culprit, accomplice or victim? *Progress in Neurobiology*, *96*(2), 190–207.

Di Napoli, M., and McLaughlin, B. (2005). The ubiquitin-proteasome system as a drug target in cerebrovascular disease: therapeutic potential of proteasome inhibitors. *Current Opinion in Investigational Drugs (London, England : 2000)*, *6*(7), 686–699.

Dick, L. R., and Fleming, P. E. (2010). Building on bortezomib: second-generation proteasome inhibitors as anti-cancer therapy. *Drug Discovery Today*, *15*(5-6), 243–9.

Dou, Q. P., and Zonder, J. A. (2014). Overview of Proteasome Inhibitor-Based Anti-cancer Therapies: Perspective on Bortezomib and Second Generation Proteasome Inhibitors versus Future Generation Inhibitors of Ubiquitin-Proteasome System. *Current Cancer Drug Targets*, *14*(6), 517–536.

Duffield, J. S., Lupher, M., Thannickal, V. J., and Wynn, T. a. (2013). Host responses in tissue repair and fibrosis. *Annual Review of Pathology*, *8*, 241–76.

Elsasser, S., Schmidt, M., and Finley, D. (2005). Characterization of the proteasome using native gel electrophoresis. *Methods in Enzymology*, *398*, 353–63.

Fernandez, I. E., and Eickelberg, O. (2012a). The impact of TGF-β on lung fibrosis: from targeting to biomarkers. *Proceedings of the American Thoracic Society*, *9*(3), 111–6.

Fernandez, I. E., and Eickelberg, O. (2012b, August 18). New cellular and molecular mechanisms of lung injury and fibrosis in idiopathic pulmonary fibrosis. *The Lancet*.

Fineschi, S., Bongiovanni, M., Donati, Y., Djaafar, S., Naso, F., Goffin, L., Argiroffo, C. B., Pache, J.-C., Dayer, J.-M., Ferrari-Lacraz, S., and Chizzolini, C. (2008). In vivo investigations on anti-fibrotic potential of proteasome inhibition in lung and skin fibrosis. *American Journal of Respiratory Cell and Molecular Biology*, *39*(4), 458–65.

Fineschi, S., Reith, W., Guerne, P. A., Dayer, J.-M., and Chizzolini, C. (2006). Proteasome blockade exerts an antifibrotic activity by coordinately down-regulating type I collagen and tissue inhibitor of metalloproteinase-1 and up-regulating metalloproteinase-1 production in human dermal fibroblasts. *The FASEB Journal : Official Publication of the Federation of American Societies for Experimental Biology*, *20*(3), 562–564.

Finley, D. (2009). Recognition and processing of ubiquitin-protein conjugates by the proteasome. *Annual Review of Biochemistry*, *78*, 477–513.

Frankland-Searby, S., and Bhaumik, S. R. (2012). The 26S proteasome complex: an attractive target for cancer therapy. *Biochimica et Biophysica Acta*, *1825*(1), 64–76.

Gaczynska, M., and Osmulski, P. A. (2015). Targeting Protein-Protein Interactions in the Proteasome Super-Assemblies. *Current Topics in Medicinal Chemistry*, *15*(20), 2056–67.

Geng, F., Wenzel, S., and Tansey, W. P. (2012). Ubiquitin and Proteasomes in Transcription. *Annual Review of Biochemistry*, *81*(1), 177–201.

Goffin, L., Seguin-Estévez, Q., Alvarez, M., Reith, W., and Chizzolini, C. (2010). Transcriptional regulation of matrix metalloproteinase-1 and collagen 1A2 explains the anti-fibrotic effect exerted by proteasome inhibition in human dermal fibroblasts. *Arthritis Research & Therapy*, *12*(2), R73.

Goldman, S. J., Chen, E., Taylor, R., Zhang, S., Petrosky, W., Reiss, M., and Jin, S. (2011). Use of the ODD-luciferase transgene for the non-invasive imaging of spontaneous tumors in mice. *PloS One*, *6*(3), e18269.

Groll, M., Bajorek, M., Köhler, a, Moroder, L., Rubin, D. M., Huber, R., Glickman, M. H., and Finley, D. (2000). A gated channel into the proteasome core particle. *Nature Structural Biology*, *7*(11), 1062–7.

Groll, M., Ditzel, L., Löwe, J., Stock, D., Bochtler, M., Bartunik, H. D., and Huber, R. (1997). Structure of 20S proteasome from yeast at 2.4 A resolution. *Nature*, *386*(6624), 463–71.

Gu, Z. C., and Enenkel, C. (2014). Proteasome assembly. *Cellular and Molecular Life Sciences*, *71*(24), 4729–4745.

Haghi, M., Ong, H. X., Traini, D., and Young, P. (2014). Across the pulmonary epithelial barrier: Integration of physicochemical properties and human cell models to study pulmonary drug formulations. *Pharmacology & Therapeutics*, *144*(3), 235–52.

Hardie, W. D., Hagood, J. S., Dave, V., Perl, A. K. T., Whitsett, J. A., Korfhagen, T. R., and Glasser, S. (2010). Signaling pathways in the epithelial origins of pulmonary fibrosis. *Cell Cycle*, *9*(14), 2769–2776.

Herndon, T. M., Deisseroth, A., Kaminskas, E., Kane, R. C., Koti, K. M., Rothmann, M. D., Habtemariam, B., Bullock, J., Bray, J. D., Hawes, J., Palmby, T. R., Jee, J., Adams, W., Mahayni, H., Brown, J., Dorantes, A., Sridhara, R., Farrell, A. T., and Pazdur, R. (2013). U.S. Food and Drug Administration approval: Carfilzomib for the treatment of multiple myeloma. *Clinical Cancer Research*, *19*(17), 4559–4563.

Hideshima, T., Richardson, P., Chauhan, D., Palombella, V. J., Elliott, P. J., Adams, J., and Anderson, K. C. (2001). The proteasome inhibitor PS-341 inhibits growth, induces apoptosis, and overcomes drug resistance in human multiple myeloma cells. *Cancer Research*, *61*(7), 3071–3076.

Hillebrandt, S., Goos, C., Matern, S., and Lammert, F. (2002). Genome-wide analysis of hepatic fibrosis in inbred mice identifies the susceptibility locus Hfib1 on chromosome 15. *Gastroenterology*, *123*(6), 2041–51.

Hinz, B., Phan, S. H., Thannickal, V. J., Galli, A., Bochaton-Piallat, M.-L., and Gabbiani, G. (2007). The myofibroblast: one function, multiple origins. *The American Journal of Pathology*, *170*(6), 1807–16.

Hoffman, L., Pratt, G., and Rechsteiner, M. (1992). Multiple forms of the 20 S multicatalytic and the 26 S ubiquitin/ATP-dependent proteases from rabbit reticulocyte lysate. *The Journal of Biological Chemistry*, *267*(31), 22362–8.

Horie, M., Stowe, M., Tabei, M., Kato, H., Nakamura, A., Endoh, S., Morimoto, Y., and Fujita, K. (2013). Dispersant affects the cellular influences of single-wall carbon nanotube: the role of CNT as carrier of dispersants. *Toxicology Mechanisms and Methods*, *23*(5), 315–22.

Huang, H., Zhang, X., Li, S., Liu, N., Lian, W., McDowell, E., Zhou, P., Zhao, C., Guo, H., Zhang, C., Yang, C., Wen, G., Dong, X., Lu, L., Ma, N., Dong, W., Dou, Q. P., Wang, X., and Liu, J. (2010). Physiological levels of ATP negatively regulate proteasome function. *Cell Research*, *20*(12), 1372–85.

Huber, E. M., and Groll, M. (2012). Inhibitors for the immuno- and constitutive proteasome: Current and future trends in drug development. *Angewandte Chemie - International Edition*, *51*(35), 8708–8720.

Imamura, T., Oshima, Y., and Hikita, A. (2013). Regulation of TGF-β family signalling by ubiquitination and deubiquitination. *Journal of Biochemistry*, *154*(6), 481–9.

Isono, E., Saito, N., Kamata, N., Saeki, Y., and Toh-E, A. (2005). Functional analysis of Rpn6p, a lid component of the 26 S proteasome, using temperature-sensitive rpn6 mutants of the yeast Saccharomyces cerevisiae. *The Journal of Biological Chemistry*, *280*(8), 6537–47.

Jang, J., Wang, Y., Kim, H.-S., Lalli, M. a, and Kosik, K. S. (2014). Nrf2, a regulator of the proteasome, controls self-renewal and pluripotency in human embryonic stem cells. *Stem Cells*, *32*(10), 2616–2625.

Jayachandran, A., Königshoff, M., Yu, H., Rupniewska, E., Hecker, M., Klepetko, W., Seeger, W., and Eickelberg, O. (2009). SNAI transcription factors mediate epithelial-mesenchymal transition in lung fibrosis. *Thorax*, *64*(12), 1053–1061.

Kabanov, A. V., and Alakhov, V. (2000). Micelles of Amphiphilic Block Copolymers as Vechicles for Drug Delivery. In *Amphiphilic Block Copolymers: Self Assembly and Applications* (pp. 134–148). Elsevier.

Kane, R. C., Bross, P. F., Farrell, A. T., and Pazdur, R. (2003). Velcade: U.S. FDA approval for the treatment of multiple myeloma progressing on prior therapy. *The Oncologist*, *8*(6), 508–513.

Katzenstein, A.-L. A., and Myers, J. L. (1998). Idiopathic pulmonary fibrosis: Clinical relevance of pathologic classification. *American Journal of Respiratory and Critical Care Medicine*, *157*(4), 1301–1315.

Kimbrel, E. a, Davis, T. N., Bradner, J. E., and Kung, A. L. (2009). In vivo pharmacodynamic imaging of proteasome inhibition. *Molecular Imaging*, *8*(3), 140–7.

King, T. E., Bradford, W. Z., Castro-Bernardini, S., Fagan, E. a, Glaspole, I., Glassberg, M. K., Gorina, E., Hopkins, P. M., Kardatzke, D., Lancaster, L., Lederer, D. J., Nathan, S. D., Pereira, C. a, Sahn, S. a, Sussman, R., Swigris, J. J., and Noble, P. W. (2014). A phase 3 trial of pirfenidone in patients with idiopathic pulmonary fibrosis. *The New England Journal of Medicine*, *370*(22), 2083–92.

King, T. E., Pardo, A., and Selman, M. (2011). Idiopathic pulmonary fibrosis. *Lancet*, *378*(9807), 1949–61.

Kish-Trier, E., and Hill, C. P. (2013). Structural biology of the proteasome. *Annual Review of Biophysics*, *42*, 29–49.

Kisselev, A. F., Callard, A., and Goldberg, A. L. (2006). Importance of the different proteolytic sites of the proteasome and the efficacy of inhibitors varies with the protein substrate. *The Journal of Biological Chemistry*, *281*(13), 8582–90.

Klingberg, F., Hinz, B., and White, E. S. (2013). The myofibroblast matrix: Implications for tissue repair andfibrosis. *Journal of Pathology*, *229*(2), 298–309.

Koca, S. S., Ozgen, M., Dagli, F., Tuzcu, M., Ozercan, I. H., Sahin, K., and Isik, A. (2012). Proteasome inhibition prevents development of experimental dermal fibrosis. *Inflammation*, *35*(3), 810–7.

Koch, A., Steffen, J., and Krüger, E. (2011). TCF11 at the crossroads of oxidative stress and ubiquitin proteasome system. *Cell Cycle*.

Komander, D., and Rape, M. (2012). The ubiquitin code. *Annual Review of Biochemistry*, *81*, 203–29.

Königshoff, M., Kramer, M., Balsara, N., Wilhelm, J., Amarie, O. V., Jahn, A., Rose, F., Fink, L., Seeger, W., Schaefer, L., Günther, A., and Eickelberg, O. (2009). WNT1-inducible signaling protein-1 mediates pulmonary fibrosis in mice and is upregulated in humans with idiopathic pulmonary fibrosis. *Journal of Clinical Investigation*, *119*(4), 772–787.

Korfei, M., Schmitt, S., Ruppert, C., Henneke, I., Markart, P., Loeh, B., Mahavadi, P., Wygrecka, M., Klepetko, W., Fink, L., Bonniaud, P., Preissner, K. T., Lochnit, G., Schaefer, L., Seeger, W., and Guenther, A. (2011). Comparative proteomic analysis of lung tissue from patients with idiopathic pulmonary fibrosis (IPF) and lung transplant donor lungs. *Journal of Proteome Research*, *10*(5), 2185–205.

Korfei, M., von der Beck, D., Henneke, I., Markart, P., Ruppert, C., Mahavadi, P., Ghanim, B., Klepetko, W., Fink, L., Meiners, S., Krämer, O. H., Seeger, W., Vancheri, C., and Guenther, A. (2013). Comparative proteome analysis of lung tissue from patients with idiopathic pulmonary fibrosis (IPF), non-specific interstitial pneumonia (NSIP) and organ donors. *Journal of Proteomics*, *85*, 109–128.

Kubiczkova, L., Pour, L., Sedlarikova, L., Hajek, R., and Sevcikova, S. (2014). Proteasome inhibitors - molecular basis and current perspectives in multiple myeloma. *Journal of Cellular and Molecular Medicine*, *18*(6), 947–961.

Lander, G. C., Estrin, E., Matyskiela, M. E., Bashore, C., Nogales, E., and Martin, A. (2012). Complete subunit architecture of the proteasome regulatory particle. *Nature*, *482*(7384), 186–91.

Lander, G. C., Martin, A., and Nogales, E. (2013). The proteasome under the microscope: The regulatory particle in focus. *Current Opinion in Structural Biology*, *23*(2), 243–251.

Leask, A., and Abraham, D. J. (2004). TGF-beta signaling and the fibrotic response. *The FASEB Journal*, *18*(7), 816–827.

Lee, J.-W., Bae, S.-H., Jeong, J.-W., Kim, S.-H., and Kim, K.-W. (2004). Hypoxia-inducible factor (HIF-1)alpha: its protein stability and biological functions. *Experimental & Molecular Medicine*, *36*(1), 1–12.

Liu, C.-W., and Jacobson, A. D. (2013). Functions of the 19S complex in proteasomal degradation. *Trends in Biochemical Sciences*, *38*(2), 103–10.

Liu, C.-W., Li, X., Thompson, D., Wooding, K., Chang, T., Tang, Z., Yu, H., Thomas, P. J., and DeMartino, G. N. (2006). ATP binding and ATP hydrolysis play distinct roles in the function of 26S proteasome. *Molecular Cell*, *24*(1), 39–50.

Liu, G., Rogers, J., Murphy, C. T., and Rongo, C. (2011). EGF signalling activates the ubiquitin proteasome system to modulate C. elegans lifespan. *The EMBO Journal*, *30*(15), 2990–3003.

Liu, H., Yu, S., Xu, W., and Xu, J. (2012). Enhancement of 26S proteasome functionality connects oxidative stress and vascular endothelial inflammatory response in diabetes mellitus. *Arteriosclerosis, Thrombosis, and Vascular Biology*, *32*(9), 2131–40.

Maharaj, S., Shimbori, C., and Kolb, M. (2013). Fibrocytes in pulmonary fibrosis: A brief synopsis. *European Respiratory Review*, *22*(130), 552–557.

Makino, D. L., Halbach, F., and Conti, E. (2013). The RNA exosome and proteasome: common principles of degradation control. *Nature Reviews. Molecular Cell Biology*, *14*(10), 654–60.

Malmsten, M. (2000). Block copolymers in pharmaceutics. In *Amphiphilic Block Copolymers: Self Assembly and Applications* (pp. 319–346). Elsevier.

Marques, A. J., Palanimurugan, R., Matias, A. C., Ramos, P. C., and Dohmen, R. J. (2009). Catalytic mechanism and assembly of the proteasome. *Chemical Reviews*, *109*(4), 1509–36.

Massagué, J. (2012). TGFβ signalling in context. *Nature Reviews. Molecular Cell Biology*, *13*(10), 616–30.

Mearini, G., Schlossarek, S., Willis, M. S., and Carrier, L. (2008). The ubiquitin-proteasome system in cardiac dysfunction. *Biochimica et Biophysica Acta - Molecular Basis of Disease*, *1782*(12), 749–763.

Meiners, S., Dreger, H., Fechner, M., Bieler, S., Rother, W., Günther, C., Baumann, G., Stangl, V., and Stangl, K. (2008). Suppression of cardiomyocyte hypertrophy by inhibition of the ubiquitin-proteasome system. *Hypertension*, *51*(2), 302–308.

Meiners, S., and Eickelberg, O. (2012). What shall we do with the damaged proteins in lung disease? Ask the proteasome! *The European Respiratory Journal : Official Journal of the European Society for Clinical Respiratory Physiology*, *40*(5), 1260–8.

Meiners, S., Eickelberg, O., and Königshoff, M. (2015). Hallmarks of the ageing lung. *The European Respiratory Journal*, *45*(3), 807–27.

Meiners, S., Hocher, B., Weller, A., Laule, M., Stangl, V., Guenther, C., Godes, M., Mrozikiewicz, A., Baumann, G., and Stangl, K. (2004). Downregulation of matrix metalloproteinases and collagens and suppression of cardiac fibrosis by inhibition of the proteasome. *Hypertension*, *44*(4), 471–7.

Meiners, S., Keller, I. E., Semren, N., and Caniard, A. (2014). Regulation of the Proteasome: Evaluating the Lung Proteasome as a New Therapeutic Target. *Antioxidants & Redox Signaling*, *21*(17), 2364–2382.

Meiners, S., Laule, M., Rother, W., Guenther, C., Prauka, I., Muschick, P., Baumann, G., Kloetzel, P. M., and Stangl, K. (2002). Ubiquitin-proteasome pathway as a new target for the prevention of restenosis. *Circulation*, *105*(4), 483–489.

Meiners, S., Ludwig, A., Lorenz, M., Dreger, H., Baumann, G., Stangl, V., and Stangl, K. (2006). Nontoxic proteasome inhibition activates a protective antioxidant defense response in endothelial cells. *Free Radical Biology & Medicine*, *40*(12), 2232–41.

Meiners, S., Ludwig, A., Stangl, V., and Stangl, K. (2008). Proteasome inhibitors: poisons and remedies. *Medicinal Research Reviews*, *28*(2), 309–27.

Micel, L. N., Tentler, J. J., Smith, P. G., and Eckhardt, S. G. (2013). Role of ubiquitin ligases and the proteasome in oncogenesis: Novel targets for anticancer therapies. *Journal of Clinical Oncology*, *31*(9), 1231–1238.

Mirabella, A. C., Pletnev, A. A., Downey, S. L., Florea, B. I., Shabaneh, T. B., Britton, M., Verdoes, M., Filippov, D. V, Overkleeft, H. S., and Kisselev, A. F. (2011). Specific cell-permeable inhibitor of proteasome trypsin-like sites selectively sensitizes myeloma cells to bortezomib and carfilzomib. *Chemistry and Biology*, *18*(5), 608–618.

Moeller, A., Ask, K., Warburton, D., Gauldie, J., and Kolb, M. (2008). The bleomycin animal model: a useful tool to investigate treatment options for idiopathic pulmonary fibrosis? *The International Journal of Biochemistry & Cell Biology*, *40*(3), 362–82.

Moore, B. B., and Hogaboam, C. M. (2008). Murine models of pulmonary fibrosis. *American Journal of Physiology. Lung Cellular and Molecular Physiology*, *294*(2), L152–L160.

Moore, B. B., Lawson, W. E., Oury, T. D., Sisson, T. H., Raghavendran, K., and Hogaboam, C. M. (2013). Animal models of fibrotic lung disease. *American Journal of Respiratory Cell and Molecular Biology*, *49*(2), 167–179.

Moran-Crusio, K., Reavie, L. B., and Aifantis, I. (2012). Regulation of hematopoietic stem cell fate by the ubiquitin proteasome system. *Trends in Immunology*, *33*(7), 357–63.

Moravec, R. A., O'Brien, M. A., Daily, W. J., Scurria, M. A., Bernad, L., and Riss, T. L. (2009). Cell-based bioluminescent assays for all three proteasome activities in a homogeneous format. *Analytical Biochemistry*, *387*(2), 294–302.

Mouratis, M. A., and Aidinis, V. (2011). Modeling pulmonary fibrosis with bleomycin. *Current Opinion in Pulmonary Medicine*, *17*(5), 355–61.

Murata, S., Yashiroda, H., and Tanaka, K. (2009). Molecular mechanisms of proteasome assembly. *Nature Reviews. Molecular Cell Biology*, *10*(2), 104–15.

Mutlu, G. M., Budinger, G. R. S., Wu, M., Lam, A. P., Zirk, A., Rivera, S., Urich, D., Chiarella, S. E., Go, L. H. T., Ghosh, A. K., Selman, M., Pardo, A., Varga, J., Kamp, D. W., Chandel, N. S., Sznajder, J. I., and Jain, M. (2012). Proteasomal inhibition after injury prevents fibrosis by modulating TGF-β(1) signalling. *Thorax*, *67*(2), 139–46.

Noble, P. W., Barkauskas, C. E., and Jiang, D. (2012). Pulmonary fibrosis: Patterns and perpetrators. *Journal of Clinical Investigation*, *122*(8), 2756–2762.

Osmulski, P. A., and Gaczynska, M. (2013). Rapamycin allosterically inhibits the proteasome. *Molecular Pharmacology*, *84*(1), 104–13.

Patel, A. S., Lin, L., Geyer, A., Haspel, J. a, An, C. H., Cao, J., Rosas, I. O., and Morse, D. (2012). Autophagy in idiopathic pulmonary fibrosis. *PloS One*, *7*(7), e41394.

Pathare, G. R., Nagy, I., Bohn, S., Unverdorben, P., Hubert, A., Körner, R., Nickell, S., Lasker, K., Sali, A., Tamura, T., Nishioka, T., Förster, F., Baumeister, W., and Bracher, A. (2012). The proteasomal subunit Rpn6 is a molecular clamp holding the core and regulatory subcomplexes together. *Proceedings of the National Academy of Sciences of the United States of America*, *109*(1), 149–54.

Phan, S. H. (2012). Genesis of the myofibroblast in lung injury and fibrosis. *Proceedings of the American Thoracic Society*, *9*(3), 148–52.

Pujols, L., Fernández-Bertolín, L., Fuentes-Prado, M., Alobid, I., Roca-Ferrer, J., Agell, N., Mullol, J., and Picado, C. (2012). Proteasome inhibition reduces proliferation, collagen expression, and inflammatory cytokine production in nasal mucosa and polyp fibroblasts. *The Journal of Pharmacology and Experimental Therapeutics*, *343*(1), 184–97.

Rafii, R., Juarez, M. M., Albertson, T. E., and Chan, A. L. (2013). A review of current and novel therapies for idiopathic pulmonary fibrosis. *Journal of Thoracic Disease*, *5*(1), 48–73.

Raghu, G., Collard, H. R., Egan, J. J., Martinez, F. J., Behr, J., Brown, K. K., Colby, T. V, Cordier, J.-F., Flaherty, K. R., Lasky, J. a, Lynch, D. a, Ryu, J. H., Swigris, J. J., Wells, A. U., Ancochea, J., Bouros, D., Carvalho, C., Costabel, U., Ebina, M., Hansell, D. M., Johkoh, T., Kim, D. S., King, T. E., Kondoh, Y., Myers, J., Müller, N. L., Nicholson, A. G., Richeldi, L., Selman, M., Dudden, R. F., Griss, B. S., Protzko, S. L., and Schünemann, H. J. (2011). An official ATS/ERS/JRS/ALAT statement: idiopathic pulmonary fibrosis: evidence-based guidelines for diagnosis and management. *American Journal of Respiratory and Critical Care Medicine*, *183*(6), 788–824.

Rechsteiner, M. (2008). The 26S Proteasome. In *Protein Science Encyclopedia* (pp. 220–247). WILEY-VCH Verlag.

Roccaro, A. M., Sacco, A., Aujay, M., Ngo, H. T., Azab, A. K., Azab, F., Quang, P., Maiso, P., Runnels, J., Anderson, K. C., Demo, S., and Ghobrial, I. M. (2010). Selective inhibition of chymotrypsin-like activity of the immunoproteasome and constitutive proteasome in Waldenstrom macroglobulinemia. *Blood*, *115*(20), 4051–60.

Rock, J. R., Onaitis, M. W., Rawlins, E. L., Lu, Y., Clark, C. P., Xue, Y., Randell, S. H., and Hogan, B. L. M. (2009). Basal cells as stem cells of the mouse trachea and human airway epithelium. *Proceedings of the National Academy of Sciences of the United States of America*, *106*(31), 12771–12775.

Rodriguez, K. A., Edrey, Y. H., Osmulski, P., Gaczynska, M., and Buffenstein, R. (2012). Altered composition of liver proteasome assemblies contributes to enhanced proteasome activity in the exceptionally long-lived naked mole-rat. *PloS One*, *7*(5), e35890.

Saeki, I., Terai, S., Fujisawa, K., Takami, T., Yamamoto, N., Matsumoto, T., Hirose, Y., Murata, Y., Yamasaki, T., and Sakaida, I. (2013). Bortezomib induces tumor-specific cell death and growth inhibition in hepatocellular carcinoma and improves liver fibrosis. *Journal of Gastroenterology*, *48*(6), 738–750.

Saeki, Y., and Tanaka, K. (2012). Assembly and function of the proteasome. *Methods in Molecular Biology*, *832*, 315–337.

Safran, M., Kim, W. Y., O'Connell, F., Flippin, L., Günzler, V., Horner, J. W., Depinho, R. A., and Kaelin, W. G. (2006). Mouse model for noninvasive imaging of HIF prolyl hydroxylase activity: assessment of an oral agent that stimulates erythropoietin production. *Proceedings of the National Academy of Sciences of the United States of America*, *103*(1), 105–10.

Sakairi, T., Hiromura, K., Takahashi, S., Hamatani, H., Takeuchi, S., Tomioka, M., Maeshima, A., Kuroiwa, T., and Nojima, Y. (2011). Effects of proteasome inhibitors on rat renal fibrosis in vitro and in vivo. *Nephrology*, *16*(1), 76–86.

Santamaria, P. G., Finley, D., Ballesta, J. P. G., and Remacha, M. (2003). Rpn6p, a proteasome subunit from Saccharomyces cerevisiae, is essential for the assembly and activity of the 26 S proteasome. *The Journal of Biological Chemistry*, *278*(9), 6687–95.

Savulescu, A. F., and Glickman, M. H. (2011). Proteasome activator 200: the heat is on... *Molecular & Cellular Proteomics*, *10*(5), R110.006890–1–8.

Schmidt, M., and Finley, D. (2014). Regulation of proteasome activity in health and disease. *Biochimica et Biophysica Acta*, *1843*(1), 13–25.

Seibold, M. A., Wise, A. L., Speer, M. C., Steele, M. P., Brown, K. K., Loyd, J. E., Fingerlin, T. E., Zhang, W., Gudmundsson, G., Groshong, S. D., Evans, C. M., Garantziotis, S., Adler, K. B., Dickey, B. F., du Bois, R. M., Yang, I. V, Herron, A., Kervitsky, D., Talbert, J. L., Markin, C., Park, J., Crews, A. L., Slifer, S. H., Auerbach, S., Roy, M. G., Lin, J., Hennessy, C. E., Schwarz, M. I., and Schwartz, D. A. (2011). A common MUC5B promoter polymorphism and pulmonary fibrosis. *The New England Journal of Medicine*, *364*(16), 1503–1512.

Seifert, U., Bialy, L. P., Ebstein, F., Bech-Otschir, D., Voigt, A., Schröter, F., Prozorovski, T., Lange, N., Steffen, J., Rieger, M., Kuckelkorn, U., Aktas, O., Kloetzel, P. M., and Krüger, E. (2010). Immunoproteasomes preserve protein homeostasis upon interferon-induced oxidative stress. *Cell*, *142*(4), 613–624.

Senft, D., and Ronai, Z. A. (2015). UPR, autophagy, and mitochondria crosstalk underlies the ER stress response. *Trends in Biochemical Sciences*, *40*(3), 141–148.

Sharon, M., Taverner, T., Ambroggio, X. I., Deshaies, R. J., and Robinson, C. V. (2006). Structural organization of the 19S proteasome lid: insights from MS of intact complexes. *PLoS Biology*, *4*(8), e267.

Shibatani, T., and Ward, W. F. (1995). Sodium dodecyl sulfate (SDS) activation of the 20S proteasome in rat liver. *Archives of Biochemistry and Biophysics*, *321*(1), 160–166.

Shore, G. C., Papa, F. R., and Oakes, S. A. (2011). Signaling cell death from the endoplasmic reticulum stress response. *Current Opinion in Cell Biology*, *23*(2), 143–149.

Sijts, E. J. A. M., and Kloetzel, P. M. (2011). The role of the proteasome in the generation of MHC class I ligands and immune responses. *Cellular and Molecular Life Sciences*, *68*(9), 1491–1502.

Smith, D. M., Chang, S.-C., Park, S., Finley, D., Cheng, Y., and Goldberg, A. L. (2007). Docking of the proteasomal ATPases' carboxyl termini in the 20S proteasome's alpha ring opens the gate for substrate entry. *Molecular Cell*, *27*(5), 731–44.

Sontag, E. M., Vonk, W. I. M., and Frydman, J. (2014). Sorting out the trash: the spatial nature of eukaryotic protein quality control. *Current Opinion in Cell Biology*, *26*, 139–46.

Soond, S. M., and Chantry, A. (2011). How ubiquitination regulates the TGF-β signalling pathway: new insights and new players: new isoforms of ubiquitin-activating enzymes in the E1-E3 families join the game. *BioEssays : News and Reviews in Molecular, Cellular and Developmental Biology*, *33*(10), 749–58.

Stadtmueller, B. M., and Hill, C. P. (2011). Proteasome activators. *Molecular Cell*, *41*(1), 8–19.

Sun, F., Kanthasamy, A., Anantharam, V., and Kanthasamy, A. G. (2009). Mitochondrial accumulation of polyubiquitinated proteins and differential regulation of apoptosis by polyubiquitination sites Lys-48 and -63. *Journal of Cellular and Molecular Medicine*, *13*(8B), 1632–43.

Tanjore, H., Blackwell, T. S., and Lawson, W. E. (2012). Emerging evidence for endoplasmic reticulum stress in the pathogenesis of idiopathic pulmonary fibrosis. *American Journal of Physiology. Lung Cellular and Molecular Physiology*, *302*(8), L721–L729.

Teicher, B. A., and Tomaszewski, J. E. (2015). Proteasome Inhibitors. *Biochemical Pharmacology*, *96*(1), 1–9.

Teixeira, L. K., and Reed, S. I. (2013). Ubiquitin ligases and cell cycle control. *Annual Review of Biochemistry*, *82*, 387–414.

Thomas, A. Q., Lane, K., Phillips, J., Prince, M., Markin, C., Speer, M., Schwartz, D. A., Gaddipati, R., Marney, A., Johnson, J., Roberts, R., Haines, J., Stahlman, M., and Loyd, J. E. (2002). Heterozygosity for a surfactant protein C gene mutation associated with usual interstitial pneumonitis and cellular nonspecific interstitial pneumonitis in one kindred. *American Journal of Respiratory and Critical Care Medicine*, *165*, 1322–1328.

Tomko, R. J., and Hochstrasser, M. (2013). Molecular architecture and assembly of the eukaryotic proteasome. *Annual Review of Biochemistry*, *82*, 415–45.

Travis, W. D., King, T. E., Bateman, E. D., Lynch, D. A., Capron, F., Center, D., Colby, T. V., Cordier, J. F., DuBois, R. M., Galvin, J., Grenier, P., Hansell, D. M., Hunninghake, G. W., Kitaichi, M., Müller, N. L., Myers, J. L., Nagai, S., Nicholson, A., Raghu, G., Wallaert, B., Brambilla, C. G., Brown, K. K., Cherniaev, A. L., Costabel, U., Coultas, D. B., Davis, G. S., Demedts, M. G., Douglas, W. W., Egan, J., Eklund, A. G., Fabbri, L. M., Henke, C. A., Hubbard, R. B., Inoue, Y., Izumi, T., Jansen, H. M., Johnston, I., Kim, D. S., Khalil, N., Lake, F. R., Lungarella, G., Lynch, J. P., Mapel, D. W., Martinez, F., Matthay, R., Newman, L. S., Noble, P. W., Ohta, K., Olivieri, D., Ortiz, L. A., Poletti, V., Rodriguez-Roisin, R., Rom, W. N., Ryu, J. H., Saldiva, P., Sansores, R. H., Schwarz, M. L., Selman, M., Smith, C. M., Tong, Z., Udwadia, Z., Valeyre, D., Wells, A., Wise, R. A., Xaubet, A., Alvarez Fernandez, E., Brambilla, E., Capelozzi, V., Cherniaev, A., Dalquen, P., Dekan, G., Hasleton, P. S., Hogg, J. C., Jambhekar, N. A., Katzenstein, A. L., Koss, M. N., Matsubara, O., Müller, K. M., Thunnissen, F. B. J. M., Waldron, J. A., Li, W. H., Friedman, P. J., Remy-Jardin, M., and McLoud, T. C. (2002). American thoracic society/European respiratory society international multidisciplinary consensus classification of the idiopathic interstitial pneumonias. *American Journal of Respiratory and Critical Care Medicine*, *165*(2), 277–304.

Van Rijt, S. H., Keller, I. E., John, G., Kohse, K., Yildirim, A. Ö., Eickelberg, O., and Meiners, S. (2012). Acute cigarette smoke exposure impairs proteasome function in the lung. *American Journal of Physiology. Lung Cellular and Molecular Physiology*, *303*(9), L814–23.

Verdoes, M., Florea, B. I., Menendez-Benito, V., Maynard, C. J., Witte, M. D., van der Linden, W. A., van den Nieuwendijk, A. M. C. H., Hofmann, T., Berkers, C. R., van Leeuwen, F. W. B., Groothuis, T. A., Leeuwenburgh, M. A., Ovaa, H., Neefjes, J. J., Filippov, D. V., van der Marel, G. A., Dantuma, N. P., and Overkleeft, H. S. (2006). A Fluorescent Broad-Spectrum Proteasome Inhibitor for Labeling Proteasomes In Vitro and In Vivo. *Chemistry and Biology*, *13*(11), 1217–1226.

Verma, R., Peters, N. R., D'Onofrio, M., Tochtrop, G. P., Sakamoto, K. M., Varadan, R., Zhang, M., Coffino, P., Fushman, D., Deshaies, R. J., and King, R. W. (2004). Ubistatins inhibit proteasome-dependent degradation by binding the ubiquitin chain. *Science*, *306*(5693), 117–120.

Vilchez, D., Boyer, L., Morantte, I., Lutz, M., Merkwirth, C., Joyce, D., Spencer, B., Page, L., Masliah, E., Berggren, W. T., Gage, F. H., and Dillin, A. (2012). Increased proteasome activity in human embryonic stem cells is regulated by PSMD11. *Nature*, *489*(7415), 304–8.

Vilchez, D., Morantte, I., Liu, Z., Douglas, P. M., Merkwirth, C., Rodrigues, A. P. C., Manning, G., and Dillin, A. (2012). RPN-6 determines C. elegans longevity under proteotoxic stress conditions. *Nature*, *489*(7415), 263–8.

Vilchez, D., Simic, M. S., and Dillin, A. (2014). Proteostasis and aging of stem cells. *Trends in Cell Biology*, *24*(3), 161–70.

Walter, P., and Ron, D. (2011). The Unfolded Protein Response: From Stress Pathway to Homeostatic Regulation. *Science*, *334*(6059), 1081–1086.

Weathington, N. M., and Mallampalli, R. K. (2014). Emerging therapies targeting the ubiquitin proteasome system in cancer. *The Journal of Clinical Investigation*, *124*(1), 6–12.

Wei, J., Rahman, S., Ayaub, E. a., Dickhout, J. G., and Ask, K. (2013). Protein misfolding and endoplasmic reticulum stress in chronic lung disease. *Chest*, *143*(4), 1098–1105.

Weiss, C. H., Budinger, G. R. S., Mutlu, G. M., and Jain, M. (2010). Proteasomal regulation of pulmonary fibrosis. *Proceedings of the American Thoracic Society*, *7*(1), 77–83.

Wolters, P. J., Collard, H. R., and Jones, K. D. (2014). Pathogenesis of idiopathic pulmonary fibrosis. *Annual Review of Pathology*, *9*, 157–79.

Wynn, T. A. (2011). Integrating mechanisms of pulmonary fibrosis. *The Journal of Experimental Medicine*, *208*(7), 1339–50.

Wynn, T. A., and Ramalingam, T. R. (2012). Mechanisms of fibrosis: therapeutic translation for fibrotic disease. *Nature Medicine*, *18*(7), 1028–40.

Zang, Y., Thomas, S. M., Chan, E. T., Kirk, C. J., Freilino, M. L., DeLancey, H. M., Grandis, J. R., Li, C., and Johnson, D. E. (2012). Carfilzomib and ONX 0912 inhibit cell survival and tumor growth of head and neck cancer and their activities are enhanced by suppression of Mcl-1 or autophagy. *Clinical Cancer Research*, *18*(20), 5639–5649.

Zhang, Y., Nicholatos, J., Dreier, J. R., Ricoult, S. J. H., Widenmaier, S. B., Hotamisligil, G. S., Kwiatkowski, D. J., and Manning, B. D. (2014). Coordinated regulation of protein synthesis and degradation by mTORC1. *Nature*, *513*(7518), 440–3.

6 APPENDIX

6.1 Abbreviations

A

α1-7	Alpha subunits 1-7 of the 20S proteasome
αSMA	Alpha smooth muscle actin
AECI	Alveolar epithelial cell type I
AECII	Alveolar epithelial cell type II
ALAT	Latin America Thoracic Society
AMC	7-amino-4-methylcoumarin
ANOVA	Analysis of variance
APS	Ammonium peroxodisulfate
ATCC	American Type Culture Collection
ATF6	Activating transcription factor 6
ATI	Alveolar type I
ATII	Alveolar type II
ATP	Adenosine triphosphate
ATS	American Thoracic Society

B

BAL	Bronchoalveolar lavage
BSA	Bovine serum albumin
BZ	Bortezomib

C

°C	Degrees Celsius
C. elegans	*Caenorhabditis elegans*
CDK	Cyclin dependent kinase
cDNA	Complementary DNA
C-L	Caspase-like
CMC	Carboxymethylcellulose
Coll-I	Collagen type I, collagen I
CP	Core particle of the proteasome
CTGF	Connective tissue growth factor
CT-L	Cymotrypsin-like

D

d	Day(s)
Da	Dalton
DAPI	4',6-diamidino-2-phenylindole
DMEM	Dulbecco's Modified Eagle's Medium
DMSO	Dimethyl sulfoxide
DNA	Deoxyribonucleic acid
dNTP	Desoxy-nucleotide-tri-phosphate
DTT	Dithiothreitol

DZL   Deutsches Zentrum für Lungenforschung

E
ECM   Extracellular matrix
ED-A   Extra domain A
EDTA   Ethylenediaminetetraacetic acid
EGF   Epidermal growth factor
EGTA   Ethylene glycol tetraacetic acid
EMT   Epithelial mesenchymal transition
ER   Endoplasmic reticulum
ERAD   Endoplamic reticulum-associated protein degradation
ERS   European Repiratory Society
ES cell   Embryonic stem cell

F
FBS   Fetal bovine serum
FDA   Food and Drug Administration (USA)
FGF   Fibroblast growth factors
FITC   Fluorescein isothiocyanate
Fn   Fibronectin
FOXO   Forkhead box O
Fw   Forward

G
g   Force
g   Gram
GAPDH   Glyceraldehyde 3-phosphate dehydrogenase
GFP   Green fluorescent Protein
Gly   Glycin

H
h   Hour(s)
h   Human
HEPES   N-2-hydroxyethylpiperazine-N-2-ethane sulfonic acid
HIF   Hypoxia-inducible factors
HRCT   High resolution computer tomography
HRP   Horseradish peroxidase

I
I   Inhibitor
IAP   Inhibitors of apoptosis
IF   Immunofluorescence
IHC   Immunohistochemistry
IL   Interleukin
INF   Interferon
IPF   Idiopathic pulmonary fibrosis
IRE1   Inositol requiring enzyme 1
I-SMAD   Inhibitory SMAD

J
JRS   Japanese Respiratory Society

K
K   Kilo
kg   Kilogram
KRT5   Cytokeratin-5

L
l   Liter
LOXL2   Lysyl oxidase-like 2
Luc   Luciferase

M
μ   Micro
m   Milli
M   Molar
mA   Milliampere
mg   Milligram
ml   Milliliter
mM   Millimolar
MMF   Medetomidin-Midazolam-Fentanyl
MMP   Matrix metalloproteinase
mRNA   Messenger RNA
MTT   3-(4,5-Dimethyl-2-thiazolyl)-2,5-diphenyl-2H-tetrazolium bromide
MUC5B   Mucin 5B

N
NF   Nuclear factor
NG   Native gel
nm   Nanometer
nM   Nanomolar
NPC   Neural progenitor cell
NTP   Nucleoside triphosphate

O
ODD   Oxygen-dependent degradation domain
OZ   Oprozomib

P
PA   Proteasome activator
PAC   Proteasome assembling chaperone
PAGE   Polyacrylamide gel electrophoresis
PBS   Phosphatate buffered saline
PCR   Polymerase chain reaction
PDGFR   Platelet-derived growth factor receptor
PERK   Protein kinase RNA-like ER kinase
PFA   Paraformaldehyde

phLF	Primary human lung fibroblast
pmATI	Primary mouse ATI cell
pmATII	Primary mouse ATII cell
pmLF	Primary mouse lung fibroblast
PMN	Polymorphonuclear leukocytes
POMP	Proteasome maturation protein
PPAR	Peroxisome proliferator-activated receptor
PVDF	Polyvinylidene difluoride

Q

qRT-PCR	Quantitave real-time Polymerase chain reaction

R

rev	Reverse
RIPA	Radio-immunoprecipitation assay
RNA	Ribonucleic acid
RP	Regulatory Particle
Rpn	Regulatory particle non-ATPase
Rpt	Regulatory particle triple A ATPase
R-SMAD	Receptor-regulated SMAD

S

SBE	SMAD-binding element
sc	Scrambled
SDS	Sodium dodecyl sulphate
SFTPC	Surfactant protein C
siRNA	Small interfering RNA

T

TEMED	N,N,N',N'-Tetramethylendiamin
TERC	Telomerase RNA component
TERT	Telomerase reverse transcriptase
TGF	Transforming growth factor
TIMP	Tissue inhibitor of metalloproteinase
T-L	Trypsin-like
TNF	Tumor necrosis factor
TR	Telomerase RNA
TRIS	Tris(hydroxymethyl)-aminomethane
TTF1	Thyroid transcription factor 1
TβRI	TGF-β transmembrane type I receptor
TβRII	TGF-β transmembrane type II receptor

U

Ub/Ubi	Ubiquitin
Ubi-K48	Lys48-Ubiquitin
UIP	Usual interstitial pneumonia
UMP	Ubiquitin-mediated proteolysis
UPR	Unfolded protein response

UPS   Ubiquitin-proteasome system

V
V   Volt
V   Volume
VEGFR   Vascular endothelial growth factor receptor
vWF   Von Willebrand factor

W
WB   Western blot

6.2 Publications

6.2.1 Original articles

Semren N, Welk V, Korfei M, Keller IE, Fernandez I, Adler H, Günther A, Eickelberg O, Meiners S. Regulation of 26S proteasome activity in pulmonary fibrosis. *American Journal of Respiratory and Critical Care Medicine,* 2015 Nov;192(9):1089-1101.

Semren N, Habel-Ungewitter NC, Fernandez IE, Königshoff M, Eickelberg O, Stöger T, Meiners S. Validation of the 2nd Generation Proteasome Inhibitor Oprozomib for Local Therapy of Pulmonary Fibrosis. *PloS One,* 10(9), e0136188.

Lenz A. G., Stoeger T., Cei D., Schmidmeir M., **Semren N.**, Burgstaller G., Lentner B., Eickelberg O., Meiners S., Schmid O. Efficient bioactive delivery of aerosolized drugs to human pulmonary epithelial cells cultured in air-liquid interface conditions. *American Journal of Respiratory Cell and Molecular Biology*, 2014 Oct;51(4):526-35

6.2.2 Review

Meiners S, Keller IE, **Semren N**, Caniard A. Regulation of the proteasome: evaluating the lung proteasome as a new therapeutic target. *Antioxidants & Redox Signaling,* 2014 Dec 10;21(17):2364-82.

6.2.3 Meeting abstracts

Welk V, **Semren N**, Korfei M, Guenther, Eickelberg O, Meiners S. Altered Protein Homeostasis in Pulmonary Fibrosis Indicates a Role for Proteasome Activator 200.
Poster presentation, ATS International Conference, Denver, USA (2015).

Semren N, Habel-Ungewitter NC, Fernandez IE, Eickelberg O, Stöger T, Meiners S. Validation of the 2nd generation proteasome inhibitor oprozomib for local therapy of pulmonary fibrosis.
Poster presentation, DZL Meeting, Hamburg, Germany (2015).

Semren N, Welk V, Korfei M, Guenther, Eickelberg O, Meiners S. Altered Protein Homeostasis in Pulmonary Fibrosis Indicates a Role for Proteasome Activator 200.
Poster presentation, ERS International Conference, Munich, Germany (2014).

Semren N, Korfei M, Fernandez IE, Günther A, Eickelberg O, Meiners S. Proteasome function in lung fibrosis.
Oral presentation, ERS International Conference, Munich, Germany (2014).

Meiners S, **Pfister N**, Korfei M, Fernandez IE, Günther A, Eickelberg O. Altered proteasome function in lung fibrosis.
Poster presentation, ATS International Conference, San Diego, USA (2014).

Semren N, Korfei M, Fernandez IE, Günther A, Eickelberg O, Meiners S. Altered proteasome function in lung fibrosis.
Poster presentation, DZL Meeting, Heidelberg, Germany (2014).

Pfister N, Fernandez IE, Eickelberg O, Meiners S. Proteasome function in lung fibrosis.
Poster presentation, Munich Lung Conference, Munich, Germany (2013).

Pfister N, Fernandez IE, Eickelberg O, Meiners S. Regulation of the proteasome in lung fibrosis.
Poster presentation, ERS International Conference, Barcelona, Spain (2013).

Pfister N, Fernandez IE, Eickelberg O, Meiners S. Regulation of the proteasome in lung fibrosis.
Poster presentation, ATS International Conference, Philadelphia, USA (2013).

Pfister N, Fernandez IE, Eickelberg O, Meiners S. Proteasome function in lung fibrosis.
Poster presentation, DZL Meeting, Bad Nauheim, Germany (2013).

Pfister N, Fernandez IE, Eickelberg O, Meiners S. Regulation of protein degradation by the proteasome in lung fibrosis.
Poster presentation, Air Symposium, Fürstenfeldbruck, Germany (2013).

Pfister N, Habel NC, Stöger T, Eickelberg O, Meiners S. Evaluation of ONX0912, a novel proteasome inhibitor, for treatment of lung fibrosis.
Poster presentation, Febs Meeting, Kusadasi, Turkey (2012).

Pfister N, Habel NC, Stöger T, Eickelberg O, Meiners S. Investigation of the novel proteasome inhibitor ONX0912 for the treatment of lung fibrosis.
Poster presentation, Munich Lung Conference, Munich, Germany (2012).

Pfister N, Habel NC, Stöger T, Eickelberg O, Meiners S. Evaluation of ONX0912, a novel proteasome inhibitor, for treatment of lung fibrosis.
Oral presentation, ERS International Conference, Vienna, Austria (2012).

Pfister N, Eickelberg O, Meiners S. Evaluation of ONX0912, a novel proteasome inhibitor, for treatment of pulmonary fibrosis.

Oral presentation, "Herbsttagung der Sektion Zellbiologie und der Sektion Infektiologie und Tuberkulose", Homburg, Germany (2011).

6.3   Acknowledgements

Coming to the end of these exiting and memorable years as a PhD student, there are many people that need to be acknowledged for their support, guidance and inspiration during this time. I could not have done it without you!

I am very grateful to **Prof. Dr. Ernst Wagner** for the supervision of my thesis at the LMU, for helpful discussions within the student seminars, and for the great support in all administrative issues.

Thanks a lot to **Prof. Dr. Oliver Eickelberg** for giving me the opportunity to do my PhD at the CPC and for providing such an inspiring, international and modern research environment.

I would like to thank my supervisor **PD Dr. Silke Meiners** for her great scientific guidance throughout this time, for allowing me to create my own ideas and projects, and for sharing the enthusiasm for my topic. Thanks a lot for the very exciting, formative, and instructive time in your lab!

For sure I could not have enjoyed the time so much without my wonderful lab-members. Therefore a great thanks to **Vanessa Welk** (thank you so much for your support during the paper revisions), **Christina Lukas** (thanks a lot for your great technical support), **Ilona Keller**, **Alessandra Mossina**, **Dr. Sabine van Rijt**, **Dr. Anne Caniard**, **Dr. Oliver Vosyka**, **Korbinian Ballweg**, **Deniz Bölükbas** and **Dr. Angela Dann** for all your scientific input, contributions of ideas, kind support and the fun we had in and outside the lab.

I further would like to thank **Nunja Habel-Ungewitter**, **David Kutschke**, **Simon Orth**, **Isis Fernandez**, **Daniela Dietel** and **Constanze Heise** for the great help with long-day animal experiments. Thanks to **Dr. Tobias Stöger** for helpful advice in animal issues and your scientific input on the oprozomib paper.

I am also very grateful to **Dr. Martina Korfei** for the great collaboration, extensive email support and your invaluable input on the Rpn6 paper.

As a "non-biologist" I have benefitted a lot from the research school "Lung Biology and Disease", and therefore I would like to thank **Dr. Dr. Melanie Königshoff** for equipping me with useful knowledge about methods and lung biology. I also thank **Camille Beunèche** and **Dr. Doreen Franke** for their administrative help.

One highlight during my time at the CPC was the great companion of my PhD fellows. Therefore I especially would like to thank **Dr. Bettina Oehrle**, **Dr. Andrea Schamberger**,